ADDIS ABABA UNIVERSITY

ADDIS ABABA INSTITUTE OF TECHNOLOGY

SCHOOL OF GRADUATE STUDIES

SCHOOL OF CIVIL AND ENVIRONMENTAL ENGINEERING

NUMERICAL MODELING OF EMBANKMENT DAMS IN LIQUEFIABLE SOILS DURING EARTHQUAKES

By

Getu Debebe

A project Submitted to the School of Graduate Studies
in Partial Fulfillment of the Requirements for the Degree of Masters in Geotechnical Engineering

Advisor

Dr. Tensay Gebremedhin

Addis Ababa University

April, 2022

Addis Ababa, Ethiopia

ADDIS ABABA UNIVERSITY

ADDIS ABABA INSTITUTE OF TECHNOLOGY

SCHOOL OF GRADUATE STUDIES

SCHOOL OF CIVIL AND ENVIRONMENTAL ENGINEERING

NUMERICAL MODELING OF EMBANKMENT DAMS IN LIQUEFIABLE SOILS DURING EARTHQUAKES

Submitted

By

Getu Debebe

Approved by the board of Examiners:

Dr. Tensay Gebremedhin Advisor	Signature	23/05/22 Date
Asrat Worku Examiner	Signature	25.05.2022 Date
Mebruk Mohammed (Dr.-Ing.) Dean, Sch... il & Environmental Engineering Chairperson	Signature	Date

Declaration

I hereby declare that this project, titled "Numerical Simulation of Embankment Dams in Liquefiable Soil During Earthquake," was written by me, that the work contained herein is my own unless otherwise stated in the text and that this work has not been submitted for any other degree or professional qualification, in whole or in part.

Getu Debebe	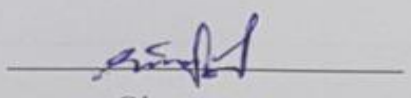	23/05/2022
Name	Signature	Date

Acknowledgments

I thank the almighty GOD for giving me the strength and bravery to complete this project.

Then my thanks go to my project adviser, Dr. Tensay Gebremedhin, who has been a great help to me throughout the study I've done, by providing insightful and timely comments, excellent advice, and spending his precious time for improving the quality of this project till it is completed.

My sincere thanks also goes to Leamlak Minwuyelet, a staff member at the school of civil and environmental engineering, for providing me with the data I required for my research, as well as the software support he gave.

Finally, I would like to thank my family and friends, for being with me in all my difficult times.

Table of Contents

List of Tables

List of figures

List of Abbreviations

ATH	Acceleration Time History
BC	Boundary Condition
CSR	Critical Stress Ratio
DBE	Design Base Earthquake
D/s	Downstream
EERC	Earthquake Engineering Research Center
Eq.	Equation
EQL	Equivalent Linear
FS	Factor of Safety
$G_{\max}$	Maximum dynamic shear modulus
H	Horizontal
K	Seismic coefficient
K_a	Correction factor for initial static stress
k_h	Horizontal seismic coefficient
K_s	Correction factor for overburden stress
k_v	Vertical seismic coefficient
KPa	Kilopascal
LL	Liquid Limit
MCE	Maximum Credible Earthquake
M_s	Surface-wave magnitude
M_W	Moment magnitude
M	Meter
N	Number of cycles of an earthquake
NL	Number of cycles required to cause liquefaction
PI	Plasticity Index
PWP	Pore Water Pressure

PGA	Peak Ground Acceleration
PGV	Peak Ground Velocity
sec	Second
T_m	Mean period
T_p	Predominant period
USGS	United States Geological Survey
U/s	Upstream
USNRC	United States National Research Center
V	Vertical
WWDSE	Water Works Design and Supervision Enterprise

Abstract

Ethiopia has built several embankment dams up to the present day for different purposes. Some dams are situated in the rift valley, which is highly susceptible to high earthquake natural disasters. Dynamic loads induced by earthquakes are often major factors in the design of earth dams founded on liquefiable soil. Earthquake-induced stresses are major factors in determining the angles of the dam slopes and significantly influence the selection of materials, the zoning of the dam, and the construction method. These have taken a great attention to dams constructed from loose or medium dense saturated cohesionless soils and subjected to strong ground shaking. This project aims to simulate the effect of earthquake shaking on the stability of the embankment dam on liquefiable soil using the finite element method-based state-of-the-art software package, Geo-Slope software. The numerical simulation of embankment dams on liquefiable soil has been carried out by taking many factors into account. Among these factors, in this project numerical simulation has been made to see the effect of dam geometry, foundation material property, and liquefiable soil foundation thickness on the stability of the dam during dynamic loading. The evaluation also has been made to determine the response of the embankment dam on liquefiable soil under different earthquake ground shaking conditions. This includes assessing the safety margins against the risks of failure due to extreme scenarios, particularly soil liquefaction of the structure's foundation. A finding of this study shows that all those aforementioned factors have a significant impact on the stability of the liquefiable foundation of the embankment dam under dynamic loading. As a result an embankment dam having with 1 to 3 slope ratios, 5 meter foundation thickness with dense sand foundation material can withstand 0.37g peak ground acceleration safely with respect to slope stability, deformation and liquefaction.

KEYWORDS: earthquakes, Geo-Slope software, liquefiable foundation, embankment dam.

1. Introduction

1.1. Background of the Study

Geotechnical earthquake engineering is a sub-specialty of geotechnical engineering that deals with the design and construction of projects in order to resist the effects of earthquakes (Day, 2006). According to (Frederick K. Lutgens, 2020) earthquakes are triggered by the movement of base rocks along fault surfaces, resulting in vibrations. The energy accumulated by elastic deformation in the rocks on both sides of a fault is adequate to rupture the rocks or overcome friction on an existing fault plane in the majority of earthquakes. The energy of the earthquake is projected outwards via elastic waves created at the fault. As these waves pass through and through the earth's crust, they shake the earth in all directions, with variable degrees of strength and oscillation patterns. The amplitude of these waves diminishes with distance in general. The quantity of energy released determines the magnitude of an earthquake. The magnitude of an earthquake can be used to determine this. The quantity of energy released is proportional to the extent of the geologic offset, fault characteristics, and the seismic hazard's effects on humans and the environment (L.Kramer, 1996). As a result, an embankment dam, which requires seismology and earthquake engineering skills, is one of the man-made constructions subject to this hazard. Liquefaction is one of the effects of the earthquake that contributes to the embankment dam instability.

Liquefaction is a loss of shear strength and/or stiffness in saturated cohesion-less soils induced by a rise in pore water pressure during fast ground movement. Saturated sandy soil’s liquefaction is a phenomenon that happens when they are subjected to seismic stress. The passage of a seismic wave reduces the soil's strength and shear stiffness, resulting in an increase in pore water pressure caused by cyclic deformations (Taiebat, Shahir and Pak, 2007). The material's sudden deconsolidation causes soil decomposition and the collapse of structures built on that type of soil. Earth dams made of or underlain by loose saturated granular soils have a significant risk of liquefaction-induced ground displacements as a result of earthquake shaking. During numerous earthquakes across the world, liquefaction-induced earth dam failures or near-failures have been documented (Taiebat, Shahir and Pak, 2007). When the underlying saturated granular soils liquefied,

cracking, settling, lateral spreading, and collapsing of the embankment occurred. To address such geotechnical issues, it is critical to design and construct geotechnical structures that take the seismic effect into account.

Dam's Seismic analysis started a few decades before. The previous most dominant analysis type of dynamic load was static or pseudo-static seismic analysis which, Pseudo-static analysis is used for simple slope design to account for seismic forces by a seismic coefficient (k_v) is related to Peak Ground Acceleration to represent horizontal inertia forces from the earthquake but it is insufficient to represent dynamics of a complex problem (Nikkar, 2014). Nowadays with the advancement of numeric-based computer applications, dynamic analysis of a dam is becoming compulsory for seismic region dams. Deformations due to earthquakes and other characters of a dam during earthquakes that cannot be captured by pseudo-static analysis can be done using dynamic analysis with the help of computer tools.

Due to seismic load, a few millimeters of deformation up to a total collapse of a project could happen. This is determined by the character of the earthquake, soil behavior of the site, dam material, and dam geometry. Using developed models to relate interaction between these factors, a dynamic analysis of an embankment dam founded in liquefiable soil has been conducted on this project to evaluate the dam's performance of serviceability and safety during an earthquake. In this case, liquefiable soil is a very problematic soil under dynamic loading taken to consider.

1.2. Statement of the Problem

An embankment dam built in a seismically active zone with liquefiable soil foundation can experience severe instability as a result of an earthquake. The dam's shape, material properties, and foundation material thickness, as well as the seismic loading conditions all have an impact on its stability. Due to a lack of attention for this aspect, dams will have a severe impact on the downstream population. For a dam that has been built or is planned to be built, it is advisable to take into account different factors during design to overcome the seismic instability of dams caused by an earthquake. It is preferable to use a numerical simulation that demonstrates the embankment dam's true response and

ensures the safety of downstream inhabitants' lives and property, as well as the economy of the country.

1.3. Objectives

1.3.1. General Objective

The general objective of this study is the use of numerical modeling to evaluate the impact of several factors on the stability of an embankment dams on liquefiable soils during earthquakes.

1.3.2. Specific Objectives

- To investigate the effect of dam geometry on the stability of the dam during earthquake.
- To examine the effect of foundation material property on the stability of the dam during earthquake.
- To investigate the influence of the thickness of the liquefiable foundation on the response of the dam under earthquake.
- To investigate the effect of earthquake conditions on the stability of the dam.

1.4. Scope of the Study

Despite the fact that an embankment dam can be made of natural materials excavated or obtained in the surrounding area without any binding, this study focused on earth fill embankment dams because they are more susceptible to earthquake-induced ground shaking failure than dams made of other materials.

Although previous studies have shown that the true response of the equivalent linear material model is less than that of the nonlinear material model, particularly in the case of liquefaction, the dynamic analysis is carried out using the equivalent linear material model because the equivalent linear material model requires soil data in a simple way. And the study is limited to secondary input data due to time and budget constraint.

1.5. Significance of the Study

Dams are used for a variety of reasons, including water supply, agriculture, hydropower, and many others. Dam failures have serious economic consequences, but they also have a negative impact on the environment and people's quality of life. Populations are also at

risk in areas downstream of big dams, which are sensitive to earthquakes. A seismic design of embankment dams on liquefiable soil has been done to eliminate seismic risks that may arise in the given site in order to reduce such damages. Another important component of this study is the evaluation of embankment dams by considering several scenarios of the embankment and foundation in order to come up with an inexpensive design for a maximum ground motion caused by an earthquake. This can be used as a reference for a preliminary design to understand the impact of changing the dam's design parameters during an earthquake.

1.6. Research Question

How do the geometry of the dam, foundation material properties, liquefiable soil foundation thickness, and earthquake conditions affect the stability of earth fill dams?

1.7. Structure of the Study

This thesis contains five chapters. The content of each chapter is described as follows: The first chapter is an introduction, which begins with a brief overview of the study field and is followed by a problem statement. The study's objectives, research questions, hypothesis, scope, and significance are all discussed in this chapter. The literature reviews are included in the second chapter. This chapter reviews past work focusing on the performance of earth fill dams in terms of dynamic analysis, liquefiable material properties, foundation material thickness, and seismic loading conditions. Following theoretical literature study, the very critical empirical literature review has been undertaken. Material and methods is the third chapter of this study, which discuses about the research material and methods employed in this study. It included, defining geometry of the dam, defining material property, method of analysis, and numerical simulation. It also clarifies how the objective of the study would be achieved. The fourth chapter is results and discussion, in which the significant findings of this study are presented in regard to the study's general objective and specific objectives, which included slope stability analysis under initial static stress and earth quake induced dynamic loading. Additionally, liquefaction of foundation, acceleration response at the dam crest, and vertical and horizontal crest deformation due to dynamic loading are all covered in depth. In the final chapter, chapter Five, conclusions have been drown based on the result obtained as discussed in chapter four and makes recommendations for further research.

2. Literature Review

2.1. Earthquake

The study of earthquake engineering necessitates a thorough understanding of the many processes that cause earthquakes and their consequences on the ground. An earthquake is mainly a result of a release of strain energy by a rupture of rock at plate boundaries. The strain energy-storing process is a result of plate tectonics. Plate tectonics is a large-scale motion of the earth's lithosphere. The most accepted explanation of the source of the plate movements is the requirement of thermo mechanical equilibrium of the earth's materials (L.Kramer, 1996).

There are two types of plate: continental plate and ocean plate. These two types of plates are different in their position, thickness, composition, and density. When these plates move, one plate might slide underneath the other. In another cases plates might rub sideways against each other, or both the plates neither go easily underneath that they crumble together. During these processes strain energy will be stored in the boundaries of the plate, which will be released when it reaches its limit. But there are other factors that can induce an earthquake. Nuclear activity and reservoir fill are among them. A reservoir fill increases the pore water pressure of a strain developing region. This reduces shear strength which results from a strain energy release (L.Kramer, 1996).

Earthquakes are divided into two types based on their origin: "Plate boundary type" and "Inland type." When a continental plate is pushed by an oceanic plate, this is known as the "Plate Boundaries Type." This happens in the vicinity of field strain energy storage. Faults generated in a continental plate may be a source of another earthquake due to the energy of plate tectonics. "Active faults" are faults that are close to the earth's surface. A focus, also known as a hypocenter, is the place where strain energy is released at plate borders. The epicenter is vertically above the focus point on the surface. The distance between the observation site and the epicenter and hypocenter, respectively, is called epicenter distance and hypocenter distance (L.Kramer, 1996).

Seismic waves of several types are emitted during earthquakes. These waves are divided into two categories: body waves and surface waves. From the hypocenter, body waves

are emitted. Primary waves and secondary waves are the two main waves of body waves. Primary waves are extremely rapid and squeeze the earth. Secondary waves have a shearing impact and travel at a slower speed than primary waves. Surface waves are waves that radiate from the epicenter, similar to a water wave in a pond caused by a thrown stone. They are caused by the interaction of body waves with the earth's surface and strata. The earth sways and rolls as a result of their action (L.Kramer, 1996).

2.2. Determination of Liquefiable Soil

Liquefaction potential may be assessed using a variety of methods, including experimentally based simpler processes and models based on nonlinear soil dynamics (Ioanna Rapti, 2016). Lose saturated sand and as observed from recent studies other soil formations like silt deposits tend to compact and decrease in volume when subjected to vibration. When drainage is not possible, the pore water pressure rises. If continuous vibration is permitted to build up the pore water pressure in the cohesion-less deposit, a state will be attained where the overburden pressure equals the pore water pressure. A load will be transmitted to pore water during this period, resulting in an increased in a pore-water pressure. This decreases the tension and internal friction angle component of shear strength by reducing the effective stress on the soil solid particle. Liquefaction will occur as it lowers. Due to their low cohesion shear strength, cohesion-less soils of loose sand and wet sand will have no residual shear strength at this state (GDP-9, 2015).

Based on the effective stress principle,

$$\sigma' = \sigma - u \quad \text{.....(2.1)}$$

Where,

$\sigma' is$ The effective stress

$\sigma\ is$ The total over burden pressure, and

u is The pore water pressure

If σ is equal to u, σ' is zero. Under this condition, the soil doesn't possess any shear strength, and it changes into a liquefied state assumed that the soil is cohesion-less in such a way that negative pore water pressure couldn't occur under dynamic loading.

This pore water pressure development primarily depends on particle shape, size, and gradation. Clean sands show the most liquefaction. Liquefaction is less likely in well-graded soils than in poorly graded soils. In the field, uniformly graded soils have caused the majority of liquefaction failures (Seged and Haile, 2010).

2.2.1. Cohesion-Less Particles Liquefaction Potential Assessment:

The first step to evaluate the potential of liquefaction is, therefore, the identification of grain size distribution of the soil. Figure 2.1 shows grain size distribution boundaries separating liquefiable and non-liquefiable soils proposed by (Tsuchida, 1988) and extensively used by geotechnical engineers worldwide. This demonstrates the necessity of understanding the dynamic behavior of liquefiable soil by determining whether it is liquefiable based on the gradation curve.

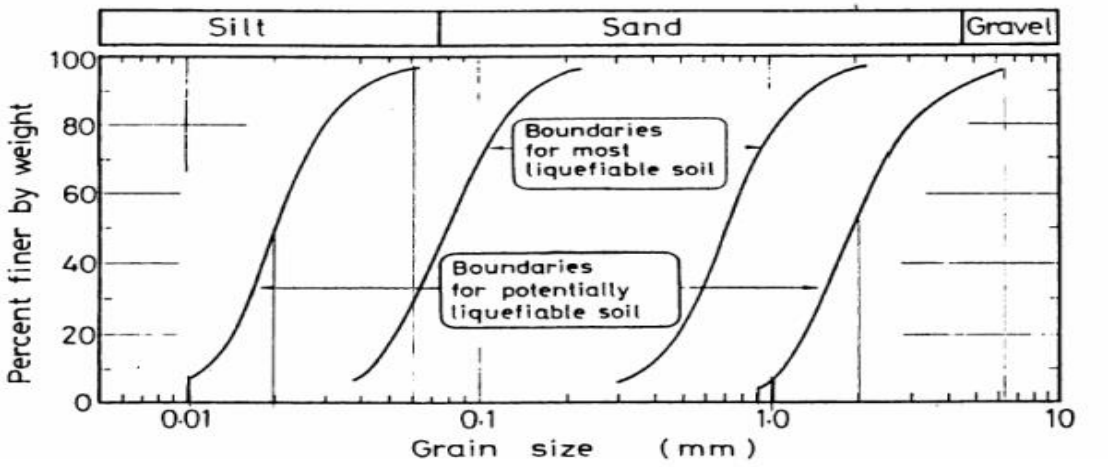

Figure 2.1 Boundaries separating liquefiable and non-liquefiable soils

2.2.2. Fine Particles Liquefaction Potential Assessment:

Several researchers have proposed using index qualities to rule out the possibility of liquefaction in fine-grained soils. A newer set of criteria based on a large number of case histories and laboratory tests is provided below. Cohesive material liquefaction assessment was done by using the model developed by (Seed H. B. and Idriss I. M., 1970) which indicates that clayey soils could liquefy if all three of the below requirements are met.

- If the PI is greater than 18, the soil may be considered non- liquefiable.

- If the PI is greater than 12, the soil may be considered non- liquefiable, provided that the water content is less than 85 percent of the Liquid Limit (LL).
- If soil does have some plasticity, even if the PI is less than 12, it may be considered non-liquefiable, provided that the water content is less than 80 percent of the LL.

Unless laboratory shear testing, in situ penetration resistance or other evidence shows otherwise, a soil that does not meet at least one of these requirements should be deemed liquefiable. If the PI is between 12 and 18, or the water content is between 80 and 85 percent of the LL, the soil is moderately vulnerable or potentially susceptible to liquefaction, and more testing is needed. For materials with even a small amount of plasticity, laboratory shear testing is often possible.

2.2.3. Other Methods of Determining Liquefaction Potential

The "simplified approach," which examines a cycle stress ratio at a particular depth for a defined design earthquake, is another fundamental procedure used in engineering practice to determine liquefaction potential. Where the cycle resistance ratio of a soil layer is the stress ratio necessary to induce liquefaction for a cohesion-free soil stratum with certain qualities at a specific depth, and the cyclic stress ratio is the seismic demand on the soil layer based on peak ground surface acceleration. Because this approach is empirical, it cannot be used everywhere, even though the underlying principle is vital for determining the liquefiable potential of the cohesion-less soil layer.

Models based on the nonlinear soil behavior using the numerical method are nowadays powerful tool used in geotechnical engineering worldwide to evaluate the stability of the geotechnical structure. One of these geotechnical structures is an embankment dam.

2.3. Embankment Dam

Embankment dam is made of natural materials excavated or obtained in the surrounding area without any binding. They can be homogeneous but the most usual structures consist of distinct zones of materials with different characteristics. There are two main types of embankment dams: earth fill and rock-fill dams depending on the materials used on the embankment. Earth fill dam is an embankment dam constructed primarily of compacted

earth either zoned or homogeneous material. An embankment dam can be characterized as an earth-fill dam, if compacted soils contribute for more than 50% of the total volume of material placed. An earth fill dam is made up primarily of selected engineering soils that have been compacted uniformly and intensively in relatively thin layers with controlled moisture content. They, usually, consist of an impermeable core made of clayey soils, filters and drains usually made of sandy and gravelly soil to prevent the core from being washed out and two shells made of variable soils to ensure the stability of the structure and the suitable weight to withstand the water load. The shells are usually protected by thin external zones of coarser soil or rock (O.Engemoen, 2012).

2.4. Dynamic Stability Analysis

Faulty design, inappropriate construction, and poor maintenance procedures, among other factors, can cause earth dams to fail. Hydraulic failure, seepage failure, piping through the dam body, structural failure, and earthquake are all possible reasons of failure. An earthquake is a sudden release of energy that causes the earth to vibrate (Tarbuck E. J. and Frederick K. L.Earth:, 1996) . (Ioanna Rapti, 2016) The focus, or the point within the earth where the earthquake rupture begins, and the epicenter, or the point on the earth's surface directly above the focus, are the two most important features. Stability and deformation are two major issues that need to be considered in assessing the seismic performance of earth-fill dams under earthquakes (Siddappa G., 2012). The Augusta dam is the first dam which is failed due to an earthquake. According to the (USCOLD, 2000) reports, less than 30 dams have failed during an earthquake. The majority of these were tailings or hydraulic fill dams, or minor embankments of doubtful design. Few large embankment dams have been severely damaged. The 25-foot high Sheffield Dam in Santa Barbara, CA, was destroyed by a catastrophic slope sliding failure induced by an earthquake (M 6.3) in 1925. This was the first time it was recognized that liquefaction failures could be caused by shaking of embankments made of low relative density materials. Experience has shown that well-compacted, impervious rolled-fill dams are resistant to earthquake forces provided they are constructed on rock or overburdened foundations resistant to liquefaction. When evaluating the seismic performance of earth dams during earthquakes, there are two key aspects to be resolved:

- Stability: Is the dam able to withstand an earthquake both during and after it?
- Deformation: How much deformation will occur in the dam?

Strain-dependent equivalent dynamic shear moduli and damping ratios as first introduced by (Seed H. B. and Idriss I. M., 1970) are essential to EQL analyses. SHAKE91 is sometimes used to obtain EQL responses for representative soil columns within the dam section (Idriss, 1992). Earth structures that are subjected to earthquake shaking have a complicated and diverse response and behavior (Kramer, 1996). In general, there are issues about:

- the movement, motion, and inertial forces that occur during the shaking
- the development of excessive pore-water pressures, and the possibility for soil shear strength to be reduced
- the effect on stability created by the inertial forces, excess pore-water pressures and potential shear strength loss, and
- after the shaking has stopped, the redistribution of excess pore-water pressures and possible strain-softening of the soil

2.4.1. Liquefaction Analysis

In geotechnical earthquake engineering, liquefaction is one of the most essential, interesting, challenging, and controversial topic. It's devastating effects sprang to the attention of geotechnical engineers in three months period in 1964 when the Good Friday earthquake (M_W = 9.2) in Alaska was followed by the Niigata earthquake (M_s = 7.5) in Japan. slope failures, bridge and building foundation failures, and flotation of buried buildings were all good examples of liquefaction-induced devastation in both earthquakes. Hundreds of scholars from all over the world have investigated liquefaction in the 30 years following these earthquakes. Much has been learned, but the road has not been smooth. Different terminology, techniques, and analysis approaches have been presented, and a dominant approach has taken a long time to develop.

Figure 2.2 Following the 1964 Nigata earthquake, liquefaction caused bearing capacity failures in kawagishi- echo apartment buildings (courtesy of USGS)

Similarly, the 6.6 Richter magnitude San Fernando earthquake struck Southern California on February 9, 1971, around 6:00 a.m. local time. The earthquake caused a liquefaction failure at the Lower San Fernando Dam and Reservoir, a water storage facility in the San Fernando community on the northern suburbs of the greater Los Angeles area. Figure 2.3.

The transformation of granular material from a solid to a liquid state as a result of increased pore pressure and lower effective stress is known as liquefaction (Marcuson W. F. III, 1978). The tendency of granular materials to compact when subjected to cyclic shear deformation causes increased pore water pressure. In loose to moderately dense granular soils with poor drainage, such as silty sands and gravel topped by or having layers of impermeable sediment, the change of condition occurred most readily.

Figure 2.3 Following failure of upstream slope in the 1971 San Fernando earthquake, Lower San Fernando Dam (Courtesy of EERC, University of California)

Liquefaction is most typically seen in shallow, loose, saturated deposits of cohesion-less soils subjected to substantial ground vibrations during earthquakes of large size. Because volume compression does not generate excess pore pressure, liquefaction does not occur in unsaturated soils. Generally, liquefaction is associated with loose fine sands. For sand to be in a loose state in the field it likely was deposited in a calm fluvial or sedimentation environment and has not been subject to past loading and unloading. In a sense, it is like the material is normally consolidated.

When cohesion-less soils are saturated, however, rapid loading occurs under un-drained conditions, so the tendency for densification causes excess pore pressures to increase and effective stresses to decrease. There are two types of liquefaction phenomena that emerge from this process (Kramer, 1996):

- Flow liquefaction and
- Cyclic mobility.

Flow liquefaction has the most severe impacts of all the liquefaction-related events, resulting in massive instabilities called flow failures. Flow liquefaction occurs when the shear stress required for static equilibrium of a soil mass (the static shear stress) exceeds the shear strength of the soil in its liquefied state. The massive deformations caused by

flow liquefaction are driven by static shear forces once they've been started. The cyclic stresses may simply bring the soil to an unstable state where its strength is low enough for the static loads to cause flow failure.

Another process that might cause unacceptably significant permanent deformations during earthquake shaking is cyclic mobility. Unlike flow liquefaction, cyclic mobility occurs when the static shear force is smaller than the liquefied soil's shear strength. The deformations due by cyclic mobility failure grow progressively during earthquake shaking. Cyclic mobility deformations, unlike flow liquefaction, are induced by both cyclic and static shear forces.

The soil strata soften when liquefaction develops, enabling massive cyclic deformations to occur. Softening is followed by a decrease of shear strength under moderate to high shear pressures, such as beneath a foundation or sloping ground, which can result in severe shear deformations or even flow failure in loose materials. Liquefaction causes transient softening and higher cyclic shear strains in moderately dense to dense materials, although a tendency to dilate during shear prevents considerable strength loss and large ground deformations. Cyclic mobility or cyclic liquefaction can occur after the liquefaction of moderately dense granular materials. Liquefaction can induce ground oscillation or lateral spread as a result of either flow deformation or cyclic mobility beneath gently sloping to level ground. When loose soils compact during liquefaction and reconsolidation, ground settlement occurs. As excess pore water pressures dissipate, sand boils may erupt (Youd and Idriss, 1997).

2.4.2. Seismic Slope Stability Analysis

Procedures for static slope stability analysis have been used for many years and calibrated against many actual slope failures. The database against which seismic slope stability analyses can be calibrated is much smaller (Kramer, 1996). The requirement to evaluate the consequences of the following two instances complicates the analysis of slope seismic stability.

- Dynamic stresses induced by earthquake shaking, and

- The effects of those stresses on the strength and stress-strain behavior of the slope materials.

Seismic slope instabilities may be grouped into two categories based on which of these effects is predominant in a given slope.

- **Inertial Instabilities,** the shear strength of the soil remains relatively constant, but slope deformations are produced by temporary exceedances of the strength by dynamic earthquake stresses.
- **Weakening Instabilities** are those in which the earthquake serves to weaken the soil sufficiently that it cannot remain stable under earthquake-induced stresses. The most common causes of weakening instability are flow liquefaction and cyclic mobility.

Several analytical techniques, based on both limit equilibrium and stress-deformation analyses, are available for both categories of seismic instability.

2.4.2.1.Analysis of Inertial Instability

Slopes can be subjected to high horizontal and vertical dynamic stresses as a result of earthquake movements. These forces cause dynamic normal and shear stresses along the slope's possible failure surfaces. When dynamic shear loads are placed on previously existing static shear stresses, the available shear strength of the soil may be exceeded, resulting in slope inertial instability. There have been several methodologies offered for analyzing inertial instability. The precision with which the seismic motion and the dynamic reaction of the slope are reproduced differs across these methodologies.

a. Pseudo Static Analysis

In the same manner as static limit equilibrium analyses create factors of safety against static slope failure, pseudo-static analyses produce factors of safety against seismic slope failure. The horizontal force is written as the product of a seismic coefficient K and the weight W of the prospective sliding mass, and the analysis is regarded as a static problem. It is sometimes assumed that the embankment dam behaves like a rigid body,

with accelerations that are homogeneous across the length and equal to ground accelerations at all times.

Although this approach of analysis is basic and clear, it has the drawback of reflecting the complex, transient, dynamic impacts of earthquake shaking with a single constant unidirectional pseudo-static acceleration, which is obviously primitive. According to (Terzaghi K., 1950), "the concept it conveys of earthquake impacts on slopes is quite wrong, to say the least," and a slope might be unstable even if the computed pseudo-static factor of safety was larger than 1, as seen in Table 2.1. Besides, the main limitations of this approach are (Seed, 1979):

- field testing have shown that all earth dams do not behave like rigid bodies
- the maximum acceleration will be developed in an embankment dam for only a short period of time, so that the deformation resulting from it may be small

Table 2. 1 Results of Pseudo static analysis of earth dams that failed during earthquakes (Seed, 1979)

Dam	K_h	FS	**Effect of earthquake**
Sheffield Dam	0.10	1.2	Complete failure
Lower San Fernando Dam	0.15	1.3	Upstream slope failure
Upper San Fernando Dam	0.15	2-2.5	Downstream shell including crest slipped about 6ft downstream
Tailing Dam (Japan)	0.2	1.3	Fail of dam with release of tailing

In their most common form, Pseudo static analyses represent the effects of earthquake shaking by Pseudo static accelerations that produce inertial forces,F_h and F_v ; which act through the centroid of the failure mass as shown in Figure 2.4. The magnitudes of the Pseudo static forces are,

$$\mathrm{F_h} = K_h W \quad \text{.....(2.2)}$$

$$F_v = K_v W \text{.....(2.3)}$$

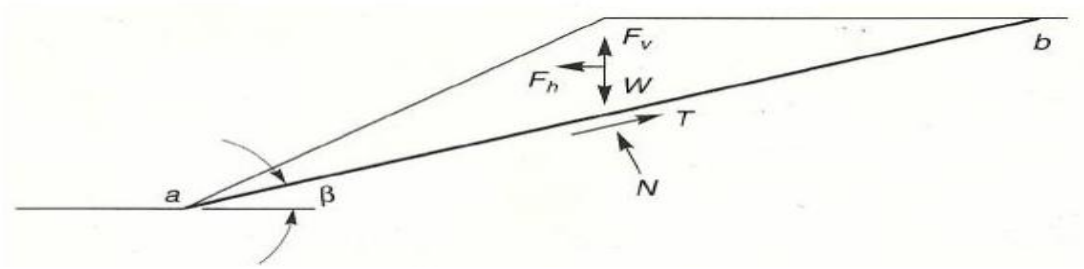

Figure 2.4 Forces acting on triangular wedge of soil above planar failure surface in Pseudo static slope stability analysis (Kramer, 1996)

$$FS = \frac{resisting\ force}{driving\ force} = \frac{cl_{ab} + [(W - F_v)cos\beta - F_h sin\beta]tan\phi}{(W - F_v)sin\beta + F_h cos\beta} \text{..... (2.4)}$$

All of the other methods are aimed at determining permanent slope displacements caused by earthquake shaking.

b. Newmark Sliding Block Analysis

By assuming that movements occur when forces on a rigid block of soils above a fixed potential failure surface exceed its sliding resistance, (Newmark, 1965) was able to calculate the displacements caused by an earthquake in embankments. He assumed that the slope deformed only when the out-of-slope earthquake pressures caused the pseudo-static factor of safety to fall below 1.0 during the earthquake.

He proposes a method for rigid-plastic materials that involves determining the yield acceleration, k_{yg} at which sliding will commence and computing the displacements that result when this acceleration is exceeded. Figure 2.5 shows how to carry out the method. If the acceleration pattern acting on a potential sliding mass is similar to the one depicted in the figure, no displacement will occur until time t_1, when the induced acceleration reaches the yield acceleration for the first cycle k_{y1}. If the yield acceleration is considered to be constant throughout the first cycle, it can be marked off as shown in Figure 2.5, and the variation in sliding mass velocity can be calculated by integrating over the shaded area. The velocity will continue to increase until time t_2, when the acceleration falls below the yield value again, and then the velocity will be lowered to

zero at time t_3, allowing the direction of the sliding mass to be determined using the velocity versus time relationship. The end outcome is represented in Figure 2.6.

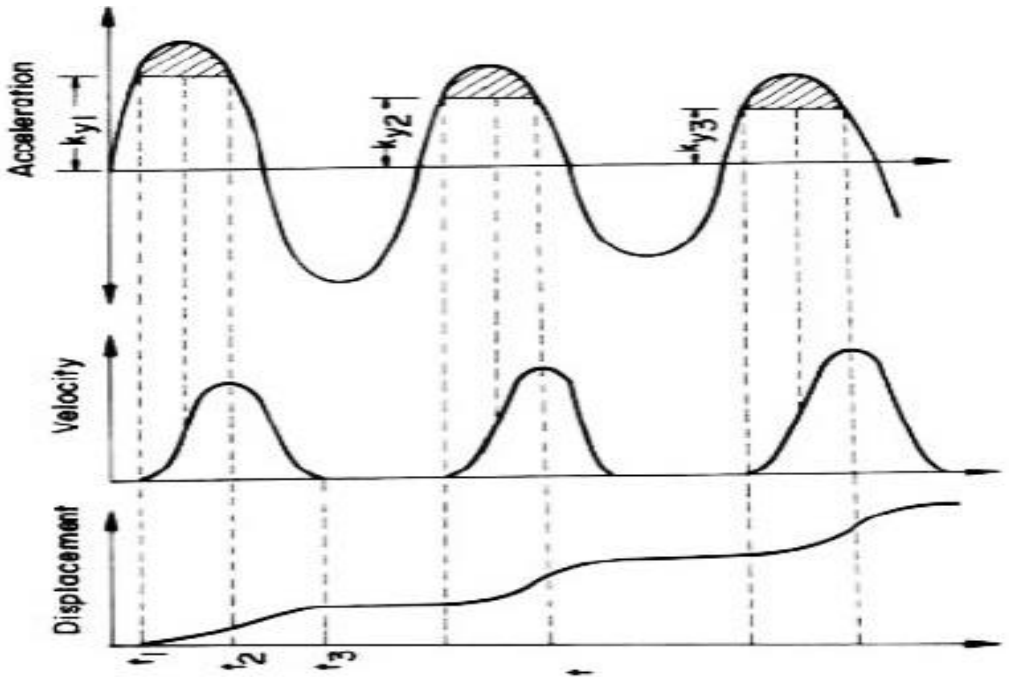

Figure 2.5 Integration of accelerograms to determine downslope displacements

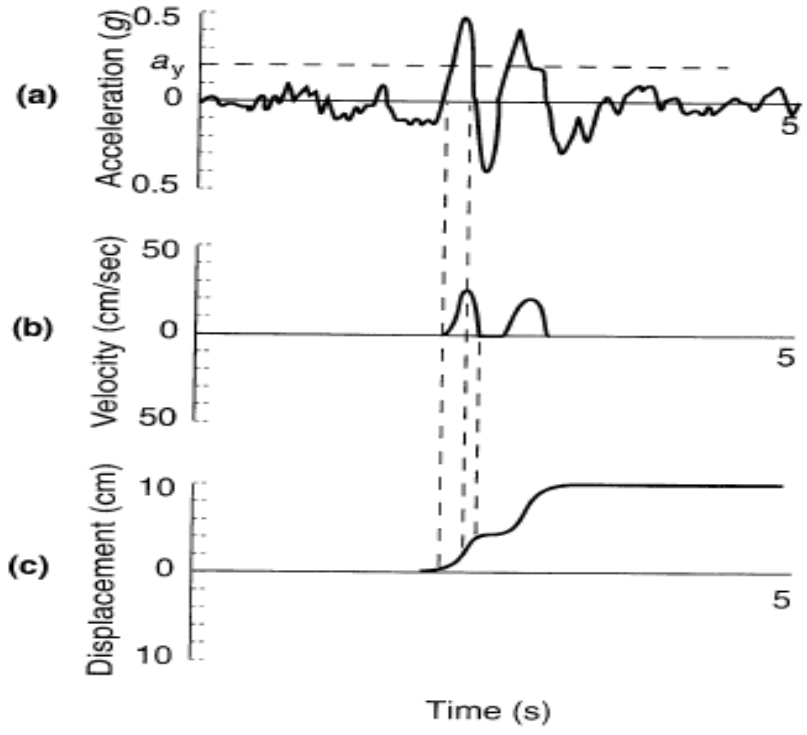

Figure 2.6 Yield acceleration effect on slope displacements

Newmark sliding block model will predict zero permanent slope displacement if earthquake-induced accelerations never exceed the yield acceleration (a_y/a_{max} = 1.0) as illustrated in Figure 2.7a. Since the permanent displacement is obtained by double integration of the excess acceleration, the computed displacements for a slope with relatively low yield acceleration (small a_y/a_{max}) will be greater than that of a slope with higher yield acceleration Figure 2.7: b, c. He found that a reasonable upper bound to the permanent displacements produced by earthquake motions was given by the following equation Eq.2.5.

$$d_{max} = \frac{{V_{max}}^2}{2a_y}\frac{a_{max}}{a_y} \dots\dots\dots\dots\dots\dots\dots\dots\dots\dots\dots\dots\dots\dots\dots\dots\dots\dots (2.5)$$

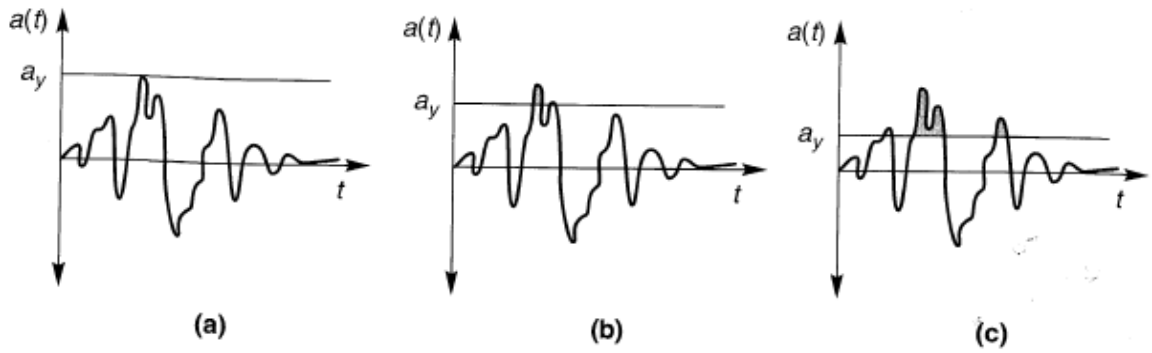

Figure 2.7 The relationship between the yield acceleration and the maximum acceleration to determines permanent slope displacements

(a) There will be no displacement if the yield acceleration of a slope is larger than the maximum acceleration of a certain ground motion. As yield accelerations decrease, as in (b) and (c), slope displacements increase quickly.

2.4.2.2.Analysis of Weakening Instability

Through a process of pore pressure generation and/or structural disturbance, earthquake-induced stresses and strains can reduce the shear strength of the soil. Weakening instabilities can occur when the reduced strength drops below the static and dynamic shear stresses induced in the slope. Weakening instabilities are usually associated with liquefaction phenomena and can be divided into two main categories, flow failures, and deformation failures).

Flow failures occur when the available shear strength becomes smaller than the static shear stress required maintain equilibrium of a slope. Flow failures, therefore, are driven by static stresses. They can produce very large deformations that occur quickly and without warning.

Deformation failures occur when the shear strength of a soil is reduced to the point where it is temporarily exceeded by earthquake-induced shear stresses. Much like inertial failures, deformation failures occur as a series of "pulses" of permanent displacement that cease at the end of earthquake shaking. Different procedures are available for the analysis of flow failures and deformation failures.

a. Flow Failure Analysis

Flow failures create substantial deformations and severe damage because they generally include a major drop in soil strength. In general, the first stage in their analysis is to identify whether or not one will happen. Procedures for estimating flow failure deformations have also been developed in order to determine the amount of damage caused by flow failures.

Conventional static slope stability evaluations employing soil strengths based on end-of-earthquake conditions are most typically used to assess potential flow slide instability (Marcuson W. F. III, 1978). Deformations Analysis if stability assessments suggest that flow failure is possible, a study of flow failure deformations can be used to estimate the extent of the zone influenced by the failure. Rough estimates of flow sliding deformations can be generated using approaches based on limit equilibrium, fluid mechanics, and stress-deformation studies by ignoring the minor deformations that precede the triggering of flow sliding.

b. Deformation Failure Analysis

Although deformation failures generally involve smaller deformations than flow failures, they are capable of causing considerable damage. The most prevalent kind of deformation failure is lateral spreading. In recent years a number of investigators have developed methods to estimate permanent displacements produced by deformation

failures. Because the mechanisms that produce deformation failures are so complicated, procedures for the prediction of the resulting displacements are largely empirical in nature.

Hamada et al (Hamada *et al.*, 1987) considered the effects of geotechnical and topographic conditions on permanent ground displacements observed in uniform sands of medium grain size in the 1964 Niigata (M = 7.5), 1971 San Fernando (M = 7.1), and 1983 Nihonkai-Chubu (M = 7.7) earthquakes. Permanent displacements were found to be most strongly influenced- by the thickness of the liquefied layer and the slopes of the ground surface and lower boundary of the liquefied zone.

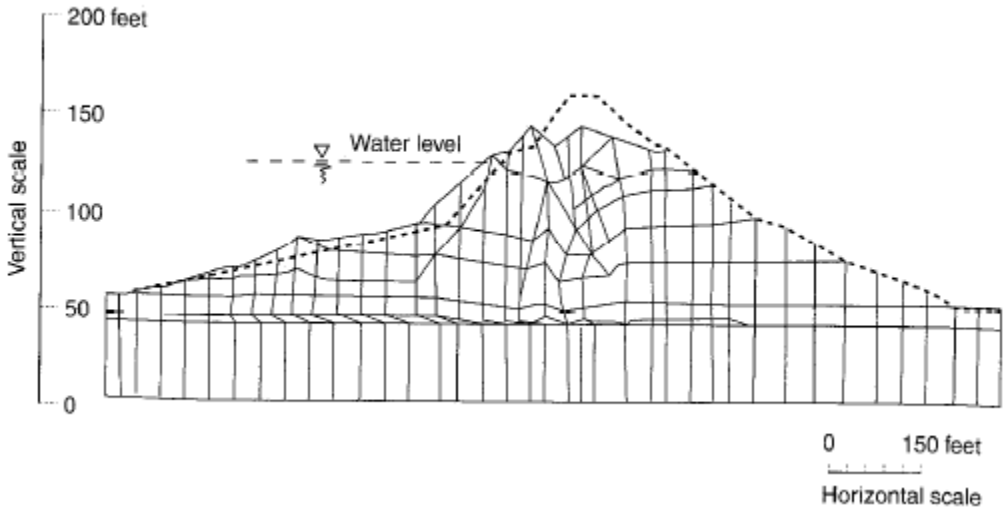

Figure 2.8 Initial (dashed) and post liquefaction (solid) configurations of Sardis Dam in Mississippi.

Note the large strains due to liquefaction in core and thin seam below the upstream shell in Figure 2.8. (Byrne P.M., Cheung H., 1978) used work-energy principles with an elastic perfectly plastic model of liquefied soil to develop expressions for estimation of permanent slope displacements. He extended this approach (Byrne P. M., 1992) to determine factors by which the initial stiffness of soil should be reduced for finite-element analysis of deformation failures. Deformations predicted by this approach were in good agreement with those observed in the 1971 failure of the Upper San Fernando Dam as shown in Figure 2.9.

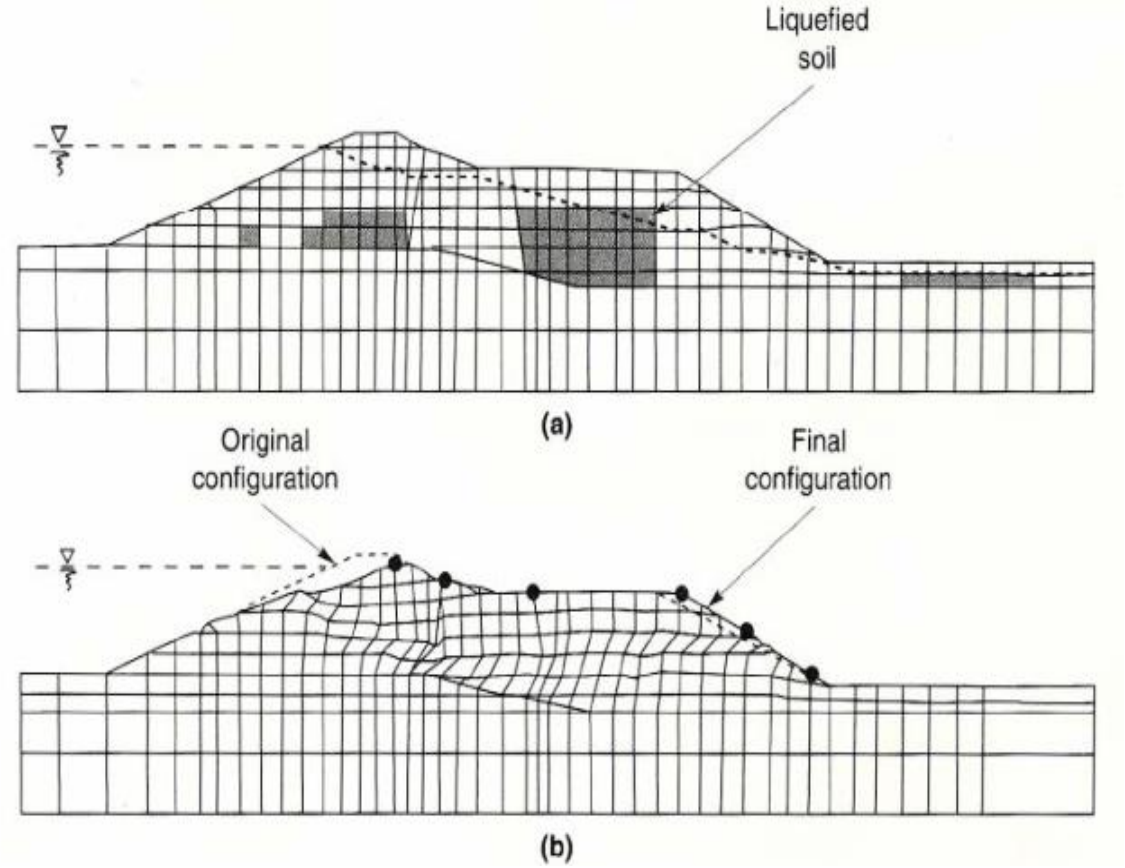

Figure 2.9 (a) Finite-element mesh for analysis of Upper San Fernando Dam with elements determined to have liquefied shaded; (b) positions of original and final meshes (displacements exaggerated by factor of 2) by procedure of (Byrne P. M., 1992)

2.5. Seismic Activity in Ethiopia

Ethiopia's construction code was updated in 2015 to divide the country into seismic zones based on the local hazard. In rock or hard ground soil, the hazard is characterized in terms of effective peak ground acceleration. If a given kind or category of structure is to be built in zones with peak ground acceleration less than 0.025g, the code suggests simplified and reduced seismic design methods. The seismic zone and their corresponding peak group acceleration for a return duration of 475 years are shown in the Table 3.1.

The 1995 Ethiopian building code had a number of drawbacks in seismic hazard analysis. Based on a recommendation of engineering community, this code was updated in 2015 (Worku, 2011). The new version is almost a direct duplicate of the European standard with the exception of the country’s peculiarities with respect to ground motion

specification in terms of seismic hazard map. The two seismic zone maps shown in Figure 2.10 and Table 2.2 do not agree and are therefore not an appropriate zoning categorization technique. Even though the table specifies the bedrock acceleration ratio for each zone, extracting any zoning information from these two extremely different maps is impossible. A range of bedrock acceleration ratios, ranging from 0.025 to 0.175 with a 0.015 increment and an undefined upper limit, is provided unnecessarily. This breaks up the contour map into thin lines and dots, making it more difficult to locate the proposed construction site and to get the corresponding bedrock acceleration ratio value. Furthermore, this code incorrectly doubles the previous version's bedrock acceleration ratio merely to take a 475-year return period rather than a 100-year return period.

Table 2. 2 Bedrock acceleration ratio for respective zones (ES EN, 2015)

Zone	5	4	3	2	1	0
$\alpha_0 = a_g/g$	0.2	0.15	0.1	0.07	0.04	0

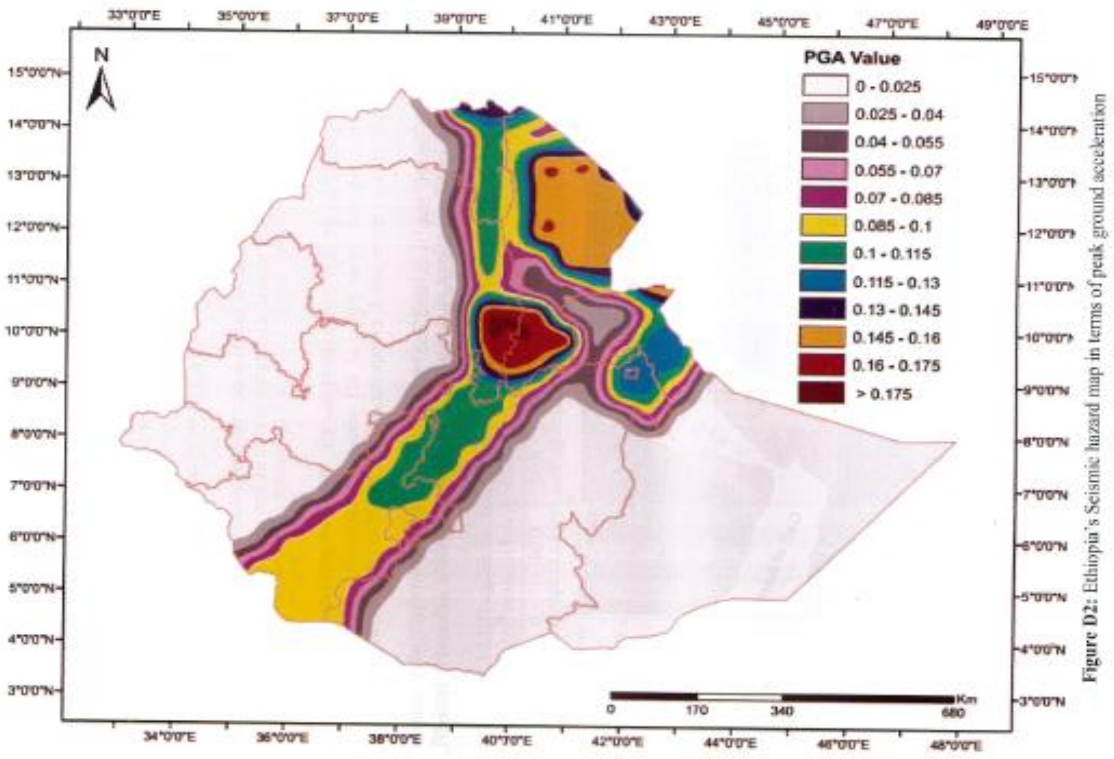

Figure D2: Ethiopia's Seismic hazard map in terms of peak ground acceleration

(a)

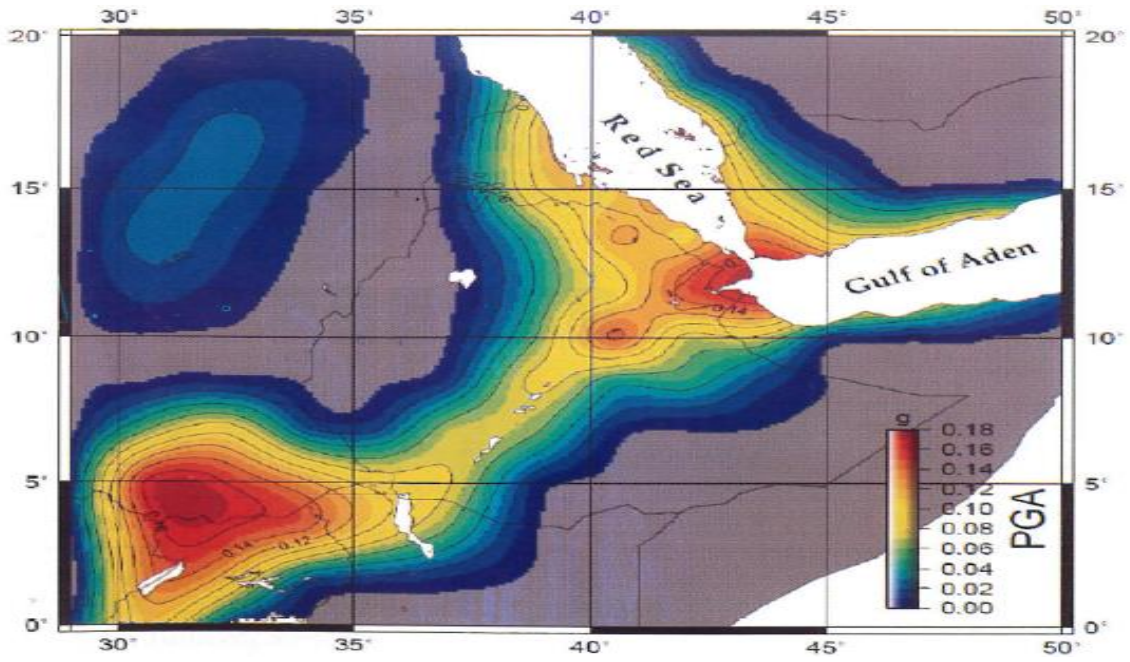

(b)

Figure 2.10 Seismic zone map of (a) along the horn of Africa and (b) Ethiopia (ES EN, 2015)

Some of Ethiopia's embankment dams are mentioned below, and they are all located in seismic areas of the country.

- Gidabo Earth Fill dam 6 ^{o} 43’80’’N and 38 ^{o} 16’80’’ E
- Midmar Earth Fill dam 14 ^{o} 20’40’’N and 38 ^{o} 91’10’’E
- Tendaho Earth Fill dam11 ^{o} 69’00’’N and 40 ^{o} 95’50’’E
- Gefersa Earth Fill dam 9 ^{o} 06’40’’N and 38 ^{o} 64’20’’E

2.6. Time-History Data

For dynamic analysis, a time history data of the amplitude of the earthquake is an essential input. Time history data of earthquake amplitude is the value of the velocity, acceleration, or displacement in a constant time interval between records for some period of the earthquake shaking. Time history data describes the set of the three earthquake motion characters in one graph: amplitude, frequency, and duration.

The cyclic shear stress in the dynamic analysis is calculated as an inertial force in every time step. To calculate this inertial force oscillating in a fraction of seconds during earthquake shaking, the time history data of acceleration usually in every 0.02 seconds

must be provided for the computation. But in most places including Ethiopia, it is hard to find recorded time history data of earthquake. If it was available even in far places from where the dam in the dynamic analysis is available, a de-convolution technique (i.e. changing the recorded surface ground motion to the source bedrock motion) can be done and applied to the bedrock under the dam in analysis. But the recently recorded time history data amplitude in Addis Ababa is so small that it undermines the probable earthquake to happen. To overcome this problem: the selection criterion to choose between elsewhere recorded data must incorporate the below factors (US.Corps of Engineers, 2003).

- Earthquake magnitude and type of faulting
- Tectonic environment
- Earthquake source to site distance
- Subsurface condition
- Response spectrum characteristics of time history data
- Duration of strong motion

Since ES EN (2015) "Design of Structure for Earthquake Resistance -Part 1: general rule-seismic action and rule for building," only applies to buildings, the International Commission on Large Dams (ICOLD) has recommended that dams be designed for earthquake resistance using two different earthquakes, the Maximum Credible Earthquake (MCE) and the Design Base Earthquake (DBE) (Seged and Haile, 2010, as cited in ICOLD, 1983). Under the presently known or presumed tectonic framework, the MCE is the largest reasonably conceivable earthquake that appears possible along a recognized fault or within a geographically defined tectonic province. The DBE is an earthquake that is expected to occur at least once during the dam's expected lifetime. The dam's structure should not be considerably affected and should remain operational under the DBE condition, according to ICOLD, even if some deformation is permissible. According to ICOLD, the MCE should not cause embankment dams (Seged and Haile, 2010, as cited in Fell R., 1992):

a. to lose its free board
b. to fail due to liquefaction of material in the dam or its foundations
c. to collapse due to movement at a slip surface in the slope or through the foundation

2.7. Previous Works on Dam Design

Dams are designed and constructed to withstand various natural forces and events that have occurred in the past or maybe expected to occur in the future. Forecasting the effects of an earthquake that would cause the dam to fail is one of the most important parts of the process of designing these structures. Earth dams made of or underlain by loose saturated granular soils face a significant risk of liquefaction-induced ground displacements as a result of earthquake shaking. During numerous earthquakes around the world, many liquefaction-induced earth dam failures or near-failures have been observed. When the underlying saturated granular soils liquefied, cracking, settling, lateral spreading, and slumping of the embankment occurred (Korhan Adalier and Michael K. Sharp, 2004).

(Seged and Haile, 2010) reported that the assessment results of liquefaction susceptibility based on grain size distribution, most of the Tendaho shell materials could be considered as non-liquefiable soils but with some potential for pore water pressure, build-up during earthquake shaking. In contrast, the alluvium foundation soils largely lie within the boundaries for potentially liquefiable soils and have, therefore, been considered to be potentially liquefiable. In the event of both site-specific Maximum Credible and Design Base Earthquakes, the alluvium foundation under the dam seat, with a depth ranging from 6 to 10 m, would liquefy, according to the dynamic analysis results. Liquefaction of the alluvium foundation would lead to excessive settlement and eventual failure of the dam. Therefore, based on the presented dynamic analysis results, complete removal of the alluvium foundation under the dam seat has been recommended and implemented during the execution of the dam.

As stated by (Stefania et.al., 2017), on one hand, the characteristics of the earthquake and the importance of the seismic hazard are crucial aspects of the dynamic response of the system. Peak ground acceleration (PGA), peak ground velocity (PGV), mean period (T_m), and predominant period (T_p), intensity measures have been demonstrated to play a significant impact in liquefaction triggering. On the other hand, the thickness of the saturated zone influences the generation of the excess pore pressure, the liquefaction apparition, and the area of failure. But also, a thin saturated layer with a thickness of 1 m can liquefy during strong base shaking.

According to a dynamic analysis of the Middle Awash Multi-Purpose Dam by (Mulat, 2015), is recommended the slope reduction of upstream from 1:1.9 to 1:1.75, while the vertical deformation is 0.48m, in creating a permanent deformation ground acceleration, shaking duration, and uniformity of peak acceleration in cycles are influential factors.

Those aforementioned researches have been conducted simply by considering the maximum credible earthquake and design base earthquake from a seismic standard of the country building code for a return period of 100 years as summarized in Table 2.2.

Table 2. 3 Summaries of horizontal and vertical MCE and DBE used for respective project

No	Project	Author	Earthquake	Horizontal	Vertical
1	Bilate Embankment Dam	Habtamu Getachew	Maximum Credible Earthquake (MCE)	0.24g	0.12g
			Design Base Earthquake (DBE)	0.12g	0.06g
2	Tendaho Earth fill dam	Hadush Seged and Messele Haile	Maximum Credible Earthquake (MCE)	0.3g	0.15g
			Design Base Earthquake (DBE)	0.18g	0.09g
3	Middle Awash Multi-Purpose Dam	Yared Mulat	Maximum Credible Earthquake (MCE)	0.4107g	0.205g
			Design Base Earthquake (DBE)	0.212g	0.106g

But a return period of 475 years of earthquakes is currently a worldwide norm for the design of the structure. This translates into an annual rate of the occurrence rate of 0.002. Recent research suggests that the use of a design PGA is of greater value.

Educators and engineers utilize numerical simulation to solve a variety of civil engineering and engineering mechanics challenges all over the world. One of the most significant benefits of using this application is that it can solve the majority of geotechnical engineering problems. Geotechnical engineering problems involving two and three-dimensional configurations, such as dynamic analysis, can be solved with the application.

The Finite Element Method is a computational method used by many computer applications. Finite element analysis is a numerical approach, according to experts. All of the issues' complexities, such as varying shape, boundary conditions, and loads, are preserved in this method, but the solutions found are approximate.

So that studying of dynamic analysis of embankment dam in liquefiable soil is required to see the effect of dam geometry, foundation material property, embankment dam material property, and thickness of non-cohesive soil foundation material on the stability of the dam under different anticipated earthquake loading conditions.

3. Materials Modeling, Earthquake Loading and Analysis Methods

3.1. Data Collection

One of the major challenges in dynamic analysis is the availability of data. Material property and earthquake data are the major input data. These data are collected from various literature. Material properties required for the dynamic response analysis using numerical approaches are total unit weights, Poisson's ratio, and dynamic shear modulus at low strain ($G_{\max}$), the relationships of the modulus reduction factors, $G/G_{\max}$, and damping ratio with shear strain. However, the dynamic characteristics of the dam materials have not been investigated through dynamic tests. Therefore, the material properties required for the dynamic analysis have been estimated with the help of the geotechnical literature as will be explained in the next sections.

3.1.1. Earthquake Data

Ground motion intensity associated to an earthquake can be assessed in terms of peak ground acceleration. This is obtained from acceleration time history; modifications and base line correction are necessary, which is important for evaluating dynamic stability of embankment dams.

a) Peak Ground Acceleration (PGA)

The design of earthquake resisting structures is based on seismic design provisions of national building codes. According to Ethiopia's seismic zoning map, the majority of the dams are located in a zone of major seismic activity, where seismic ground shaking could cause damage. Table 3.1 under section 2.6 summarizes the relationship between seismic zones and horizontal ground accelerations.

With its plenty of issues as discussed in section 2.5, the Ethiopian building code (ES EN, 2015) specifies a bedrock acceleration ratio of 0.2 for zone 5, a value that is expected to increase as soil sites possess the ability to amplify rock-surface accelerations (Worku, 2011). Based on the study conducted as indicated in Table 3.1, the peak acceleration is then specified ranging from 0.12g to 0.37g. For these simulations, the author uses the PGA values, as shown in table 3.2, where the PGA data corresponds to the MCE.

Table 3.1 Considered peak ground acceleration for the dynamic analysis

PGA					
0.12	0.17	0.22	0.27	0.32	0.37

Zone factors summarized in the above Table 3.2 are for MCE. The vertical PGA is half of the horizontal component, according to international design standards (Kramer, 1996). And, according to Seged and Haile (2010), the alluvium foundation liquefies (where liquefaction means zero effective stress) earlier in the case of MCE than in the case of DBE after the earthquake shaking begins, but for these simulations only the horizontal PGA of MCE has been used to see the maximum effect of earthquake induced dynamic load on the dam.

b) Acceleration Time History (ATH)

The dam's dynamic analysis was carried out using Geo-Slope International Ltd's QUAKE/W, a state-of-the-art computer program based on the Finite Element Method (QUAKE/W, 2018). Although both horizontal and vertical acceleration time histories are important inputs for QUAKE/W analysis, horizontal acceleration time histories are used in this study.

Therefore, site-specific horizontal ATH for embankment dams should be produced using the peak accelerations and records of actual earthquakes. In the case of if there are no ATH records near the dam site, actual accelerographs recorded elsewhere have been used. The selection of the time history data is mainly based on the earthquake magnitude and hypo-central distance. Based on this fact three recorded data elsewhere are selected and used in the dynamic analysis of the dam. The Kara Kore earthquake recordings, which have a Richter magnitude of 3.5-6.5, are considered to be the most similar to the 1940 Elcentro record, which has a magnitude of 6.7. However, in order to represent other possible earthquakes with different magnitude, time duration, and frequency content, the 1995 Kobe JMA record and the Hachinohe record have been considered.

The following ATH data were used for the purposes of the analysis.

I. THE 1940 Elcentro Record, USA (M=6.7, H=11 km, R=11.5 km).

II. The 1995 Kobe JMA record, Japan (M=7.2, H=14.3 km, R=19 km).

III. The 1968 Hachinohe record, Japan (M=7.9, H=0 km, R=200 km).

c) Data Modification

Once the data have been imported into QUAKE/W, the data can be modified to suit the needs of a particular site or analysis (QUAKE/W, 2018). It is possible to specify the desired peak acceleration and duration. After that, the record is scaled to the provided values. The imported data of the 1940 Elcentro record has a peak acceleration of 0.318g.

The peak acceleration is then specified ranging from 0.12g to 0.37g with an increment of 0.05 for the modeled embankment dam site; the entire record is scaled so that the peak is 0.12g, 0.17g, 0.22g, 0.27g, 0.32g, and 0.37g. The form of the record remains the same, only the amplitudes are adjusted. Similarly, the duration between the first and last exceedance of a certain threshold value of acceleration, usually 0.05g, has been modified based on Bolt (1969). Extraneous data is frequently seen at the beginning and end of earthquake records. From a numerical performance standpoint, these data are removed in QUAKE/W. As shown in Figure 3.2, the extraneous data are in between 0 to 0.02 seconds and above 40 seconds, because these intervals do not contain peak values.

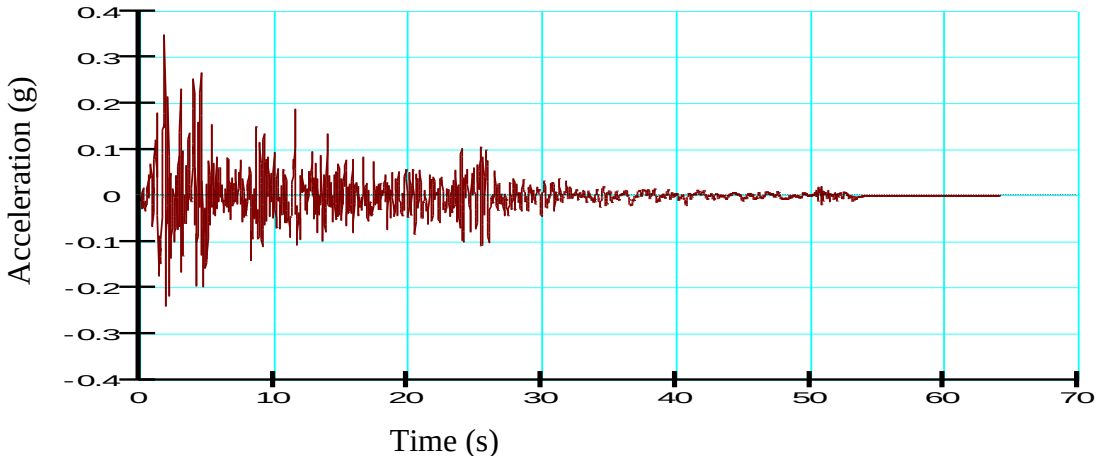

Figure 3.1 Horizontal maximum credible earthquake - 1940 Elcentro record

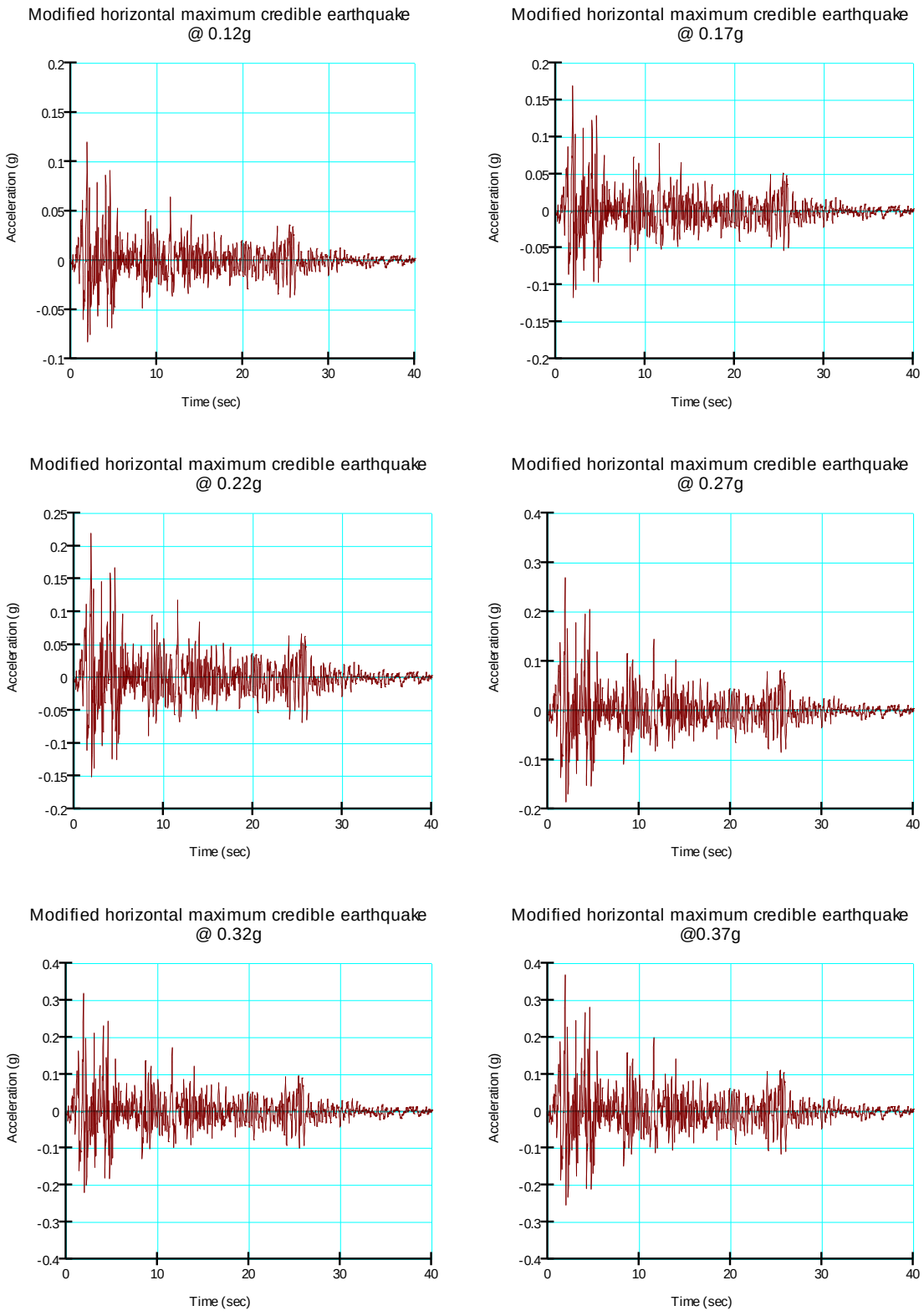

Figure 3.2 Modified horizontal maximum credible earthquake - 1940 Elcentro record

d) Baseline Correction

Data in earthquake records are commonly distorted. This has little effect on a structure's dynamic response analysis, but it does result in an erroneous picture of displacement calculated from the acceleration record's double integration. QUAKE/W can do a baseline correction to eliminate this drift (QUAKE/W, 2018). The QUAKE/W baseline correction is calculated using simple linear regression. The goal is to keep the area under the curve the same above and below the axes of zero acceleration (that is, the slope of the modified linear regression line is zero). This does not mean that a double integration displacement curve near the end of the recording will always return to zero. Even so, the curve may show some cumulative shift. The basic linear regression correction, on the other hand, helps to reduce the offset of zero displacements at the end of the record. Unwanted displacement offsets can be further decreased by removing as much redundant data as feasible from the beginnings.

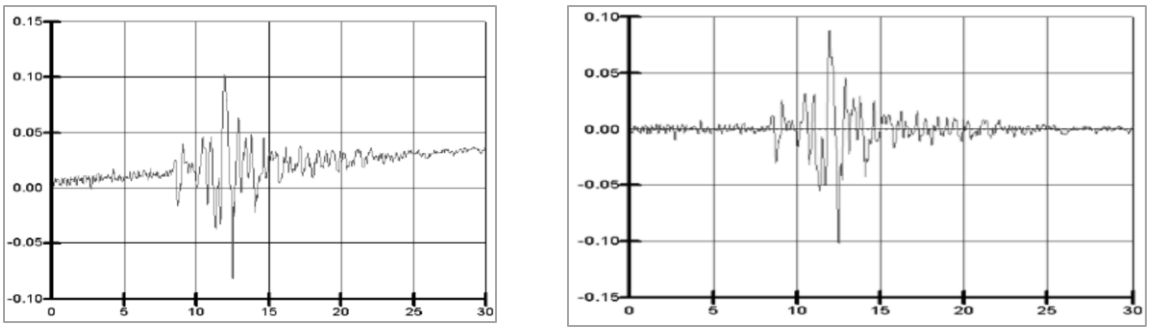

(a) (b)

Figure 3.3 (a) an earthquake record with some drift in the data (b) an earthquake record with a baseline correction(QUAKE/W, 2018)

3.2. Geometry and Material Properties

3.2.1. Geometry of the Dams

The proposed dam is zoned earth fill dam with a clayey central core that is impervious to water. A central core has the benefit of delivering more pressure at the point where the core meets the foundation, minimizing the risk of leakage and piping. A 1.94m core top width has been given. As a result, the core's base will be around 27 meters wide with side Slope of 1V:2.5H. The dam geometry used for this model with reference to the existing dam geometry as shown in Table 3.3. Figure 3.4 depicts a representative zonal earth fill

dam section and materials used in the case of 10 meter liquefiable foundation thickness and 1V:3H slope ratio of the upstream and downstream embankment, while Appendix B has the rest of the model.

Table 3.2 Initial dam geometry of the model with reference to existing dam

Dam	Gefersa-I/II	Middle Awash	Gidabo	Bilate	For Simulation
Crest width(m)	5	12	3		4
U/s slope	1:2.58	1:1.9	1:3	1:2.2	1:1.5 to 1:3.2
D/s slope	1:2.27	1:1.65	1:3	1:1.7	1:1.5 to1:3.2
Core slope			1:2.5		1:2.5
Height (m)	18.94	40 to 50	19.25 to 30.6	42.5	20
U/s berms width(m)	-	4	-	-	-
D/s berms width(m)	-	-	-	5	-
Foundation thickness(m)	-	15		2 to 15	5 to 15
Free board(m)				5.5	5

3.2.2. Material Properties of the Dams

Engineering properties of soils are vital components of any geotechnical analysis. Thus, these geotechnical soil parameters used in the analysis of the present study are extracted from the geological and geotechnical investigation report and final design report of Gidabo earth fill dam (WWDSE, 2008, 2009) and summarized in the upcoming sections.

a. Strength Parameters

Table 3.3 Analysis shear strength parameters and unit weight (adapted from (WWDSE, 2009)

No.	Description	γ(kN/m3)	ϕ' (^{0})	c' (KPa)
1	Impervious clay core	16	20	10
2	Gravel shell	19	32	0
3	Transition/Filter layer	18	34	0
4	Foundation	17	28	0
5	Compacted alluvium/liquefiable foundation	17	26	0
6	Rock toe	22	40	0

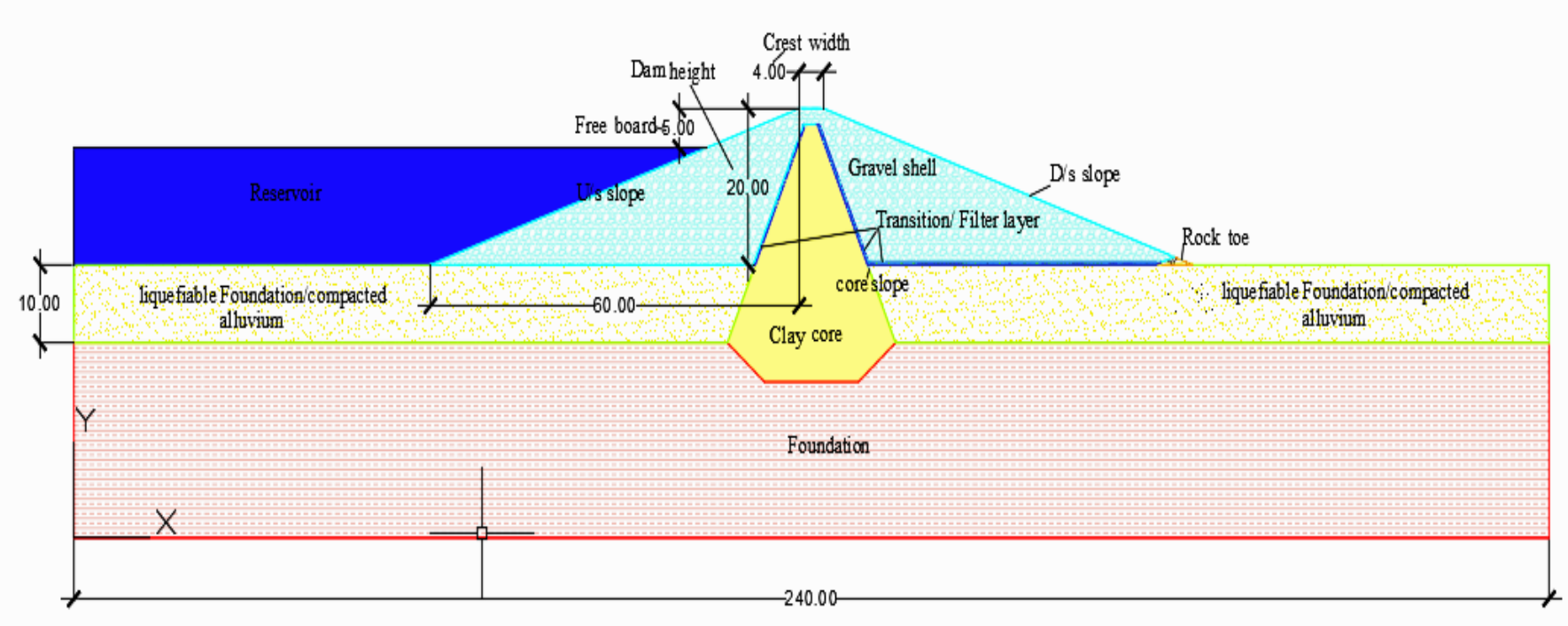

Figure 3.4 Representative zoned earth fill dam section and materials used in the case of 10 meter liquefiable foundation thickness and 1V:3H slope ratio of upstream and downstream embankment.

3.2.3. Soil Model and Dynamic Material Properties

A. Equivalent Linear Soil Model

The Equivalent Linear model and the linear-elastic model are remarkably similar. The distinction is that in the case of equivalent linear model, the soil stiffness G is changed at each time step. This soil model starts a dynamic analysis with the specified soil stiffness using the Equivalent Linear model. Their adoption of nonlinear analyses, however, appears to be restrained by uncertainty in how to develop the input parameters required for available nonlinear models, and by the lack of well-documented validation studies for those models. QUAKE/W explores the complete earthquake record, identifying the peak shear stresses at each Gauss numerical integration point in each element. After that, the shear modulus is changed using a G reduction function, and the procedure is repeated until all of the needed G adjustments are within a certain tolerance. While stepping through the earthquake record, the crucial behavior to understand is that G is a constant. G may be modified for each pass through the record, but remains constant during one pass. This is visually depicted in Figure 3.4. During one iterative trip through the earthquake, the straight lines show that G is constant.

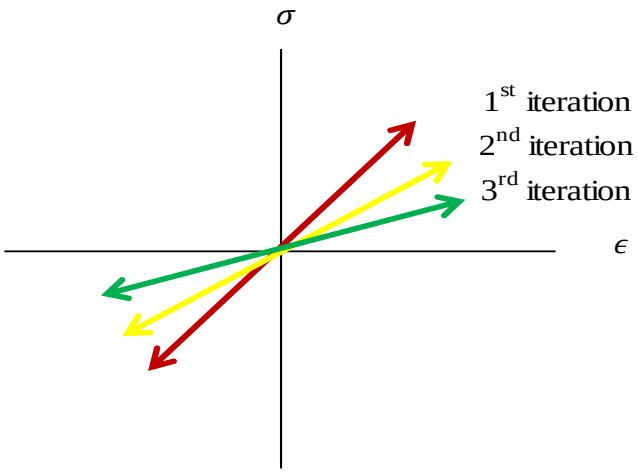

Figure 3.5 Change in G with each iteration through the earthquake

An equivalent linear soil model has become widely used because it is computationally efficient and yields reasonable results in many circumstances, particularly when small strains (1-2 percent) and modest accelerations (0.3-0.4 g) are present (Kramer and Paulsen, 2004).

Material properties used in this model are summarized as follows:

- Unit weight, Poisson's ratio, c' and ϕ'
- Damping ratio constant or function
- K_a and K_s functions
- Pore-water pressure function
- Cyclic number function
- G reduction function
- G_{max} constant or function

B. Dynamic Material Properties

The dynamic characteristics of the dam materials have not been investigated employing dynamic tests. Therefore, the material properties required for the dynamic analyses were estimated with the help of the geotechnical literature as explained as follows.

i. Stiffness as a Function of Depth

The soil stiffness is generally a function of the stress state. As the confining stress increases, the soil stiffness increases. QUAKE/W uses the following relationship to describe the soil stiffness as a function of depth (QUAKE/W Tutorial, 2018).

$$G = k_G(\sigma'_m)^n \quad \ldots\ldots\ldots\ldots\ldots\ldots\ldots\ldots \quad (3.1)$$

Where G is the shear modulus, K_G is a soil modulus, σ'_m is the mean effective stress, and n is a power exponent (generally n is taken as 0.5). To determine G_{max} and the corresponding soil modulus K_G, the following widely used empirical equation, which was developed by (Seed H. B. and Idriss I. M., 1970) has been utilized.

$$G_{max} = 220\ .\ K_{2max}(\sigma'_m)^{0.5} \quad \ldots\ldots\ldots\ldots\ldots\ldots \quad (3.2)$$

From Equations, (Eq.3.1 and Eq.3.2) $(in\ KPa)$, we get,

$$k_G = 220\ .\ K_{2max} \quad \ldots\ldots\ldots\ldots\ldots\ldots\ldots\ldots \quad (.3.3)$$

According to (Seed *et al.*, 1986) the magnitude of K_{2max} for gravels ranges 80 to 180. The K_{2max} values of the dam materials are determined based on the curves published by (Seed H. B. and Idriss I. M., 1970). The shell materials of the dam used for the modeling

are composed of rock fill, thus a K_{2max} value of 90 is used. Table 3.5 summarizes the K_{2max} values and the corresponding k_G values used in the analyses. Assumed Poisson"s ratios (υ) for each material are also shown in these tables. The K_{2max} value for the clay core is determined based on the publication by (Malla S. et.al., 2005). Figure 3.6 shows the G_{max} functions used in this study for various embankment and foundation materials.

Table 3.4 K_{2max}, k_G and υ values are based on Eq. (3) (Seged and Haile, 2010), and E is based on (WWDSE, 2016)

No.	Material	K_{2max}	k_G	υ	Modulus of Elasticity, E (kPa)
1	Impervious Clay Core	50	11000	0.4	20,000
2	Transition/Filter layer	70	15400	0.3	50,000
3	Gravel Shell	90	19800	0.3	100,000
4	Foundation	90	19800	0.3	100,000
5	Compacted Alluvium/ Liquefiable foundation	85	18700	0.3	100,000
6	Rock Toe	90	19800	0.3	50,000

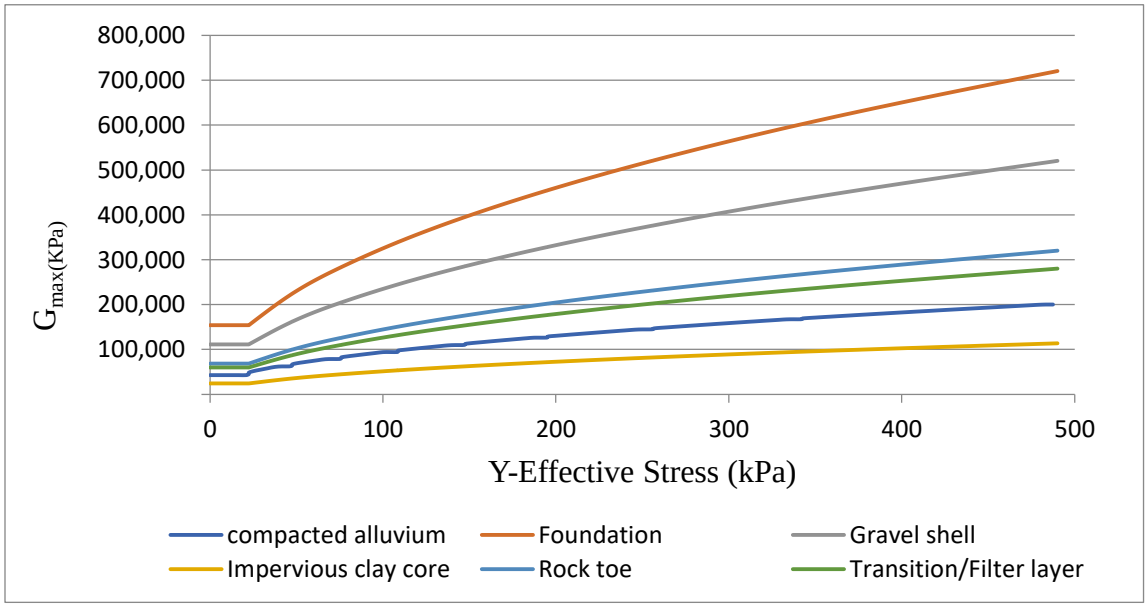

Figure 3.6 G_{max} functions for various embankment and foundation materials

ii. Shear Modulus Reduction and Damping Ratio Functions

As the dynamic shear strain increases, the effective dynamic shear modulus becomes smaller than the maximum value G_{max}. At the same time, the nonlinear response at higher dynamic strains leads to a higher rate of energy dissipation, which is represented

by a damping ratio that increases at higher strain levels. The strain-dependent dynamic shear modulus reduction function and damping ratio function for different soils and rock were utilized for the dynamic analysis. An overview of these functions is shown in Figures 3.7 and 3.8.

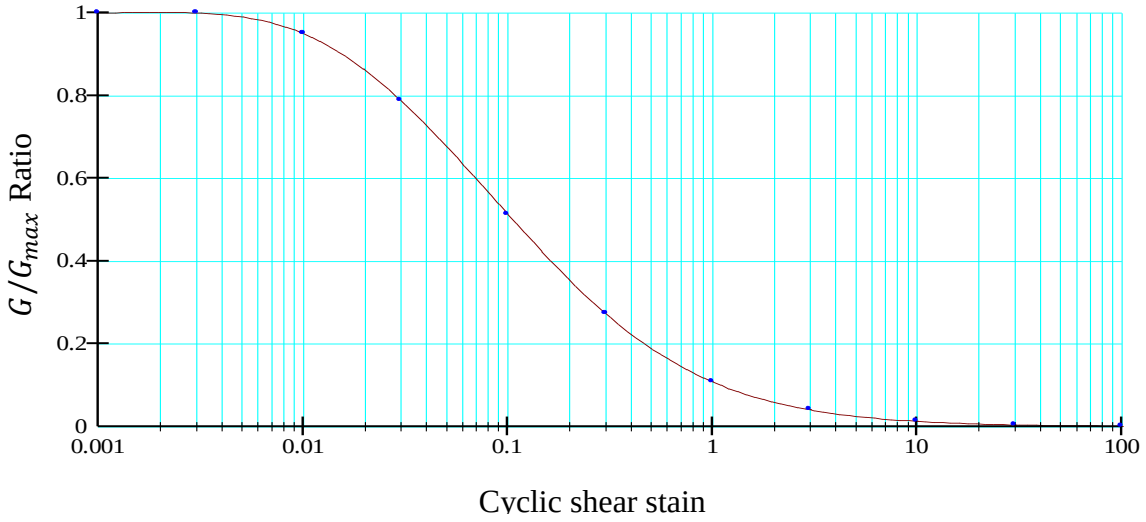

Figure 3.7 Sample Shear modulus reduction function

As with G_{max}, the damping ratio in QUAKE/W can be specified as a function. The damping ratio is a function of the cyclic shear strain, the same as the G-reduction function. A typical damping ratio function is presented in Figure 3.8.

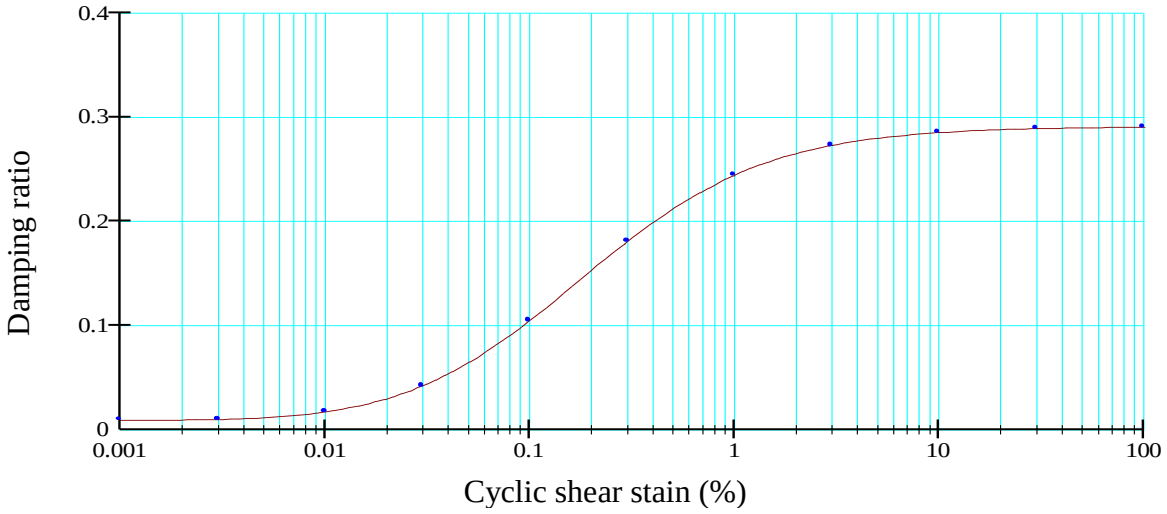

Figure 3.8 Sample damping ratio function

For confining pressures stated in KPa and plasticity index, the above damping ratio and shear modulus reduction function formula have been constructed.

iii. Pore Pressure Function

The pore pressures developed during earthquake shaking are a function of the equivalent number of uniform cycles (N) for a particular earthquake and the number of cycles which will cause liquefaction for a particular soil (NL), under a particular set of stress condition. The ratio of N/NL is then related to a pore pressure parameter, u (Kramer, 1996). Albaisa, (1974) and DeAlba P., (1975) found that the pore pressure function can be described by the following equation Eq.3.4:

$$r_u = \frac{1}{2} + \frac{1}{\pi} sin^{-1}\left[2\left(\frac{N}{N_L}\right)^{\frac{1}{\alpha}} - 1\right] \ldots\ldots\ldots\ldots\ldots\ldots\ldots\ldots\ldots\ldots\ldots\ldots (3.4)$$

Eq.3.4 is used to estimate the pore pressure function in QUAKE/W. For saturated sand α= 0.7 (Das, 1993). As described above, the compacted alluvium foundation is largely comprised of weakly compacted sandy silt that has been assumed to be a potentially liquefiable soil. Therefore, the pore pressure function shown in Figure 3.9 (obtained using Eq.3.4, for α = 0.7) has been used for the compacted alluvium foundation of the dam.

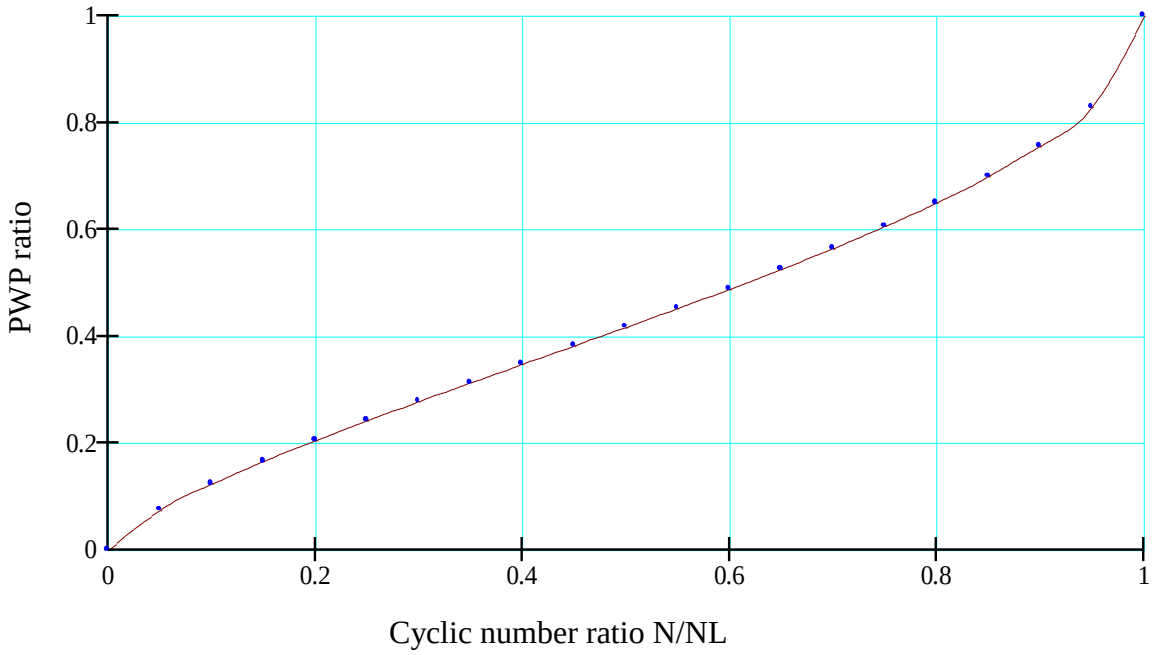

Figure 3. 9 Pore pressure function used for alluvium foundation (DeAlba P., 1976)

iv. Cyclic Number Function

A Cyclic Number Function must be attached to the Pore Pressure Function so that NL is defined. For high shear stress ratios (defined as the ratio of cyclic deviatoric stress to initial static effective vertical stress), only a few cycles may be required to cause liquefaction, while for low ratios, a larger number of cycles are required. The cyclic number function specifies this relationship. DeAlba P.(1976) and USNRC (1985) have published cyclic number function curves obtained from shaking table tests on sand as shown in Figure 3.9. Based on these publications and characteristics of soils based on relative density (Roy, 2017) as shown in Table 3.6, the cyclic number function shown in Figure 3.10 has been used for the compacted alluvium foundation of the dam.

Table 3. 5 Characteristics of soils based on relative density (Roy, 2017)

Relative density (%)	Soil compactness
0-15	Very loose
15-35	Loose
35-65	Medium
65-85	Dense
85-100	Very dense

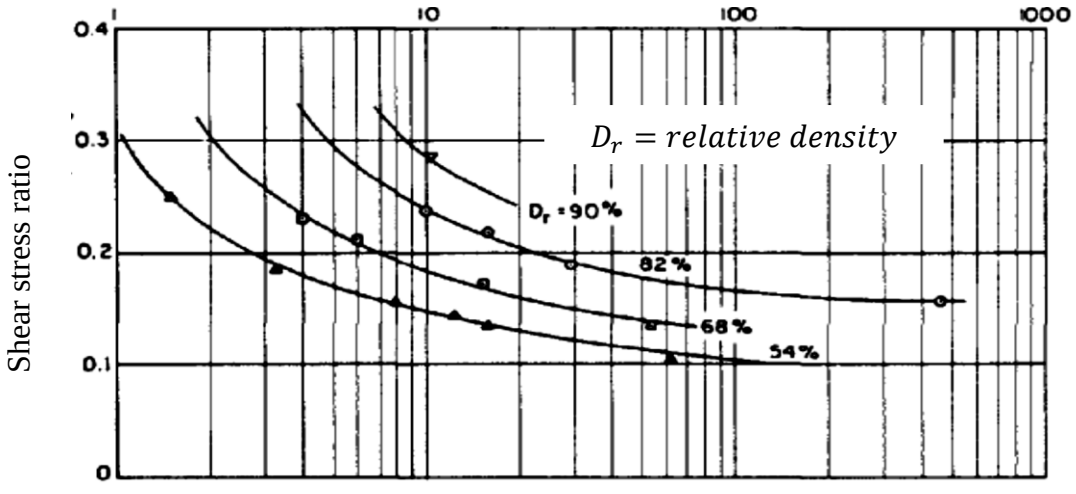

Figure 3. 10 Cyclic number function used for analysis (DeAlba P., 1976)

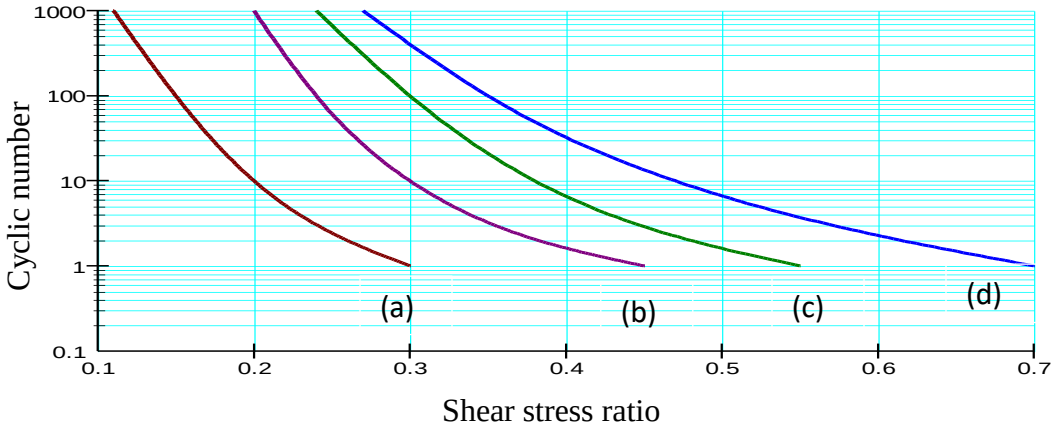

Figure 3. 11 Cyclic number function used for the analysis, (a) very loss sand, (b) loss sand, (c) medium dense sand, and (d) dense sand

v. Overburden Pressure Correction Function, K_σ

The cyclic shear stress required to trigger liquefaction increases as the confining stress increases (Kramer, 1996). In QUAKE/W a K_σ function is specified to account for this. (Marcuson W. F. III, 1990) reported variation of correction factor K_σ with effective overburden pressure for different soils. The K_σ correction function is attached to the cyclic number function and is specified as part of the cyclic number function data. The overburden correction factor influences N_L and therefore has an effect on the pore-water pressure value that is computed.

Based on the work of (Marcuson W. F. III, 1990), the K_σ function shown in Figure 3.11 (corresponding to the estimated average curve for sand) has been used for the compacted alluvium foundation of the dam.

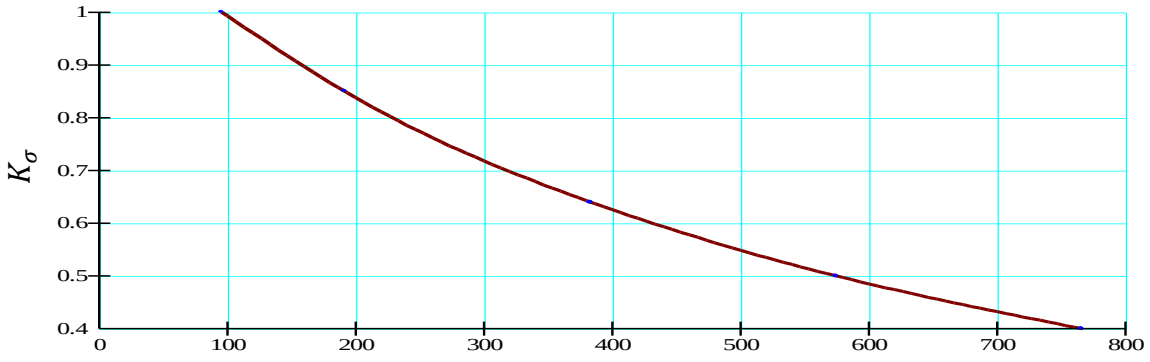

Figure 3. 12 K_σ correction function used for the analysis

vi. Shear Stress Correction Function, K_α

The initial in-situ static shear stresses also influence the cyclic stress required to trigger liquefaction (Kramer, 1996) This function is dependent on the density of the soil. (Seed H. B. and Harder, 1990) reported the shear stress correction function for different relative densities as shown in Figure 3.13.

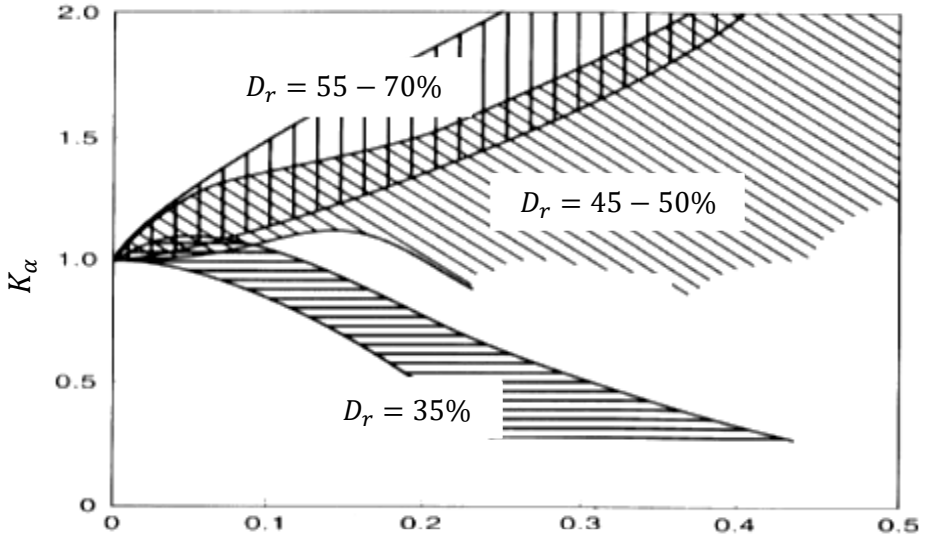

Figure 3. 13 K_a Correction factor (Seed H. B. and Harder, 1990)

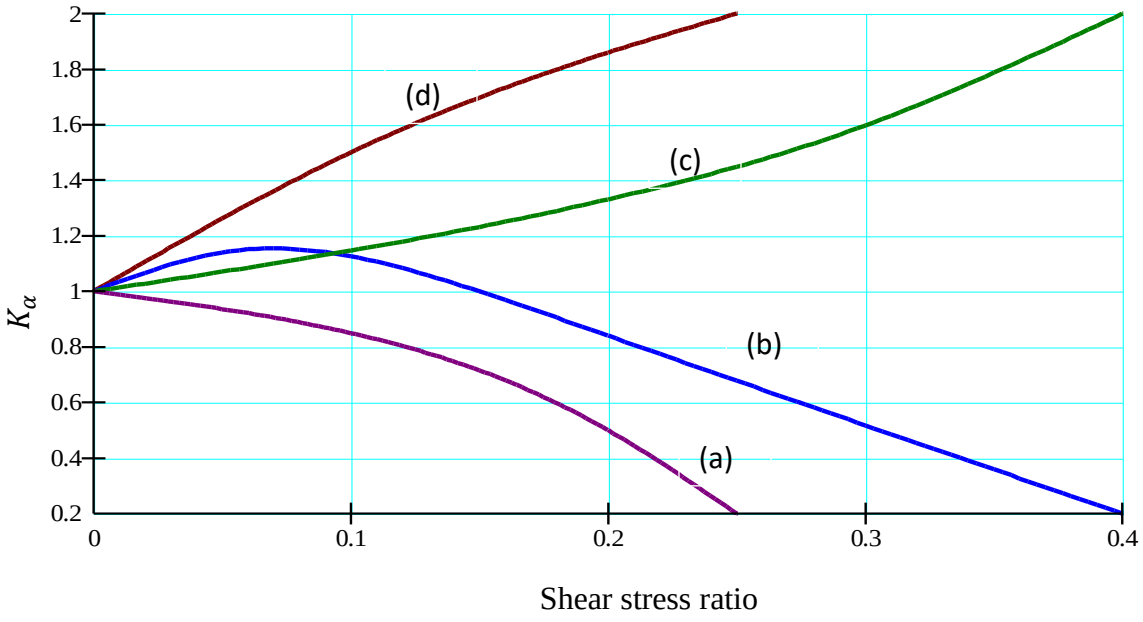

Figure 3. 14 K_α correction function used for analysis (a) very loss sand, (b) loss sand, (c) medium dense sand, and (d) dense sand

Based on Figure 3.13 for a given range of relative density of a soil, the K_α function shown in Figure 3.14 has been used for the compacted alluvium foundation of the dam.

3.2.4. Boundary Conditions

All boundary conditions in Quake/W must be applied to geometry elements directly, such as area faces, region lines, free lines, or free points. A Boundary Condition (BC) cannot be applied directly to an element edge or node. Connecting the BC to the geometry has the advantage of making it independent of the mesh, which allows the mesh to be altered if required without losing the boundary condition definition (QUAKE/W, 2018).

The ground can move freely in the vertical direction in the in-situ stress state, which exists before the earthquake, but it is fixed in the horizontal direction. The dam is also secured along the base. This is performed by setting the horizontal (x) and vertical (y) displacements to zero in both directions. For the dynamic analysis, the boundary conditions at the problem's vertical ends must be altered. The vertical movement is now restricted, but the ground may now move laterally. When horizontal earthquake accelerations are applied, these circumstances cause the ground to sway from side to side.

3.3. Methods of Analysis

The field of geotechnical earthquake engineering is broad. Different types of analysis are required for different conditions. Multiple approaches must be used since it is impossible to solve all of the problems with a single dynamic analysis. Slope/W analysis, Quake/W analysis, and Sigma/W analysis are all available with Geo-integrated studio's feature. It is important to use all of them together to examine the various aspects of earthquake engineering.

3.3.1. Initial Static Stress

The initial static stress is done before the dynamic analysis. The initial static stress determination is done by the Sigma/W model. The constitutive material model selected for the analysis is elastic-plastic. In the analysis, pore pressure influences to the strength of the soil by altering the matric suction.

The Sigma/W analysis has a boundary condition constrained in both left and right borders by zero horizontal displacements. And the lower border of the analysis is also constrained by both zero vertical and horizontal displacements.

3.3.2. Slope Stability Analysis before the Earthquake Shaking

This section of the analysis is used to compare the instability that occurred on the slope due to the static stresses from self-weight of dam material and reservoir pressure before shaking. To do this the SLOPE/W component of the Geo-studio software has been used.

The SLOPE/W component of the software uses the SIGMA/W Stress analysis technique in the numeric. For both the upstream and downstream face of the dam at a steady-state, the slope stability factor of safety is determined before the earthquake. It can easily be guessed that the factor of safety for the upstream is more than for the downstream, because of the additional hydrostatic normal force of the impounded water in the upstream face. The constitutive model for the materials is Mohr-Coulomb. The material parameters used for slope stability determination for different dam zones are provided in table 3.4.

3.3.3. Dynamic Analysis with QUAKE/W

(QUAKE/W, 2018) is a geotechnical finite element software program for dynamic analysis of earth structures subjected to earthquake shaking and other sudden impact loadings. The shear stresses due to self-weight, pore pressure, hydrostatic pressure, and cyclic shear stress are calculated using dynamic analysis. To determine the specific dynamic shear stress, which is responsible for deformations and slope instability, the stress determined by the initial static stress is subtracted from the dynamic analysis stress.

a) **Dynamic Finite Element Equation:**

The equation used in Geo studio is similar to all of other finite element equations. The stiffness matrix, damping matrix, mass matrix, displacement, velocity, and acceleration are all included in this part of the equation. A stiffness matrix is a characteristic matrix that describes the stiffness of an element. A damping matrix and a mass matrix are two types of characteristic matrices that describe an element's damping and mass respectively. The rate of change of velocity with time is the acceleration, and the velocity is the change of

displacement with time. The displacement is the main unknown in this equation. All of this is driven by a force on the right-hand side of the equation, which is the effective driving force.

$$[M]\left\{\frac{\partial^2 u}{\partial t^2}\right\} + [D]\left\{\frac{\partial u}{\partial t}\right\} + [K]\{u\} = \{F_t\} = [M]\{i\}\ddot{u}_g(t) \ldots\ldots\ldots\ldots\ldots\ldots (3.5)$$

Where,

$[M]$ = Element mass matrix

$[D]$ = Element damping matrix

$[K]$ =Element stiffness matrix

$\left\{\frac{\partial^2 u}{\partial t^2}\right\}$ = Acceleration vector

$\left\{\frac{\partial u}{\partial t}\right\}$ = Velocity vector

$\{u\}$ = Displacement vector

$\{F_t\}$ = Effective force vector

$\{i\}$ = Influence vector

$\ddot{u}_g(t)$= Exciting ground acceleration

3.3.4. Seismic Slope Stability Analysis

Using the same method as that of slope stability before an earthquake, the slope stability during an earthquake is calculated by the slice method. In the finite element method, which uses the stresses calculated by the Quake/W for all those fractions of seconds the slope stability is assessed for all potential slip surfaces and the critical one is considered. Additional inertial loads and dynamic shear stresses decrease the factor of safety from the static condition results.

a) Stability and Deformation Analysis

Integration of stability and deformation analyses with SLOPE/W allows the factor of safety to be determined at every phase of the dynamic analysis process utilizing limit equilibrium or stress-based analyses. To account for the consequences of strength loss, liquefied zones indicated by QUAKE/W might be given steady-state strength. Use SLOPE/W with simulated ground accelerations in a Newmark deformation study to

determine irreversible plastic deformation (e.g., dam crest settling). Alternatively, by spreading stresses inside liquefied zones and other over-stressed locations, SIGMA/W may be used to compute permanent deformation. This enables the evaluation of earth structure failure modes and overtopping.

3.3.5. Liquefaction Assessment

During an earthquake, excessive pore-water pressures can cause liquefaction, which can lead to large-scale deformations or global failure. QUAKE/W simulates excess pore-water pressure generation utilizing either a functional connection between volumetric straining (and hence pore-water pressure response) and cyclic number or a conventional cyclic stress ratio and pore-water pressure relationship. At each time step, liquefied zones are shown to better simulate deformations and verify stability.

In an Equivalent Linear analysis, a key parameter obtained is the Cyclic Stress Ratio (CSR). This number is used together with the Cyclic Number function discussed earlier Figure 3.9 to indicate the possibility of liquefaction. Without going into much detail, generally the higher the CSR, the higher the possibility of liquefaction. In this study, CSR's greater than about 0.2 will indicate liquefaction is possible (QUAKE/W Tutorial, 2018).

The shear stress ratio (CSR) in QUAKE/W is defined as below Eq.3.6:

$$CSR = \frac{q_d}{2\sigma'_{v(static)}} * 0.65 \dots\dots\dots\dots\dots\dots\dots\dots\dots\dots\dots\dots\dots\dots\dots\dots\dots\dots\dots\dots\dots\dots\dots\dots (3.6)$$

The 0.65 constant is specified under the define analyses advanced tab Figure 3.9. It is called the coefficient of equivalent shear stress. It is used to view the irregular earthquake shaking in terms of equivalent uniform cycles.

The term q_d in the CSR equations is the peak dynamic deviatoric stress.

The term $\sigma'_{v(static)}$ is the static vertical effective stress before the earthquake shaking (the initial static conditions or time = zero conditions) (QUAKE/W Tutorial, 2018).

4. Results and Discussion

4.1. Initial Static Stress

The elastic-plastic constitutive material model was chosen for the study. A pore pressure that contributes to the soil's strength and characterized by the matric suction is employed in the study. A boundary condition is specified to both the left and right vertical ends of the SIGMA/W model to restrict horizontal movement. The analyses' lower border is constrained in both vertical and horizontal directions. The outcome of effective stresses in the embankment zone is depicted with a labeled contour below in Figure 4.1.

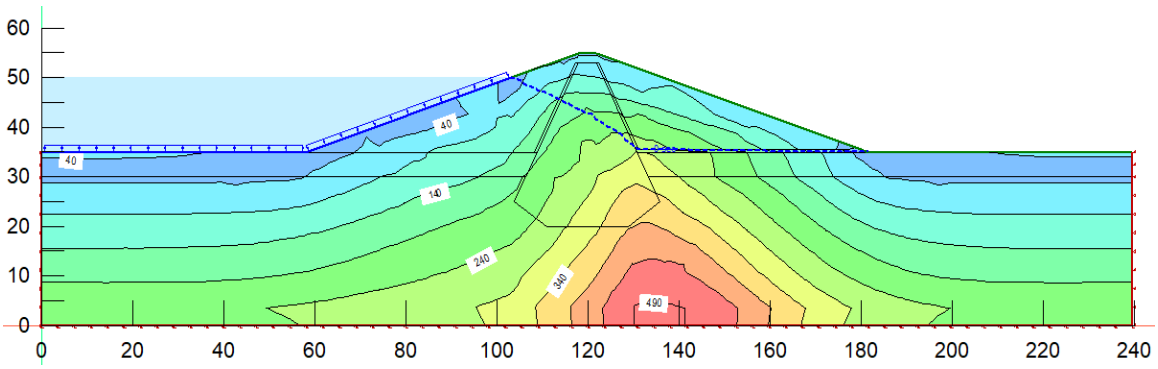

Figure 4.1 Effective stresses distribution in the dam

As the graphic result presents, maximum effective stress is recorded at the bottom of downstream toe of the clay core (490 KPa). Effective stress is computed by deducting pore water pressure from total stress. Due to the stored-water pore pressure, the upstream face is a region where minimum effective stress is obtained.

4.2. Slope Stability Analysis before the Earthquake Shaking

It is good practice to look at stability under static conditions before earthquake shaking. The finite element analysis method results for both upstream and downstream slope stability analysis before an earthquake has done for the assurance of static stability. For the upstream slope the calculated factor of safety in slope 1V to 2.6H is 1.576 against slope, instability. For the downstream slope the calculated factor of safety in slope 1V to 2.8H is 1.515 against slope instability as shown in Figure 4.2 and Figure 4.3,

respectively. The corresponding factor of safety with sliding masses and slip surfaces are presented by the appendix D of the rest of the analysis result.

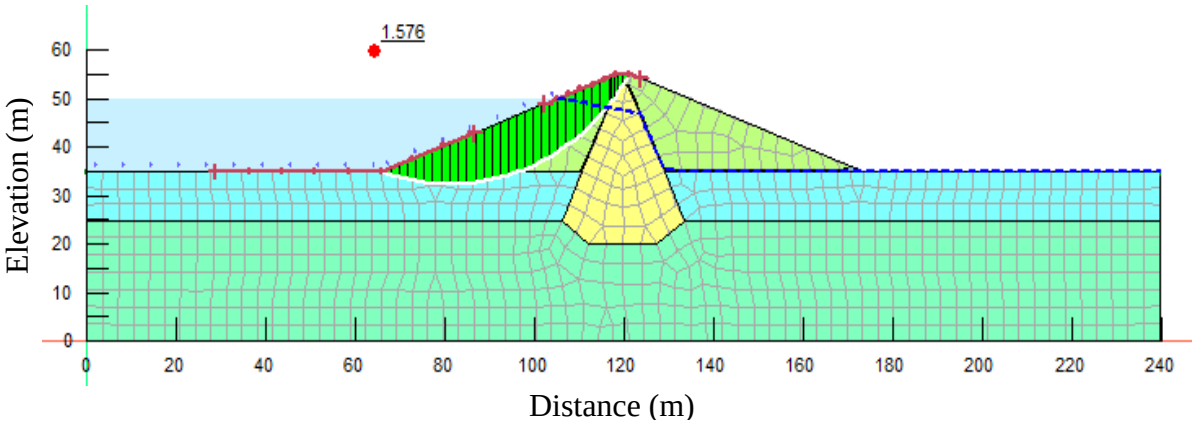

Figure 4.2 1V to 2.6H Upstream slope static stability of 10 meter thick liquefiable foundation of the dam

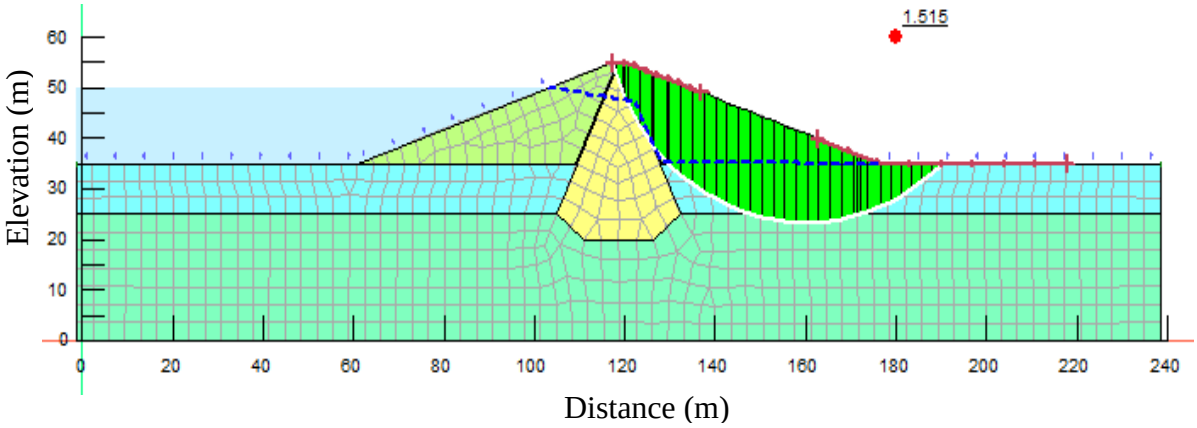

Figure 4.3 1V to 2.8H Downstream static slope stability of 10 meter thick liquefiable foundation of the dam

Despite the fact that all of the slopes considered in this study have a factor of safety greater than 1.0, the lowest required factor of safety for a static case is 1.5 (US.Corps of Engineers, 2003). As shown in Table 4.1, the safety factor for the downstream slope when steeper than 1V to 2.6H does not satisfy this requirement. The 1V to 2.8H embankment dam does satisfy this requirement under static loading condition, according to the results of marginal safety factors for both upstream and downstream slope of 10 meter liquefiable foundation thicknesses. For 5 and 15 meter liquefiable foundation thicknesses and slope of 1V to 3H, the factors of safety for downstream slope of embankment are 1.628 and 1.530, and the factors of safety for upstream slope of

embankment are 3.458 and 1.703 respectively, as shown in appendix D. As a result, multiple methods of analysis should be used to verify dynamic stability.

Table 4.1 Factors of safety for upstream and downstream slope stability before earthquake shaking for liquefiable foundation thicknesses of 10 meters and different dam slopes

Liquefiable foundation thickens(m)		Slope							
		1:1.5	1:2	1:2.2	1:2.4	1:2.6	1:2.8	1:3	1:3.2
10	upstream	1.104	1.305	1.483	1.490	1.576	1.638	1.682	1.826
	downstream	1.052	1.257	1.282	1.350	1.424	1.515	1.590	1.641

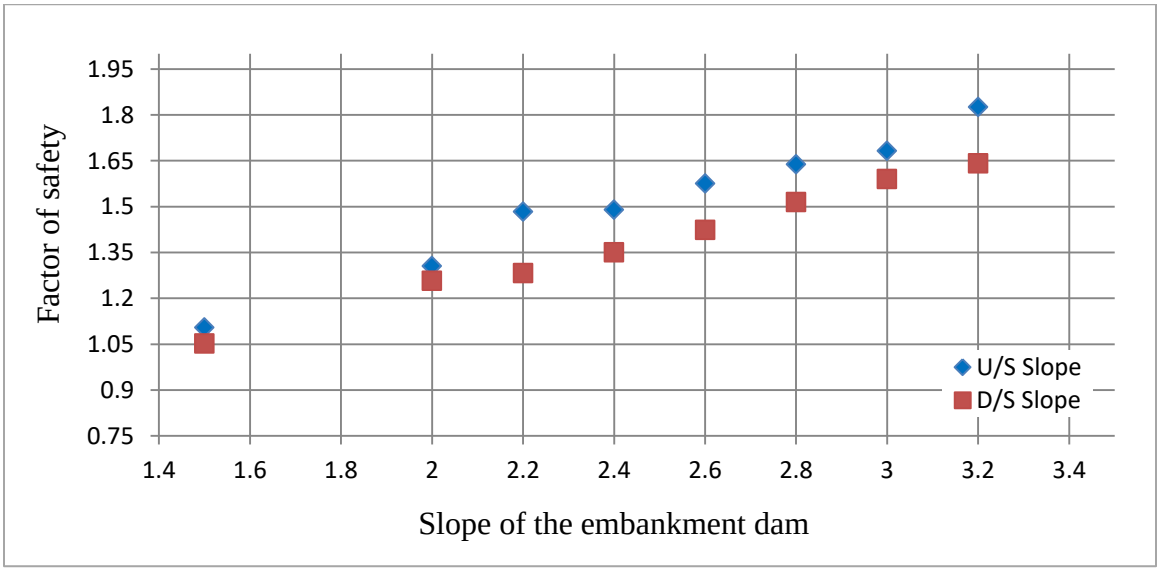

Figure 4.4 Upstream and downstream slope stability before earthquake shaking for 10 meter liquefiable foundation thicknesses and different slope of the dams

4.3. Dynamic Analysis

The finite element model is done with both structured and unstructured mesh, depending on the geometry. In the case of 10-meter liquefiable foundation thickness and slope of a 1Vto 3H as shown in Figure 4.5, the model consists of 884 nodes in which equations are checked, and 816 elements, where material properties are extracted. The Geo-Studio manual recommends elements not more than 1000 to shorten the time of analysis and to avoid results that might be complex for interpretation. In all cases also all node and mesh meet the Geo-Studio manual recommendation since the embankment dam in this study is not as such very large with a height of 20 m. The quadrilateral and triangular element

geometry is selected for their compatibility in an unstructured mesh. To minimize the disturbance due to the boundary wave reflection in the dynamic analyses, the side boundaries were extended by 100 m (about 4 times the dam height) in both left and right directions

The dynamic analyses for three different earthquake records have been examined in the following sections. The earthquake-induced accelerations, displacements, liquefaction, and as well as, the embankment's stability, are assessed during the ground motion.

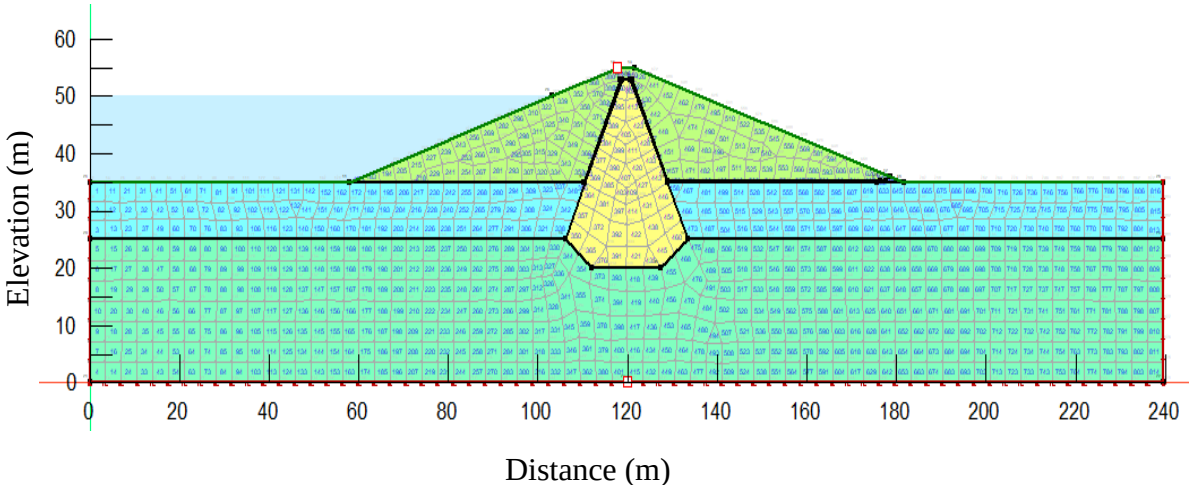

Figure 4.5 QUAKE/W finite element model to show mesh elements and nodes

4.4. Seismic Slope Stability Analysis

The slope stability is determined using the finite element approach in the same way as the static (pre-earthquake) analysis. The difference is that the analysis is performed at each time step of the earthquake motion (0.02 sec.). The additional dynamic shear stress in each element at the base of a slice is averaged and added to the static finite element slope stability analysis for each time step in the finite element method analysis. The calculated factor of safety for upstream slope during the 0.37 g earthquake shaking is 0.750 for 1V to 2.6H slope. Since these dams were satisfy the requirement under static conditions, the calculated factor of safety for the downstream slope during the 0.37 g earthquake shaking is 0.872 for 1V to 2.8H Slope.

However, when the slope of the embankment is changed the calculated factor of safety during earthquake shaking is also changed. Figure 4.6 and Figure 4.7 shows downstream

and upstream slope calculated factor of safety of 1V to 3.2H slope for liquefiable foundation thickens 10m is 1.113 and 1.033 respectively. And downstream and upstream slope calculated factor of safety of 1V to 3H slope for liquefiable foundation thicken of 5m are 1.334 and 1.748 respectively. Therefore the dynamic analysis of the embankment dam at a slope of 1V to 3H and 1V to 3.2H for the foundation thickness 5m and 10m respectively satisfy the requirement. For 15 meter liquefiable foundation thicknesses and slope of 1V to 3H, the factor of safety for downstream slope of embankment is 0.900 and the factor of safety for upstream slope of embankment is 0.764. In general, this study suggests that finite element approaches (SLOPE/W with QUAKE/W) are important in determining the slope factor of safety for embankment dams.

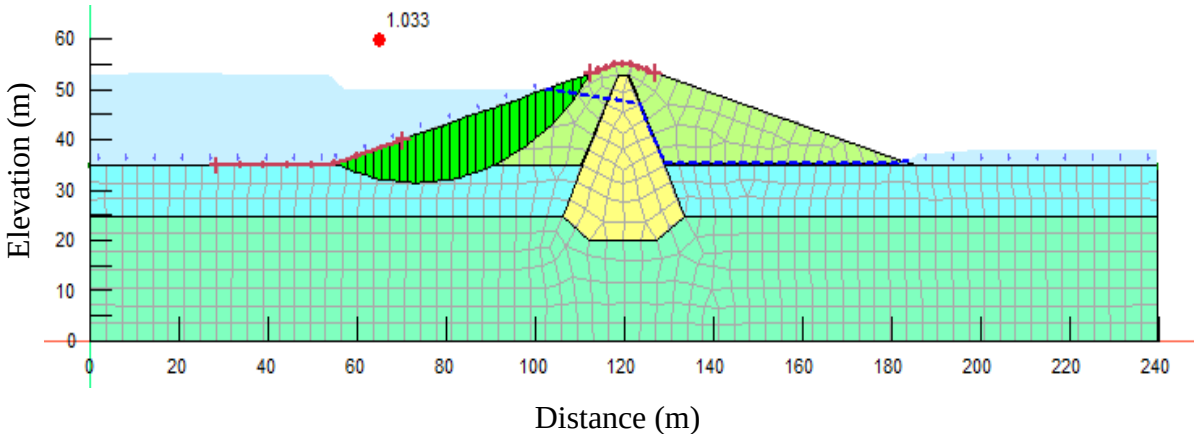

Figure 4.6 1V to 3.2H Upstream slope stability of 10 meter thick liquefiable foundation of the dam corresponding to 0.37g earthquake shaking

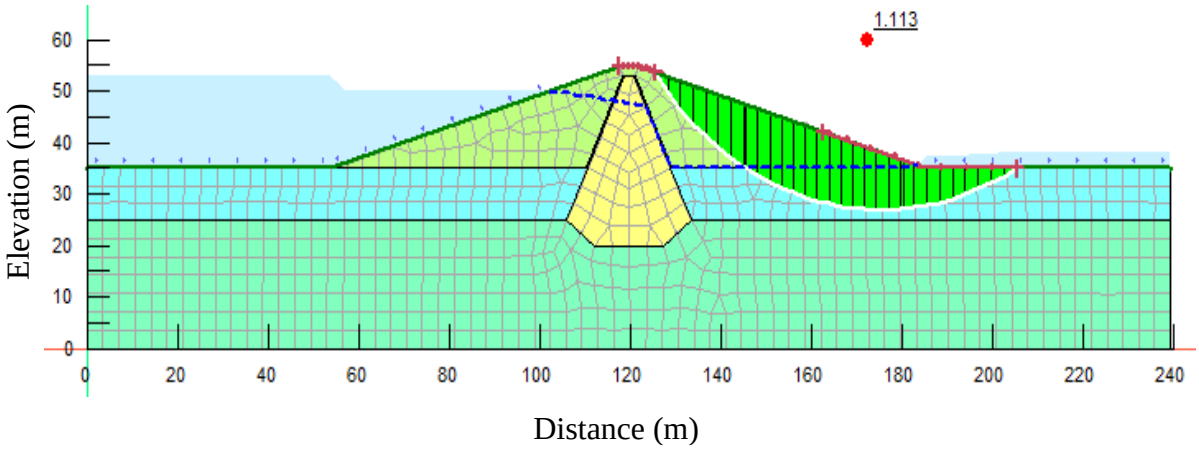

Figure 4.7 1V to 3.2H Downstream slope stability of 10 meter thick liquefiable foundation of the dam corresponding to 0.37g earthquake shaking

Table 4.2 shows the summary of the factor of safeties for the upstream and downstream slopes during the 0.37g earthquake shaking for 10 meter foundation thicknesses and different slope of the dam.

Table 4.2 factor of safety for upstream and downstream slope stability under 0.37g earthquake shaking for liquefiable foundation thicknesses of 10 meters

Liquefiable foundation thickens(m)		Slope							
		1:1.5	1:2	1:2.2	1:2.4	1:2.6	1:2.8	1:3	1:3.2
10	upstream	0.469	0.627	0.682	0.692	0.750	0.773	0.831	1.033
	downstream	0.702	0.835	0.848	0.851	0.865	0.872	0.923	1.113

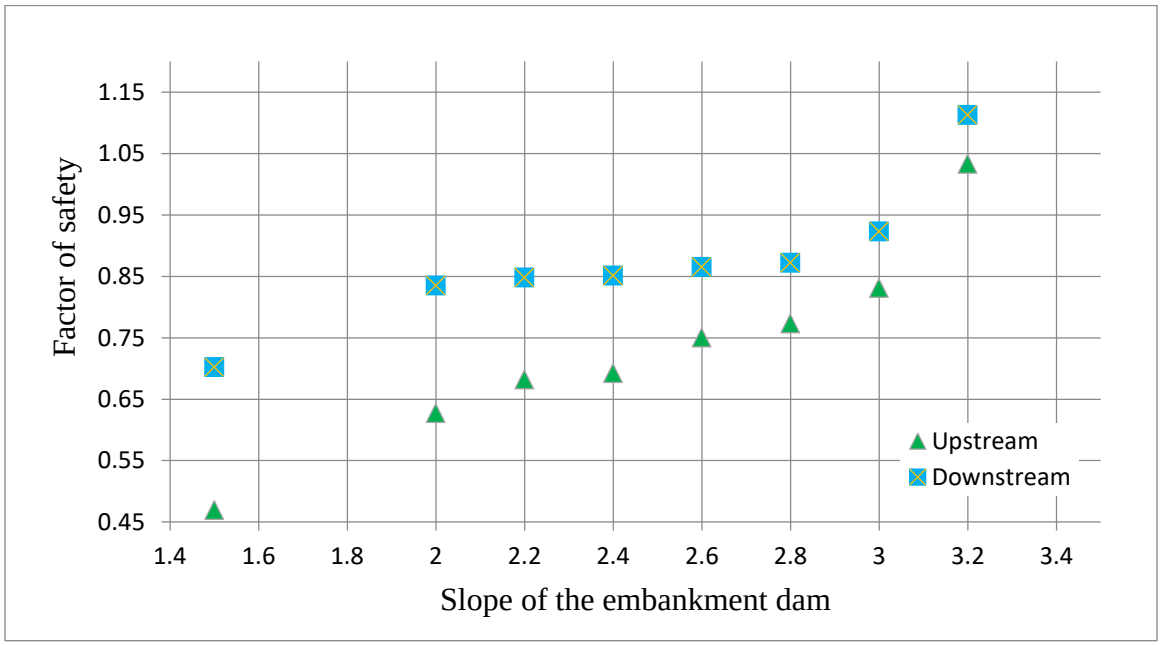

Figure 4.8 Upstream and downstream slope stability during earthquake shaking for 10 meter liquefiable foundation thicknesses and slope of the dams

4.5. Comparison of Static and Seismic Slope Stability

For varied foundation thicknesses and slopes, this study looked at the upstream and downstream slope stability of dams before and during earthquake shaking. The results revealed in Figure 4.9 that in static conditions, the upstream slope of the dam has a bigger magnitude of a factor of safety than the downstream slope of the dam, owing to the hydraulic pressure of the reservoir on the upstream side contributing to the dam's stability. However, in a dynamic study, the reservoir's hydraulic pressure causes the

downstream slope of the dam to be more unstable than the upstream slope, as reflected by a low factor of safety.

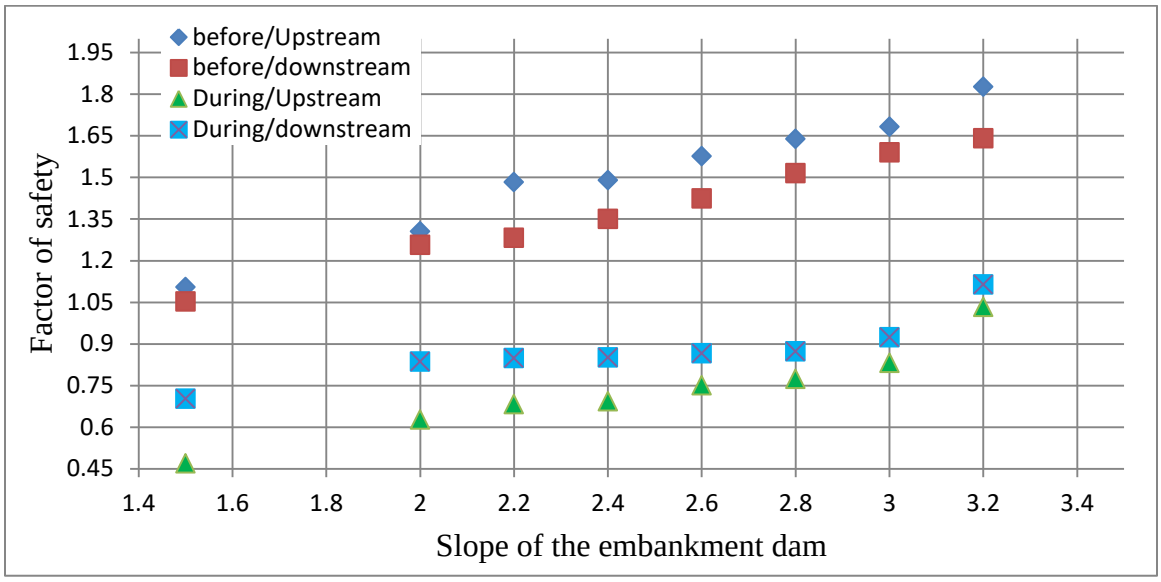

Figure 4.9 Upstream and downstream slope stability before and during earthquake shaking for 10 meter liquefiable foundation thicknesses and slope of the dams

Furthermore, because the critical slip surface passing through this foundation is less than that of 10 and 15-meter foundation thickness, both pre-earthquake and during -earthquake upstream slope stability of the dam at 5m liquefiable foundation thickness exhibited a high value of factor of safety as shown in Figure 4. 10.

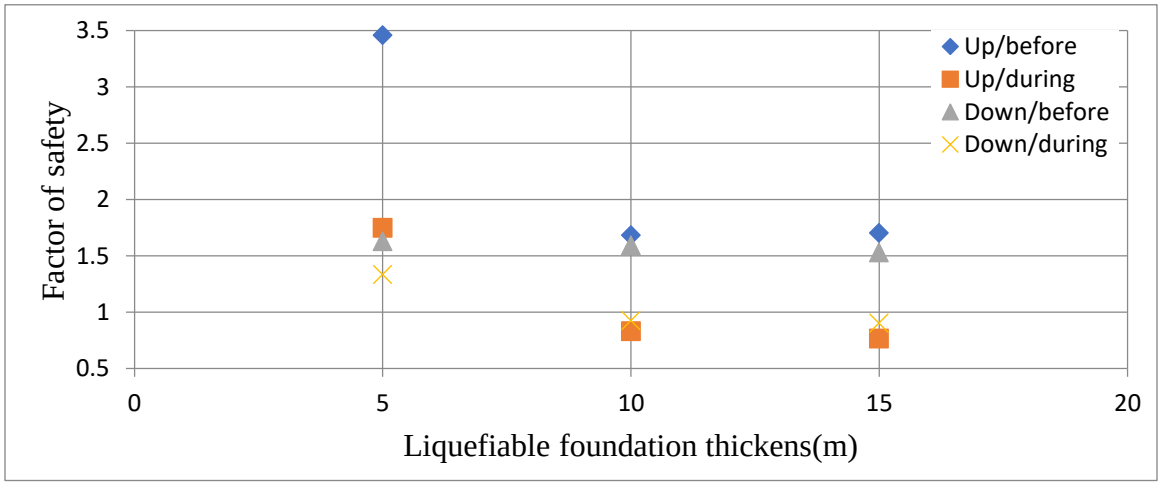

Figure 4.10 Upstream and downstream slope stability before and during earthquake shaking for liquefiable foundation thicknesses of 5, 10, and 15 meters, and dams with a 1V:3H slope

4.6. Liquefaction Result

The liquefaction result demonstrates that the liquefied parts of the foundation material is less at the commencing of earthquake, both in the upstream and downstream parts of the foundation, compared to the final time step of 40 seconds. Because the culmination of cyclic shear stresses at time step 40 resulted in a higher progressive increase of pore pressure, a larger section of the foundation was liquefied. However, because of the lower value of peak ground acceleration, the liquid fraction of foundation material is smaller under small ground motion than under peak ground motion.

The result of the liquefaction study at a 6.2 second time step and PGA of 0.17g earthquake shaking demonstrates that the foundation section near the clay core is not liquefied. These parts have a higher value of effective stresses as shown in Figure 4.1. Increments of effective stresses reduce the liquefaction potential of the material. Appendices C include figures of the results for different thicknesses of liquefiable foundation.

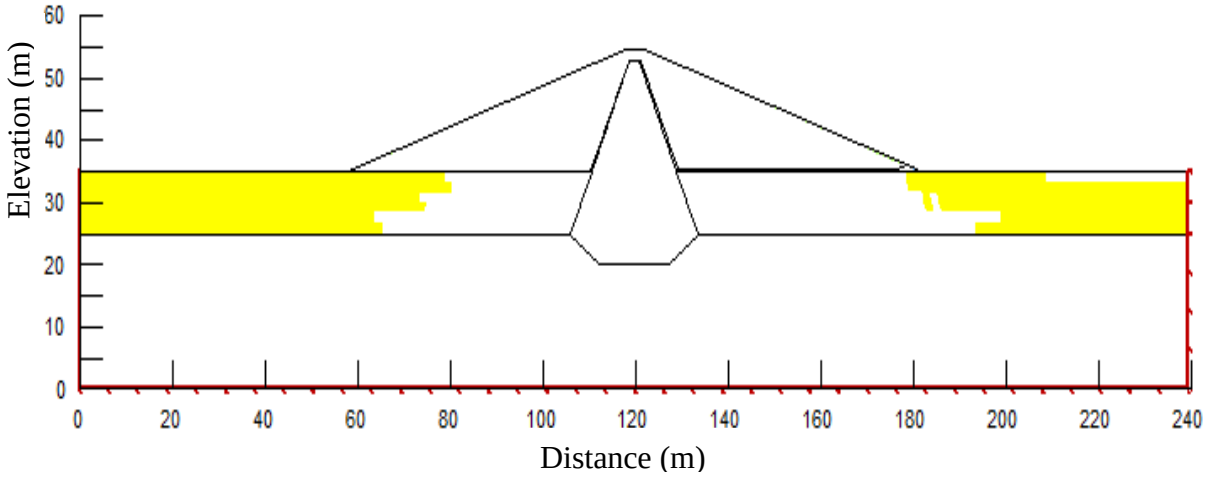

Figure 4.11 Liquefaction of 10 meter medium dense sand foundation at 6.2s and PGA of 0.17g earthquake shaking

Table 4.3 shows that during 0.37g magnitudes of earthquake shaking, the upstream component of the foundation entirely liquefied before the downstream parts of the foundation for all foundation thicknesses. There is no liquefaction for the upstream and downstream parts of the foundation and all liquefiable foundation thicken (m) at PGA of 0.12g, but there is liquefaction for the upstream and downstream parts of the foundation

and all liquefiable foundation thicken (m) at PGA of 0.37g. These findings show that independent of frequency and acceleration time history, high peak ground acceleration produces complete liquefaction more than low peak ground acceleration.

Table 4.3 Time(s) of upstream and downstream medium dense sand foundation fully liquefaction during different magnitude of earthquake shaking and liquefiable foundation thickens

Liquefiable foundation thickens(m)		PGA					
		0.12	0.17	0.22	0.27	0.32	0.37
5	upstream	DNL	DNL	38	34	26	24.6
	downstream	DNL	DNL	40	40	40	40
10	upstream	DNL	40	40	24	12	5.52
	downstream	DNL	40	40	32	14.2	8
15	upstream	DNL	40	9.8	7.72	4.6	4.2
	downstream	DNL	40	16.4	8.6	5.8	4.72

DNL refers do not fully liquefied

Table 4.4 shows that during 0.37g magnitudes of earthquake shaking; very loose sand liquefiable foundation material entirely liquefied at 4.02 seconds for both upstream and downstream parts of the foundation for all foundation thicknesses. No liquefaction is observed in both the upstream and downstream parts of dense sand foundation material and all liquefiable foundation thickens (m) at PGA of 0.37g. These findings indicate that very loose sand liquefiable foundation material is more vulnerable to earthquakes than loose sand, loose sand liquefiable foundation material is more vulnerable to earthquakes than medium dense sand, and dense sand foundation material is not vulnerable to earthquakes, regardless of frequency or acceleration time history.

Table 4.4 Time(s) of upstream and downstream alluvium deposit fully liquefaction during 0.37g magnitude of earthquake shaking for different liquefiable foundation thickens

Liquefiable foundation thickens(m)		Liquefiable foundation material			
		Very loose sand	Loose sand	Medium dense sand	Dense sand
5	upstream	4.02	4.02	21.2	DNL

	downstream	4.02	4.02	40	DNL
10	upstream	4.02	4.02	10	DNL
	downstream	4.02	4.02	11.2	DNL
15	upstream	4.02	4.02	4.02	DNL
	downstream	4.02	4.02	4.52	DNL

4.7. Acceleration Response at the Dam Crest

Figure 4.12 depicts the acceleration response at the dam crest during the earthquake in case of 10m liquefiable foundation thickness and 1V to 3H slope of embankment. Appendices E include figures of the results for different magnitude of earthquake shaking which ranged from 0.12g to 0.37g with a 0.05g increment. As shown in Table 4.5, the response ground accelerations at the dam crest are 0.340g, 0.499g, 0.594g, 0.607g, 0.674 g, and 0.784g, for the corresponding accelerations and foundation thickness of 5 meters, and the response ground accelerations at the dam crest are 0.332g, 0.434g, 0.529g, 0.604g 0.672g and 0.739g, for the corresponding accelerations and foundation thickness of 10 meters, and for the foundation thickness of 15 meters, the response ground accelerations at the dam crest are 0.274g, 0.404g, 0.518g, 0.586g, 0.653g, and 0.717g, for the corresponding accelerations respectively. Figure 13 shows the amplification of acceleration at the dam crest for the given case study. This acceleration amplification at the crest is expected. Appendices E include graphs of the results for different acceleration amplifications.

Table 4.5 Acceleration response at the dam crest for different magnitude of earthquake shaking and different liquefiable foundation thickens

Liquefiable foundation thickens(m)	PGA(g)					
	0.12	0.17	0.22	0.27	0.32	0.37
5	0.340	0.499	0.594	0.607	0.674	0.787
10	0.332	0.434	0.529	0.604	0.672	0.739
15	0.274	0.404	0.518	0.586	0.653	0.717

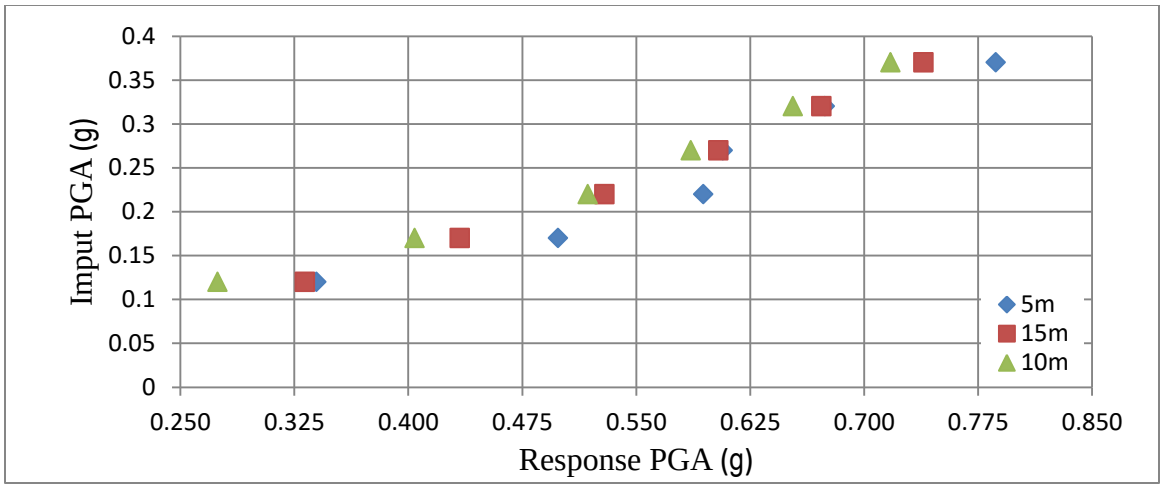

Figure 4.12 Response PGA at the crest of the dam for three different liquefiable foundation thicknesses

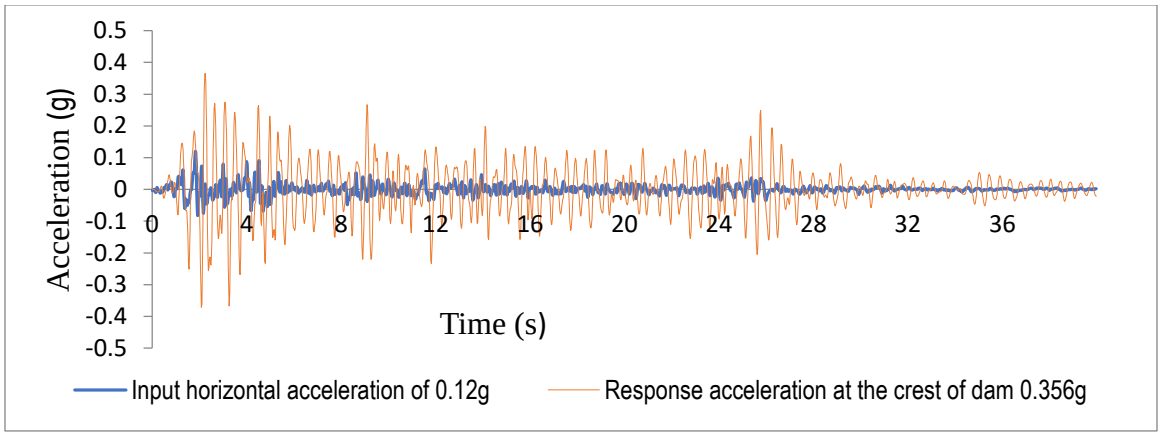

Figure 4.13 Dam crest responses in case of 10 meter liquefiable foundation thickness and 1V to 3H slope of embankment

4.8. Deformation Result

4.8.1. Vertical Crest Deformation

Figure 4.14 depicts the model's typical dynamic response, with the horizontal and vertical displacements given during the ground motion. One of the most essential aspects of dynamic analysis is deformation analysis after an earthquake has stopped shaking. The output findings from the QUAKE/W dynamic analysis will contain the updated soil total stresses and pore-water pressures at each saved time step. At each time step, SIGMA/W may take the output from QUAKE/W, subtract it from the previous time step, and construct an incremental force at each node. A deformation will occur as a result of the force. The vertical crest deformation increases as the input PGA increases, as seen in

figure 4.15. As stated in Table 4.6, the greatest displacement was determined to be 0.743m, equivalent to a PGA of 0.37g, which is less than the dam's freeboard section. As a consequence, the outcome is within acceptable bounds.

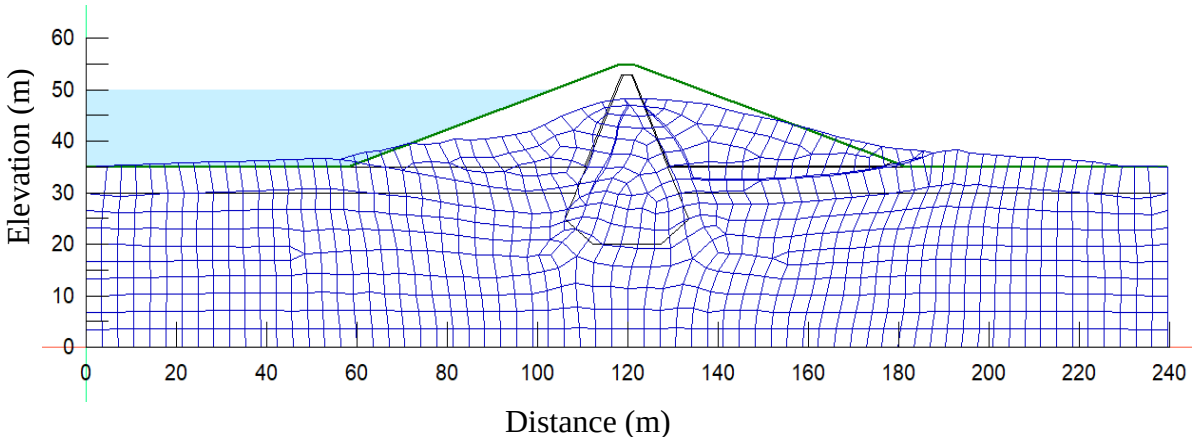

Figure 4.14 Deformation of the dam at maximum vector length 43 and magnification 2

Table 4.6 Vertical crest deformation for 10m liquefiable foundation thicknesses as a function of earthquake magnitude

Liquefiable foundation thickens(m)	PGA(g)					
	0.12	0.17	0.22	0.27	0.32	0.37
10	0.461	0.575	0.581	0.610	0.646	0.743

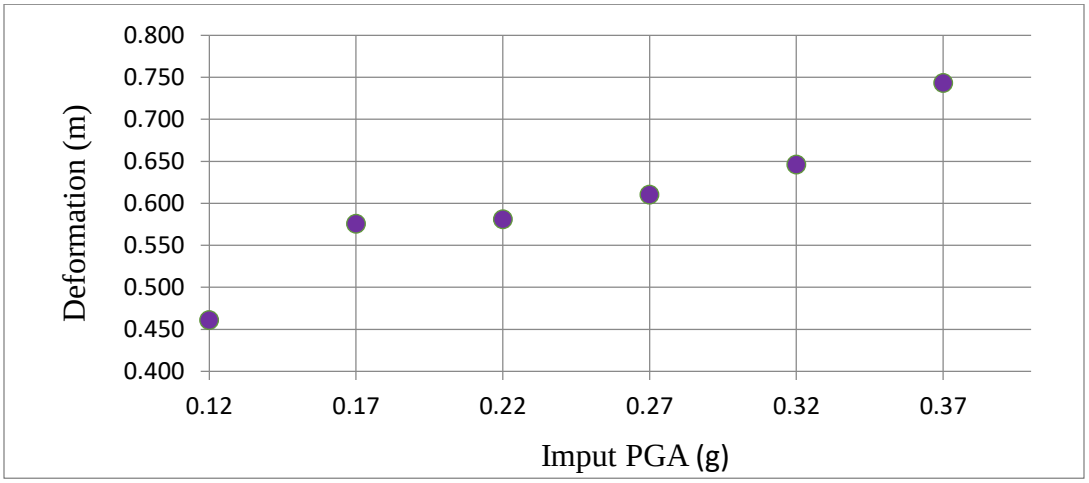

Figure 4.15 Vertical crest deformation for 10 meter liquefiable foundation thicknesses during various magnitudes of earthquake shaking

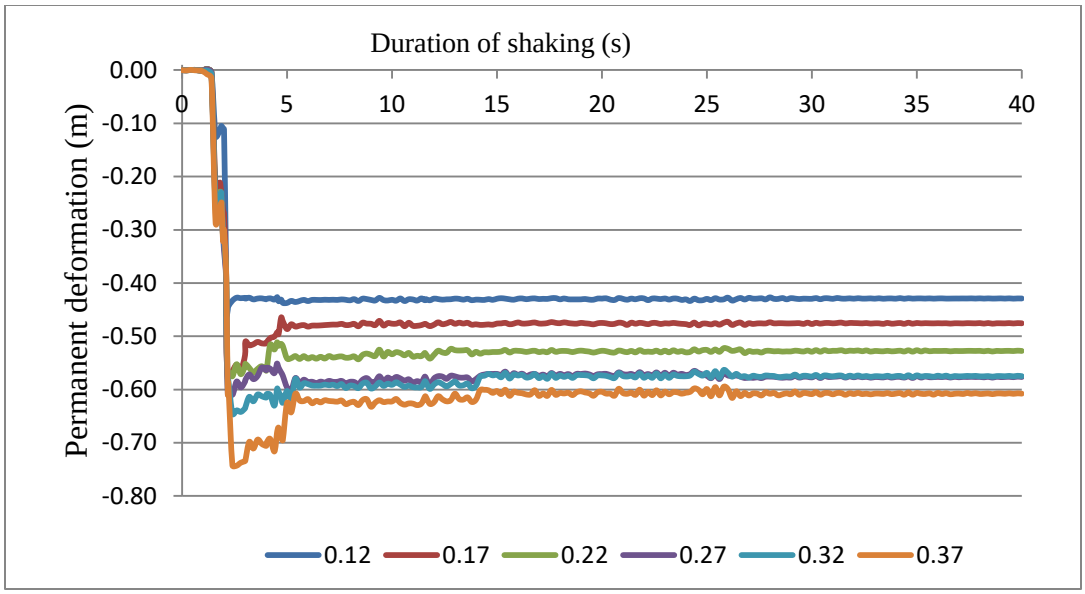

Figure 4.16 Vertical crest deformations for 10 meter liquefiable foundation thickness during various magnitudes of earthquake shaking

4.8.2. Horizontal Crest Deformation

Earthquake shaking creates inertial forces. These inertial forces cause the stresses in the ground to varying with time. In response to inertial forces, the mobilized shear strength increases and decreases along a possible slip surface. The mobilized shear strength may exceeds the available shear resistance at points throughout the shaking, resulting in a temporary loss of stability. The ground may experience some displacement if the safety factor is less than unity. Permanent deformation results from the accumulation of these displacements.

Dynamic study of dams includes examining the permanent deformations induced by dynamic inertial forces, as shown in figure 4.18 (QUAKE/W, 2018). By integrating the QUAKE/W computed results with the Newmark sliding block idea, (SLOPE/W, 2018) in the Geo-studio program executes earthquake-induced permanent deformations in dams. When the overall (static and dynamic) driving force exceeds the available resisting force, the Newmark method assumes that a potential sliding mass behaves like a rigid body, sliding down a slope. The important value of the resultant acceleration that causes the sliding mass to move is the yield acceleration. The factor of safety against sliding is 1.0 for the resulting acceleration. As indicated in Table 4.7, the greatest displacement

based on this concept is 2.738, which corresponds to a PGA of 0.37g. As the PGA increases, the horizontal crest deformation increases, as shown in figure 4.17.

Table 4.7 Horizontal crest deformation during different magnitude of earthquake shaking for different foundation thickens

Liquefiable foundation thickens(m)	PGA					
	0.12	0.17	0.22	0.27	0.32	0.37
10	0.889	1.259	1.629	1.998	2.367	2.738

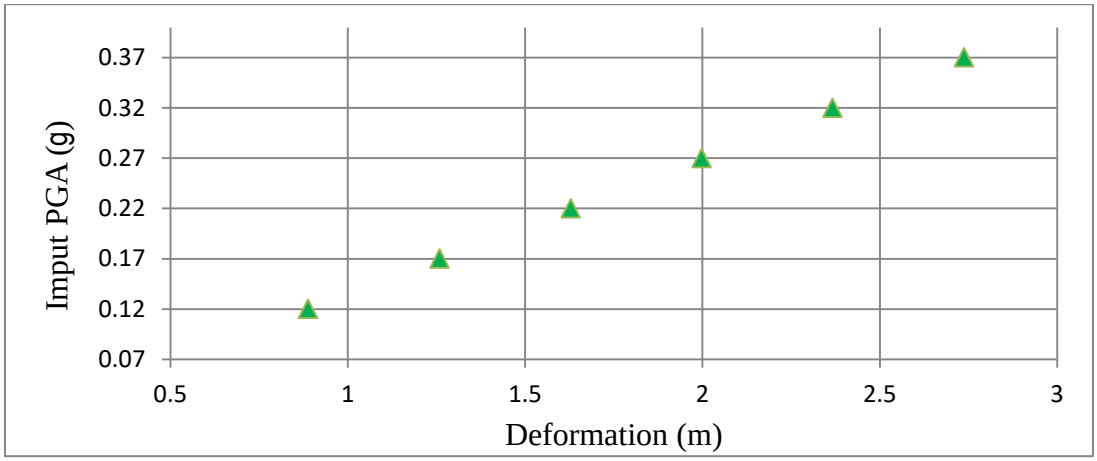

Figure 4.17 Horizontal deformation as a function of input PGA at the crest of the dam for 10meter liquefiable foundation thicknesses

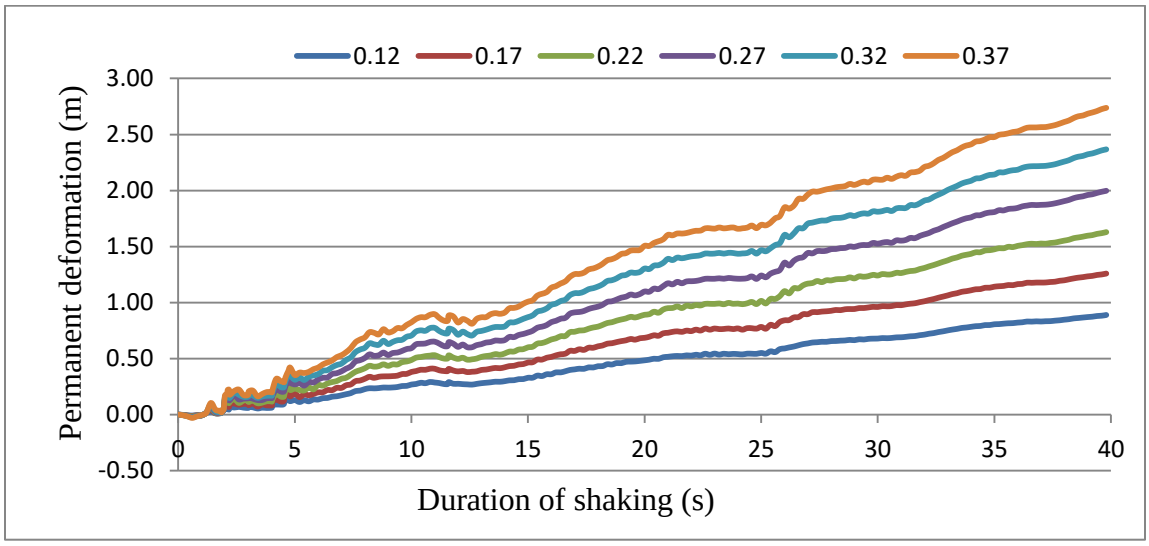

Figure 4.18 Horizontal deformation as a function of input PGA at the crest of the dam for 10 meter liquefiable foundation thicknesses

5. Conclusion and Recommendation

5.1. Conclusions

In this project, evaluation on dynamic stability of embankment dam is done considering Elcentro, Kobe JMA, and Hachinohe acceleration time history. The earthquake-induced accelerations, displacements, liquefaction, and as well as, the embankment's stability, are assessed during the ground motion simultaneously with an extended several parameters evaluation.

- All scenario shows amplification of acceleration at the dam crest regardless of the condition of earthquake except the magnitude of amplification increases as the amplitude increases and liquefiable foundation thickness decreases.
- Significant amount of both horizontal and vertical crest deformation during different magnitude of earthquake shaking and for 10m foundation thickens have been obtained even if they are with in permissible limit. The horizontal deformation is increased from 0.889m to 2.738m corresponding to 0.12g and 0.37g. The vertical deformation is increased from 0.461m to 0.743m corresponding to 0.12g and 0.37g.
- No liquefaction for the upstream and downstream parts of the foundation at PGA of 0.12g, but there is liquefaction at PGA of 0.37g. These findings show that independent of frequency and acceleration time history, high peak ground acceleration produces complete liquefaction more than low peak ground acceleration. And loose sand liquefiable foundation material is more vulnerable to earthquakes than dense sand, and dense sand foundation material is not vulnerable to earthquakes.
- The upstream slope of the dam has a larger magnitude of factor of safety than the downstream slope of the dam in static conditions; however the upstream slope of the dam is more unstable in a dynamic analysis than the downstream slope. In this considered case, the slope satisfy the requirement under dynamic loading of 0.37g are 1V to 3H and 1V to 3.2H slope for 5m and 10m liquefiable foundation thickness respectively.

5.2. Recommendations

In this study all of the input data is obtained from secondary sources, which degrade the accuracy of the result. Instead by conducting dynamic test, more realistic result can be obtained. Moreover, the dynamic analysis is conducted by considering equivalent linear material model, but apparently, the result showing the true response of the model is less than nonlinear material model especially in the case of liquefaction occurrences.

References

1. Albaisa (1974), 'Earthquake Induced Settlements in Saturated Sands,' *Journal of the soil mechanics and foundation division.*, vol.100., pp. 387-403.
2. Bolt BA (1969) 'Duration of Strong Motion', in *4th World Conference on Earthquake Engineering*. Santiago, Chile, pp. 1304–1315.
3. Byrne P. M., J. H. and S. R. (1992), 'Soil parameters for deformation analysis of sand masses,' vol.3., pp. 1407–1412.
4. Byrne P.M., Cheung H., and Y. L. (1978), 'Soil parameters for deformation analysis of sand masses,' *Canadian Geotechnical Journal*, vol.24(3)., pp. 366–376.
5. Das, B. M. (1993), '*Principles of Soil Dynamics*,' Seventh Ed. Edited by H. Gowans. Global Engineering.
6. Day, R. W. (2006), '*Foundation Engineering Handbook Design and Construction with the 2006 International Building Code*.'
7. DeAlba P., C. C. K. and S. H. B. (1975), 'Determination of Soil Liquefaction Characterstics by Large Scale Laboratory Tests,' *Earthquake engineering center ; University of California. - Berkeley*, (Report EERC), pp. 75–25.
8. DeAlba P., S. H. B. and C. C. K. (1976), 'Sand Liquefation in Large Scale Simple Shear Tests,' *ASCE Geotechnical engineering*, vol.102., pp. 909–927.
9. ES EN (2015), 'Design of Structures for Earthquake Resistance - Part 1: General Rules-Seismic Action and Rules for buildings,' Addis Ababa, Ethiopia: Minister of Construction, p. 207.
10. Frederick K. Lutgens, S. R. L. (2020), '*An Introduction to Physical Geology*,' *The Geographical Journal*. thirteenth. doi: 10.2307/1785582.
11. GDP-9 (2015), 'Liquefaction Potential of Cohesionless Soils,' New York State of Department, Department of Transportation, Office of Technical Services, Geotechnical Engineering Bureau.
12. Hamada, M. *et al.* (1987), 'Study on permanent ground displacement induced by seismic liquefaction,' *Computers and Geotechnics*, 4(4), pp. 197–220. doi: https://doi.org/10.1016/0266-352X(87)90001-2.
13. Idriss, I. M. (1992), 'Response of Soft Soil Sites during Earthquakes,' *Memorial*

Symposium to honor Professor Harry Bolton Seed. California: Berkeley.

14. Ioanna Rapti (2016), '*Numerical Modeling of Liquefaction-Induced Failure of Geostructures Subjected to Earthquakes*,' Construction hydraulique. Université Paris-Saclay - CentraleSupélec. Available at: https://tel.archives-ouvertes.fr/.
15. Korhan Adalier and Michael K. Sharp (2004), 'Dynamic Behavior of Embankment Dam on Liquefiable Foundation Subject to Moderate Earthquake Loading.'
16. Kramer, S. L. (1996), '*Geotechnical Earthquake Engineering*,' H. Edited by W. J. Hall. Prentice-Hall: University of Washington, International Series in Civil Engineering and Engineering Mechanics.
17. Kramer, S. L. and Paulsen, S. B. (2004), 'Practical use of Geotechnical Site Response Models,' *Proceedings, Int. Workshop on Uncertainties in Nonlinear Soil Properties and their Impact on Modeling Dynamic Soil Response, PEER Center Headquarters, Richmond, California*, pp. 1–10.
18. L.Kramer (1996), '*Geotechnical Earthquake Engineering*,' Edited by W. J. Hall. Washington DC, Upper Saddle River: Prentice-Hall International Series.
19. Malla S. et.al. (2005), 'Seismic Analysis and Safety Assessment of Earthfill Dam Founded on Alluvium Soil,' *Commission Internationale*. Barcelona.
20. Marcuson W. F. III, H. P. F. and L. R. H. (1978), 'Defnition of terms related to liquefaction ASCE,' *Journal of geotechnical engineering division.*, pp. 1197-1200.
21. Marcuson W. F. III, H. P. F. and L. R. H. (1990), 'Evaluation and Use of Residual Strength in Seismic Safety Analysis of Embankments,' *Earhquake Spectra*, pp. 529-572.
22. Mulat, Y. (2015), '*Dynamic Analysis of Middle Awash Multi-Purpose Dam*,' Addis Ababa University, Civil Environmental Engineering in partial fulfillment of the Degree of Masters of Science in Civil Engineering (Major in Hydraulic Engineering).
23. Newmark, N. M. (1965), 'Effects of earthquakes on dams and embankments,' *Geotechnique*, vol.15., pp. 139–160.
24. Nikkar, T. A. and A. (2014), 'Evaluation of the Pseudostatic Analyses of Earth Dams Using FE Simulation and Observed Earthquake-Induced Deformations:

Case Studies of Upper San Fernando and Kitayama Dams,' *The Scientific World Journal*.

25. O.Engemoen (2012), 'Embankment Dams,' *Association of Dam Safety Officials - Dam Safety 2008*. U.S. Department of the Interior Bureau of Reclamation, p. 100.
26. QUAKE/W (2018), 'Dynamic Modeling with QUAKE/W,' Geo-Slope international ltd, p. 165.
27. QUAKE/W Tutorial (2018), 'QUAKE / W Tutorial – Getting Started,' Canada: GEO-SLOPE International Ltd., pp. 1–12.
28. Roy, S. (2017), 'Role of Geotechnical Properties of Soil on Civil Engineering Structures,' PSIT College of Engineering, Kanpur, Uttar Pradesh, India.
29. Seed, B. H. B. *et al.* (1986) ,'Moduli and Damping Factors for Dynamic Analyses of Cohesion less Soils,' *Journal of geotechnical engineering,ASCE*, vol.112., pp. 1016–1032.
30. Seed, H. B. (1979), 'Considerations in the earthquake - resistant design of earth and rockfill dams,' Vol. 29., pp. 215-263.
31. Seed H. B. and Harder (1990), 'Variation of Correction Factor Ka with Initial /Normal Stress Ratio,' in. BiTech Publishers Ltd, p. 364.
32. Seed H. B. and Idriss I. M. (1970), 'Soil Moduli and Ddamping Factors for Dynamic Response Anayses,' University of California. - Berkeley : Earthquake engineering research center, p. Report no. EERC/70-10.
33. Seged and Haile (2010), 'Earthquake Induced Liquefaction Analysis of Tendaho Earth-Fill Dam,' *Journal of EEA*, 27, p. 8.
34. Siddappa G. (2012), 'Effect of Earthquake onembankment dams,' *Proceeding of innovative dam and levee design and construction.* USA : the united states society of dams.
35. SLOPE/W (2018), 'Stability Modeling with SLOPE/W 2018 Version,' Geo-Slope international ltd, p. 252.
36. Stefania et.al. (2017), 'Numerical Analysis of Soil Liquefaction Induced Failure of Embankments,' 6th ECCOMAS Thematic Conference on Computational Methods in Structural Dynamics and Earthquake Engineering.
37. Taiebat, M., Shahir, H. and Pak, A. (2007), '*Study of Pore Pressure Variation During Liquefaction Using Two Constitutive Models for Sand*,' *Soil Dynamics*

and Earthquake Engineering. doi: 10.1016/j.soildyn.2006.03.004.

38. Tarbuck E. J. and Frederick K. L.Earth: (1996), 'An introduction to physical Geology,' New Jersy, Prentice Hall.
39. Terzaghi K. (1950), 'Mechanics of landslides,' *Geological society of America, Engineering geology volume.*
40. Tsuchida, J. P. K. and T. (1988), 'Earthquake-Induced Liquefaction of Fine-Grained Soils-Considerations from Japanese Research,' Washington, DC 20314-1000: Department of the Army US Army Corps of Engineers Under CWRD Work Unit 32255.
41. US.Corps of Engineers (2003), 'Engineering and design Time-History Dynamic Analysis of Concrete Hydraulic Structures.'
42. USCOLD (2000), 'Observed Performance of Dams During Earthquakes,' *Committee of earthqukaes.* -, vol.II., p. 461. doi: Denver,USA.
43. USNRC (1985), 'Safety of Dams: Flood and Earthquake Criteria,' *National Academy Press, Washington, DC*.
44. Worku, A. (2011) 'Recent Developments in the Definition of Design Earthquake Ground Motions Calling for a Revision of the Current Ethiopian Seismic Code - EBCS 8: 1995', Zede Journal, 28(0), pp. 1–15.
45. WWDSE (2008), 'Seismic Analysis and Safety Assessment of Earthfill Dam Founded on Alluvium Soil,' Addis Ababa.
46. WWDSE (2009), 'Final Detail Design Report of Gidabo Earth Fill dam,'Addis Ababa.
47. WWDSE (2016), '*Middle Awash Feasibility Study and Detail Design of Multipurpose Dam Project*,' *Volume-Iii, Annex-Iii, Site Specific Seismic Hazard Assessment Final Report, Addis Ababa, Ethiopia.*
48. Youd, T. L. and Idriss, I. M. (1997), 'Proceeding of the NCEER workshop on evaluation of liquefaction resistance of soils,' *Technical Report NCEER-97-0022,* p. 281.

Appendix A: Input Ground Motion

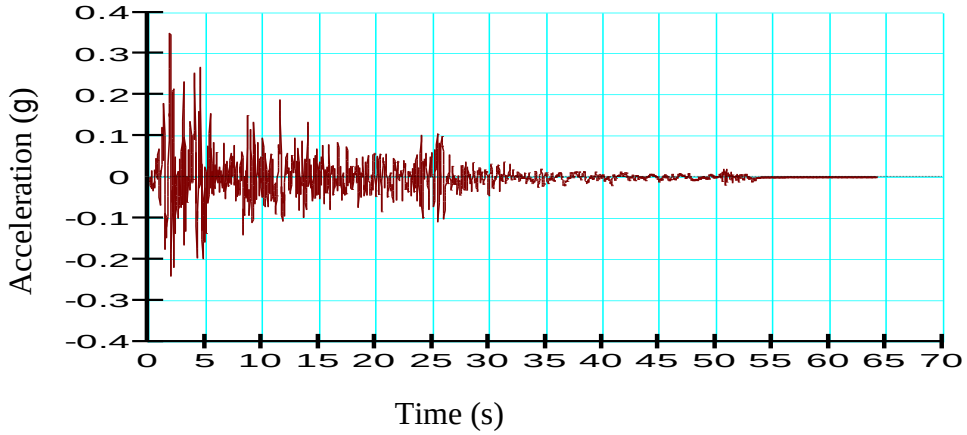

Appendix A: 1. Horizontal maximum credible earthquake – 1940 Elcentro record

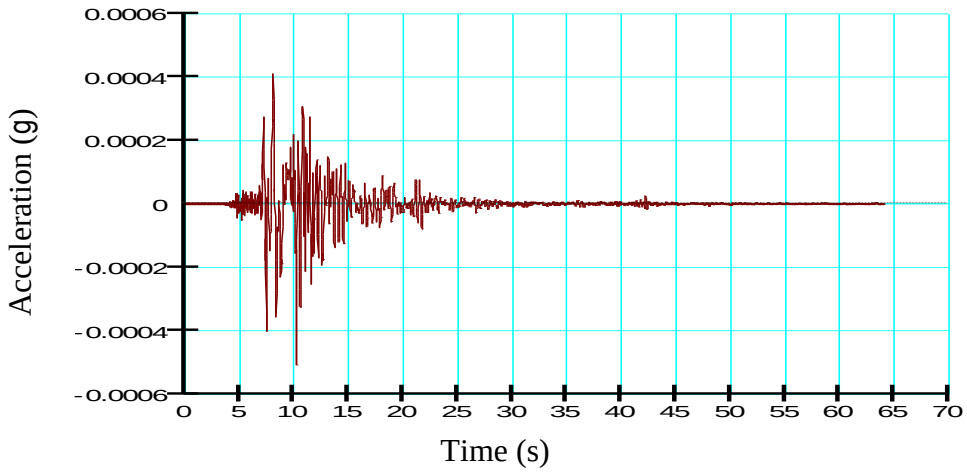

Appendix A: 2. Horizontal maximum credible earthquake – 1995 Kobe JMA record

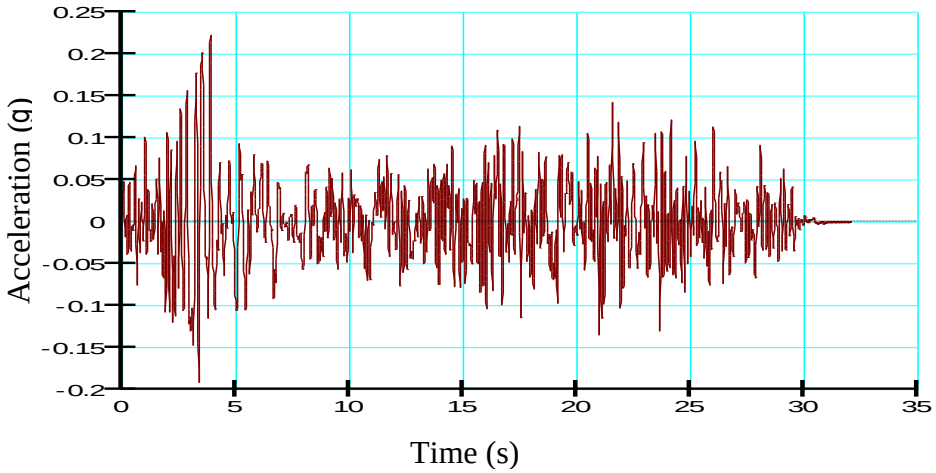

Appendix A: 3. Horizontal maximum credible earthquake – 1968 Hachinohe record

Appendix B: Dam Geometry

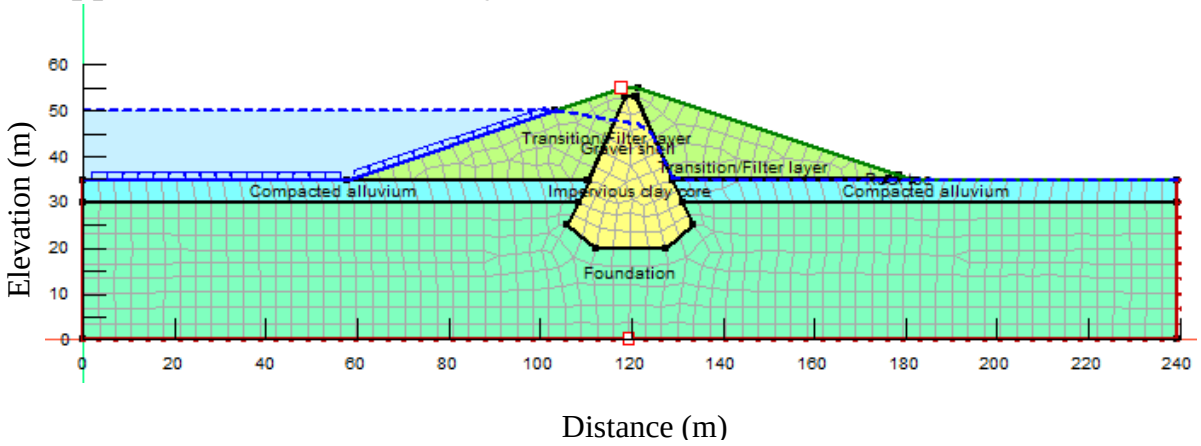

Appendix B: 1. Model of zoned earth fill dam with 5 meter thick liquefiable foundation and slope of 1:3

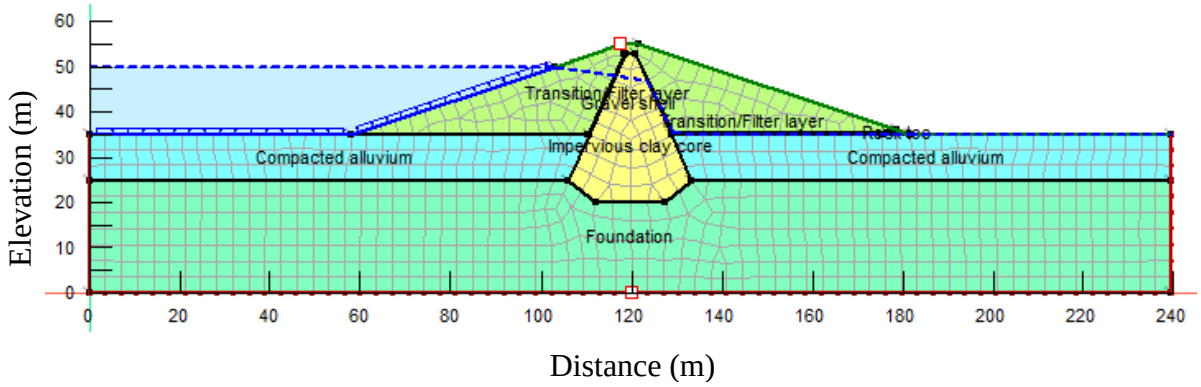

Appendix B: 2. Model of zoned earth fill dam with 10 meter thick liquefiable foundation and slope of 1:3

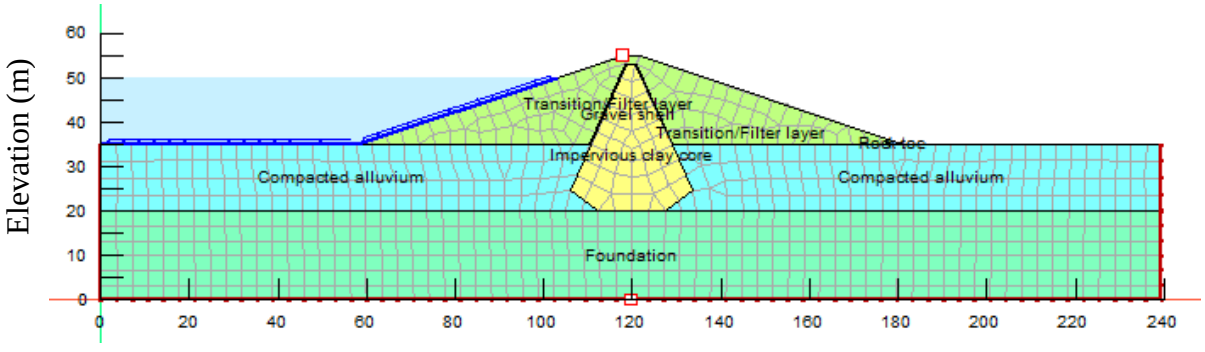

Appendix B: 3. Model of zoned earth fill dam with 15 meter thick liquefiable foundation and slope of 1:3

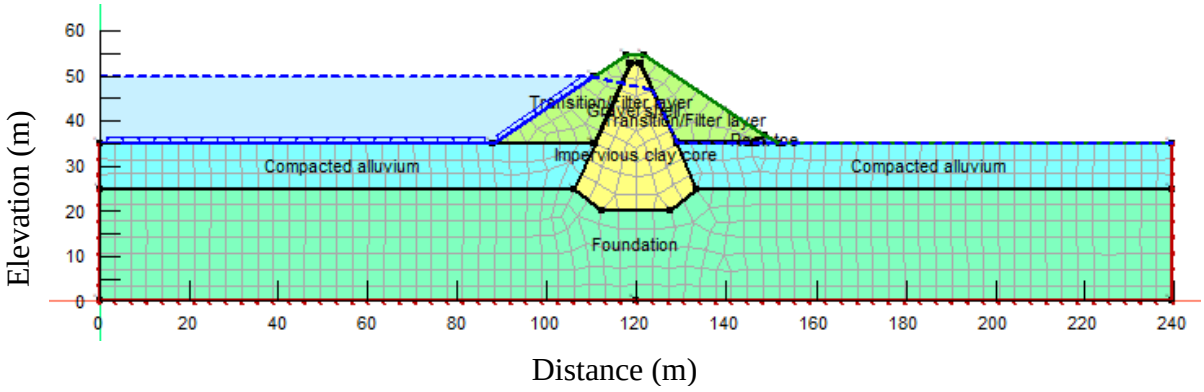

Appendix B: 4. Model of zoned earth fill dam with 10 meter thick liquefiable foundation and slope of 1:1.5

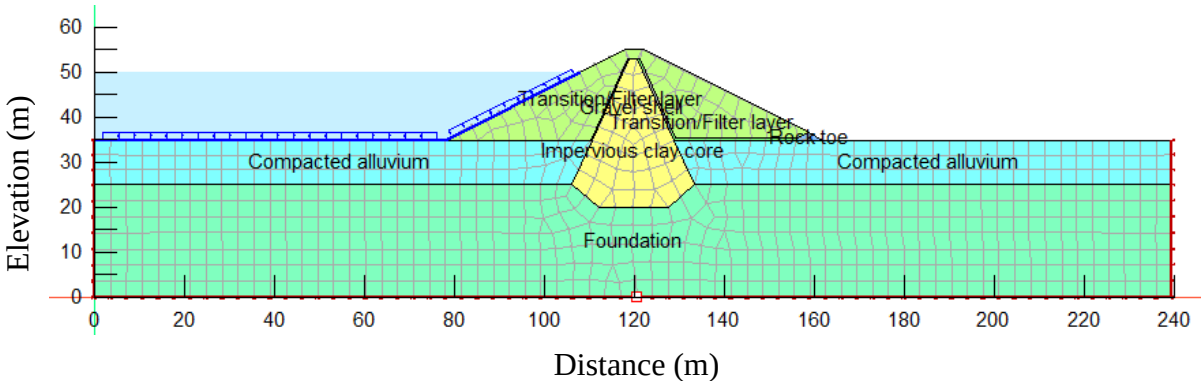

Appendix B: 5. Model of zoned earth fill dam with 10 meter thick liquefiable foundation and slope of 1:2

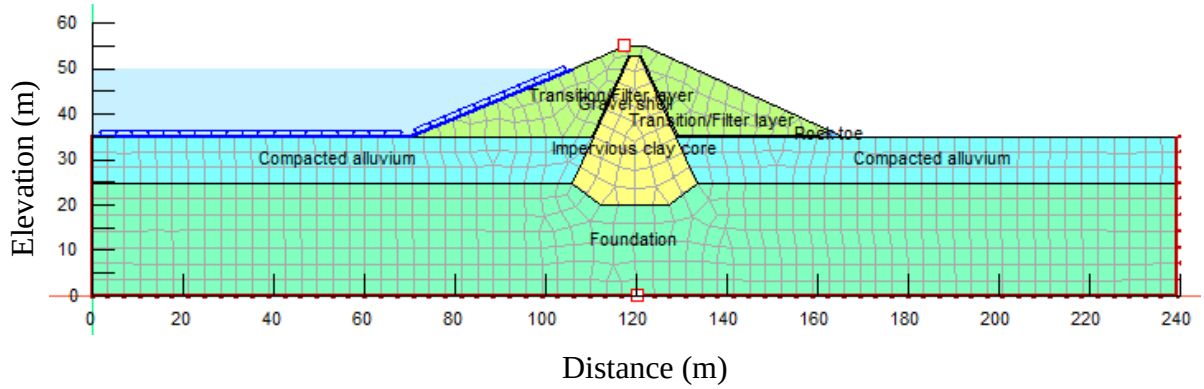

Fig Appendix B: 6. Model of zoned earth fill dam with 10 meter thick liquefiable foundation and slope of 1:2.2

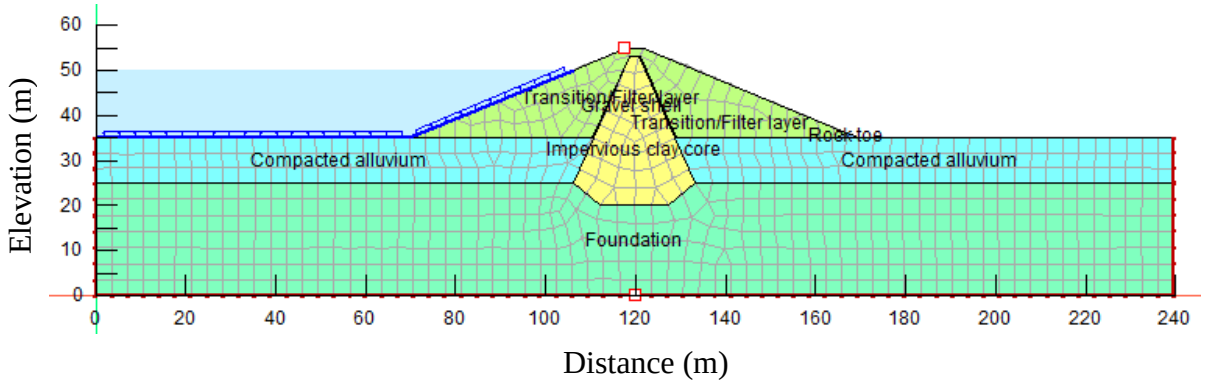

Appendix B: 7. Model of zoned earth fill dam with 10 meter thick liquefiable foundation and slope of 1:2.4

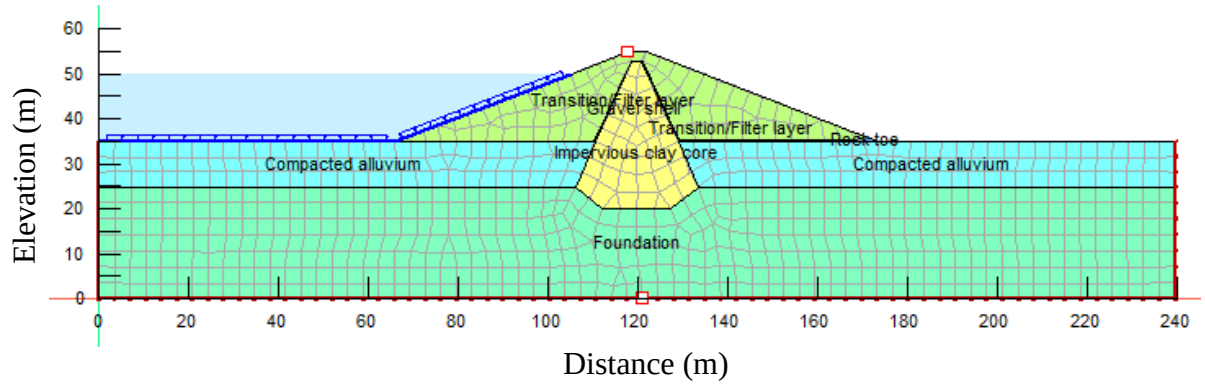

Appendix B: 8. Model of zoned earth fill dam with 10 meter thick liquefiable foundation and slope of 1:2.6

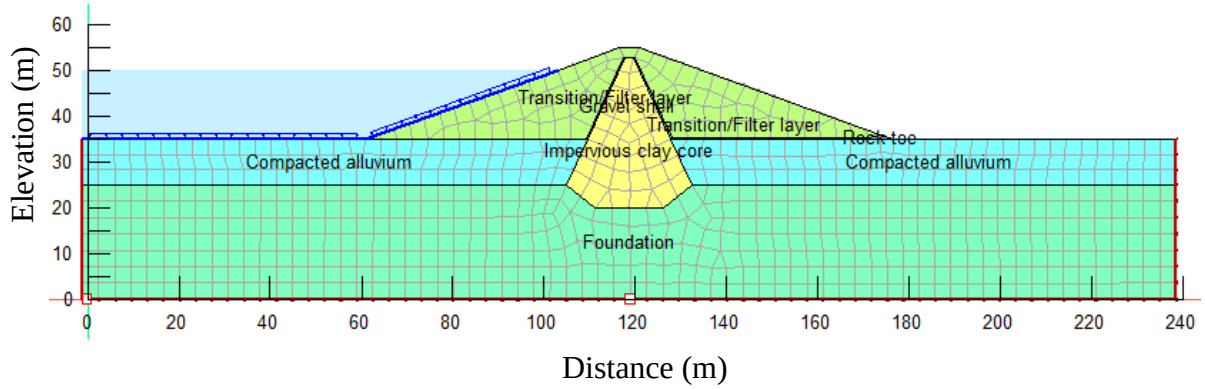

Appendix B: 9. Model of zoned earth fill dam with 10 meter thick liquefiable foundation and slope of 1:2.8

Appendix C: Liquefaction Result

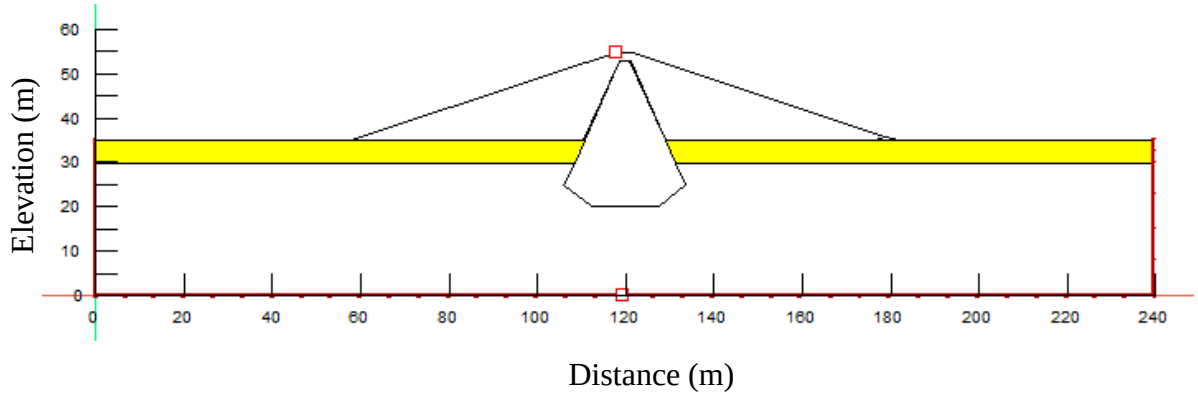

Appendix C.1: Fully liquefaction of 5 meter thick liquefiable foundation of the dam during 0.37g earthquake shaking

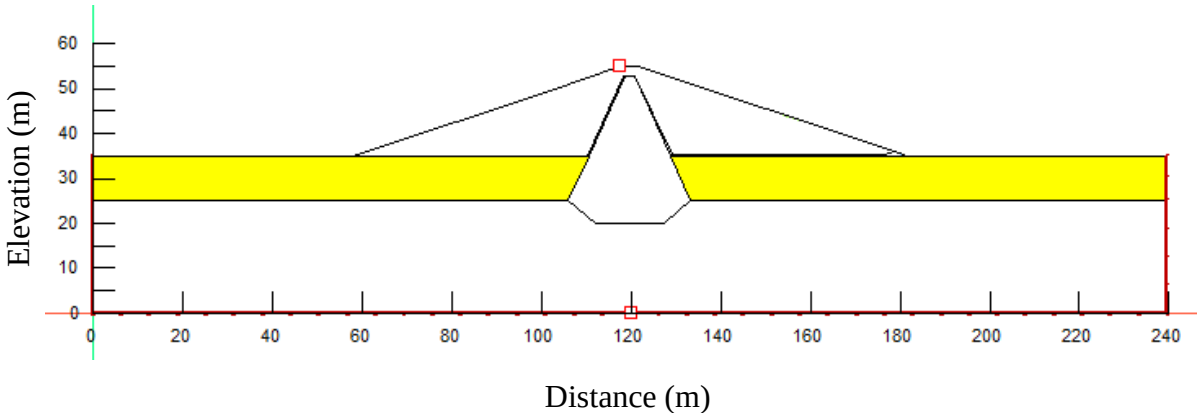

Appendix C.2: Fully liquefaction of 10 meter thick liquefiable foundation of the dam during 0.37g earthquake shaking

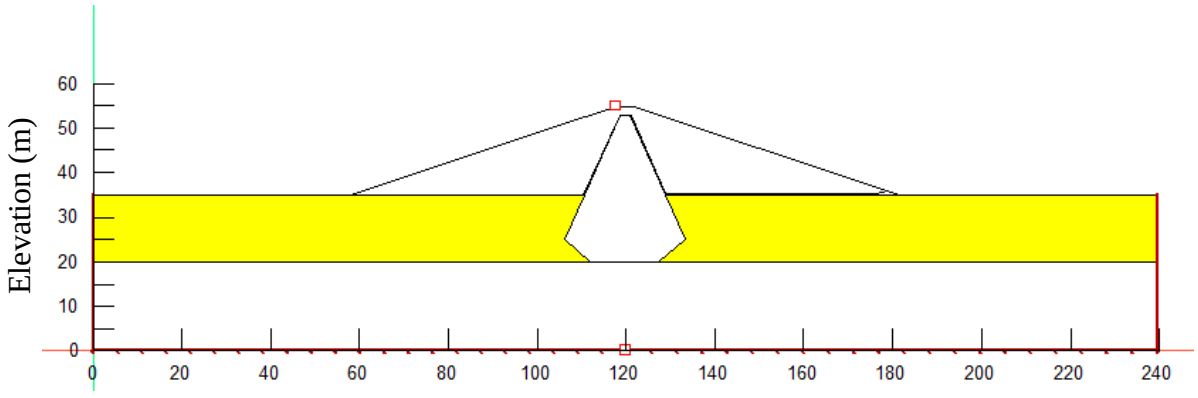

Appendix C.3: Fully liquefaction of 15 meter thick liquefiable foundation of the dam during 0.37g earthquake shaking

Appendix D: Static and Seismic Slope Stability

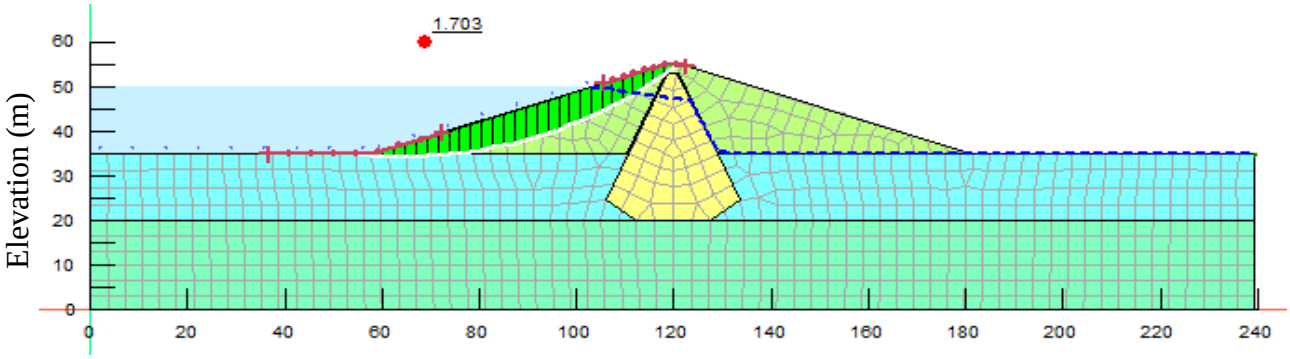

Appendix D.13: 1V:3H upstream slope stability of 15 meter thick liquefiable foundation of the dam

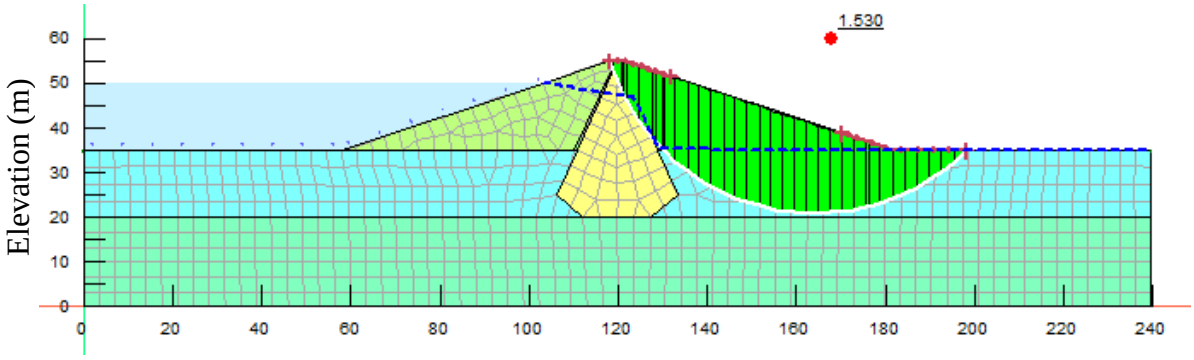

Appendix D.14: 1V:3H downstream slope stability of 15 meter thick liquefiable foundation of the dam

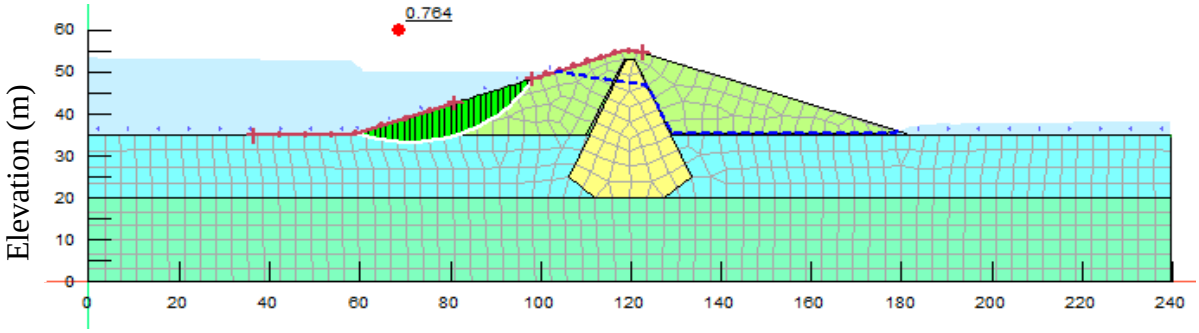

Appendix D.16: 1V:3H upstream slope stability of 15 meter thick liquefiable foundation of the dam corresponding to 0.37g earthquake shaking

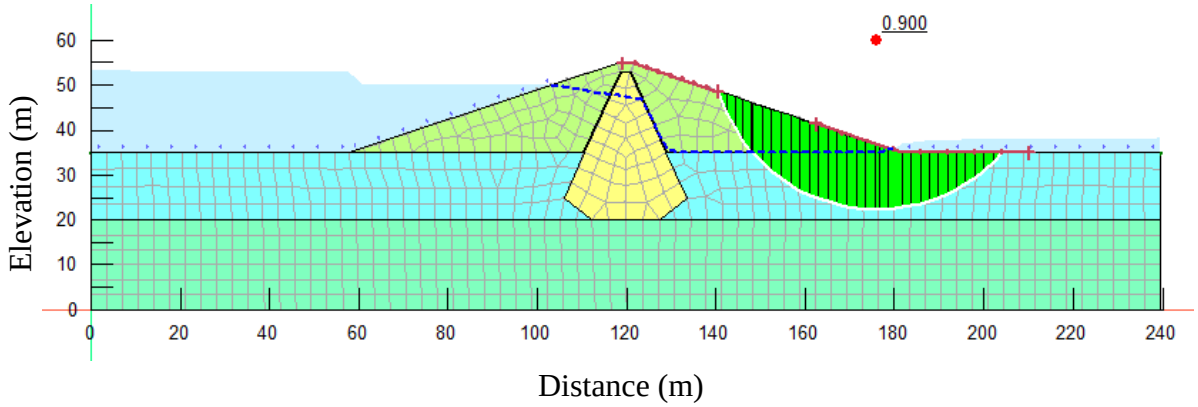

Appendix D.15: 1V:3H downstream slope stability of 15 meter thick liquefiable foundation of the dam corresponding to 0.37g earthquake shaking

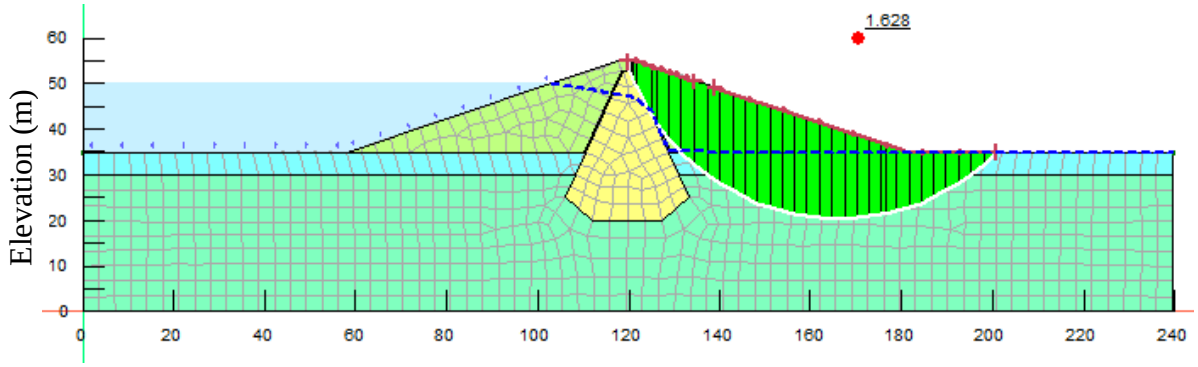

Appendix D.9: 1V:3H downstream slope stability of 5 meter thick liquefiable foundation of the dam

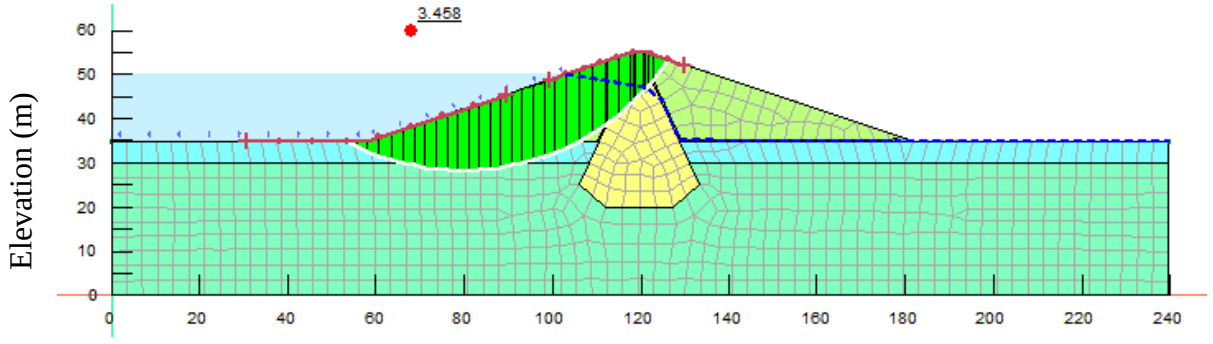

Appendix D.10: 1V:3H upstream slope stability of 5 meter thick liquefiable foundation of the dam

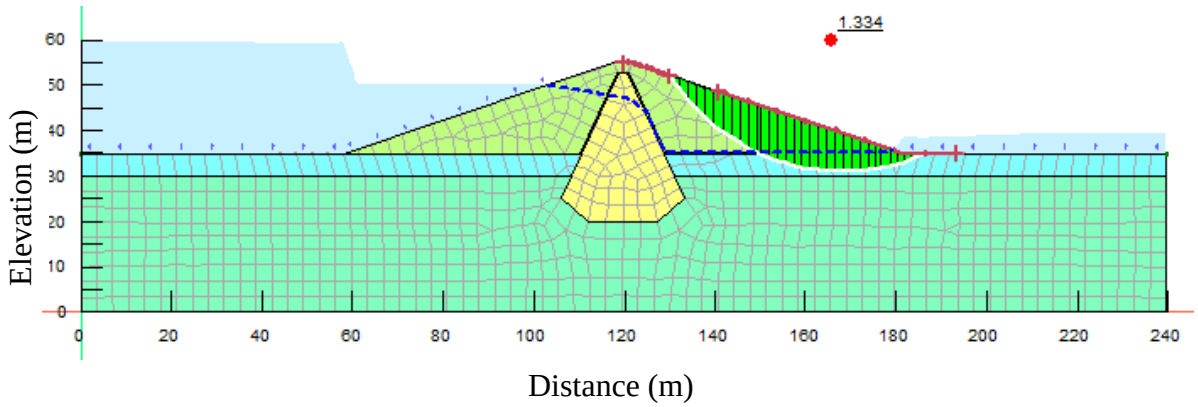

Appendix D.11: 1V:3H downstream slope stability of 5 meter thick liquefiable foundation of the dam corresponding to 0.37g earthquake shaking

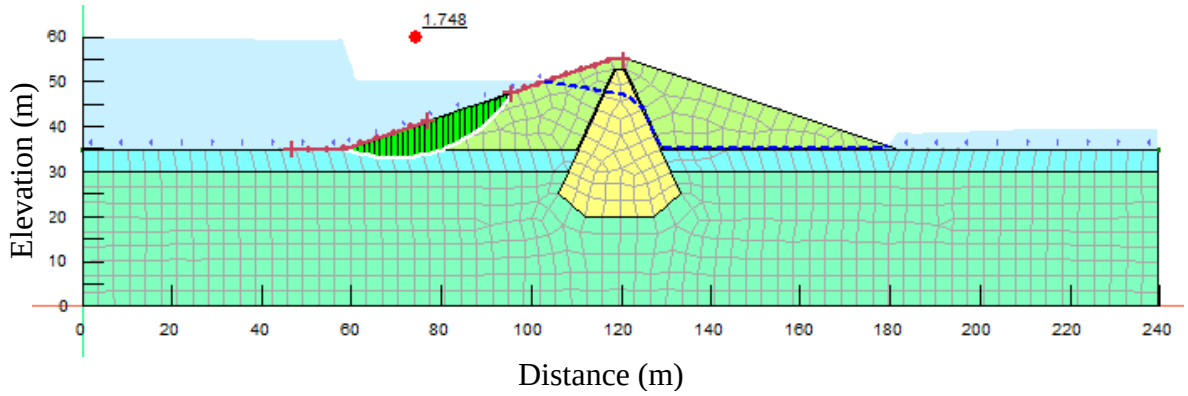

Appendix D.12: 1V:3H upstream slope stability of 5 meter thick liquefiable foundation of the dam corresponding to 0.37g earthquake shaking

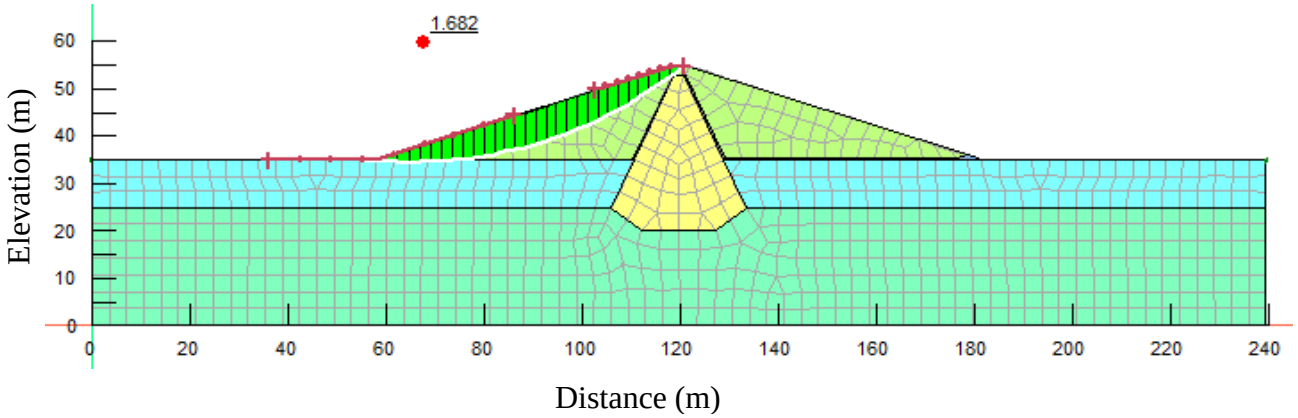

Appendix D.2: 1V:3H upstream slope stability of 10 meter thick liquefiable foundation of the dam

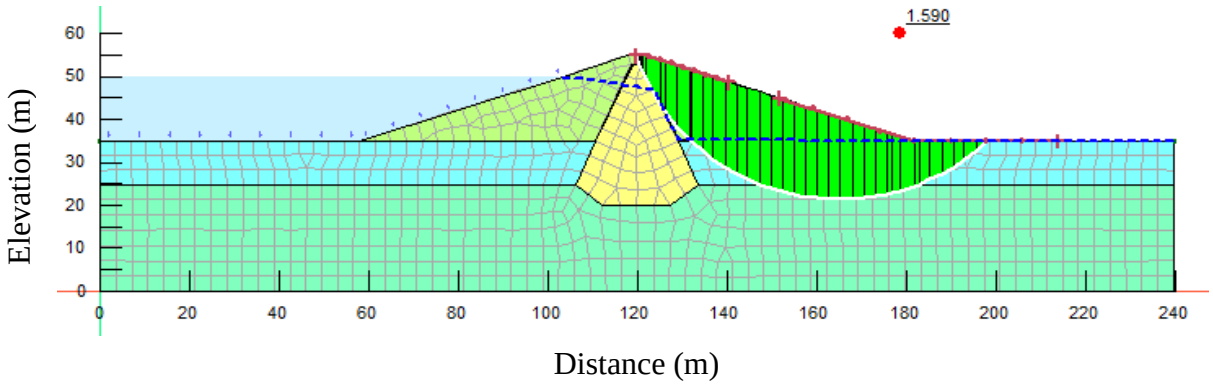

Appendix D.1: 1V:3H downstream slope stability of 10 meter thick liquefiable foundation of the dam

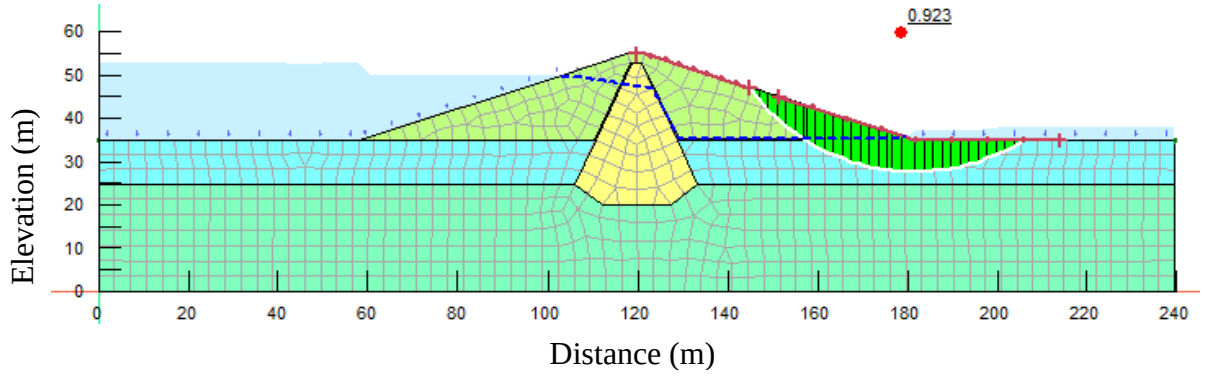

Appendix D.3: 1V:3H downstream slope stability of 10 meter thick liquefiable foundation of the dam corresponding to 0.37g earthquake shaking

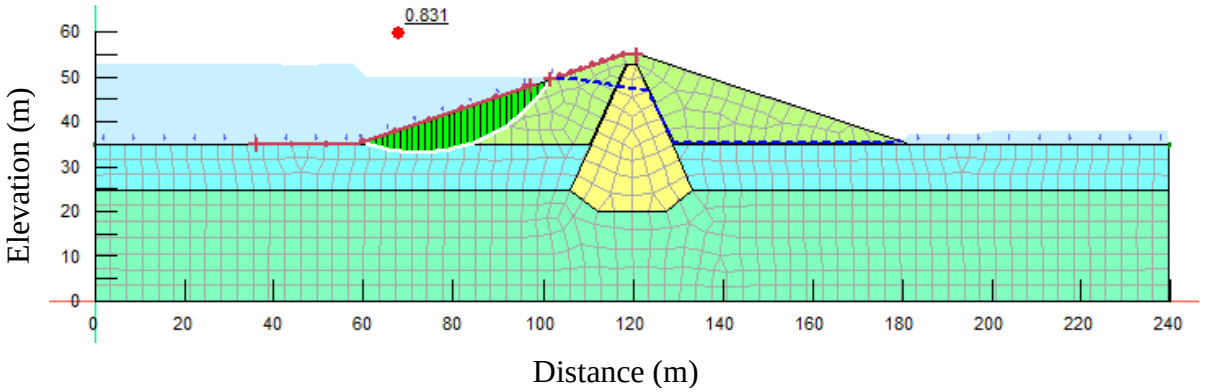

Appendix D.4: 1V:3H upstream slope stability of 10 meter thick liquefiable foundation of the dam corresponding to 0.37g earthquake shaking

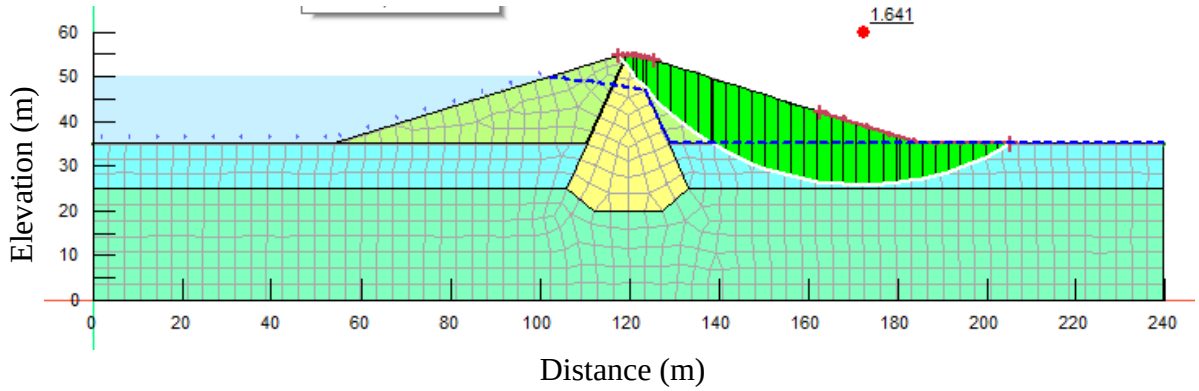

Appendix D.5: 1V:3.2H downstream slope stability of 10 meter thick liquefiable foundation of the dam

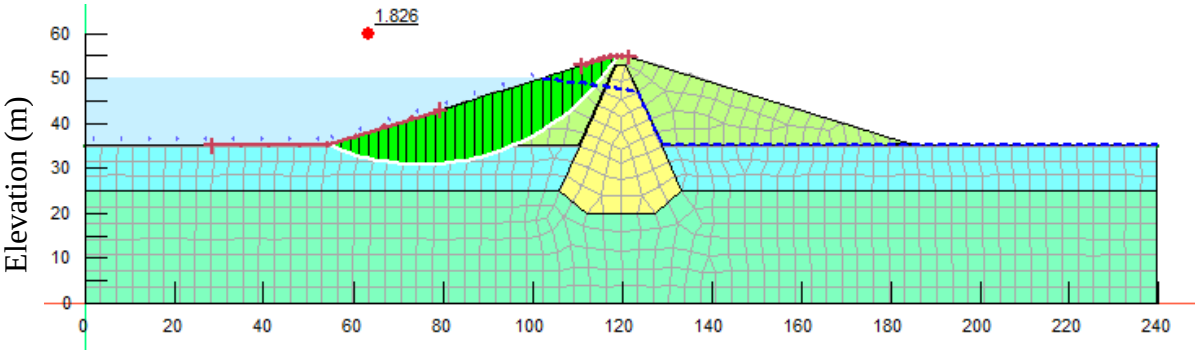

Appendix D.6: 1V:3.2H upstream slope stability of 10 meter thick liquefiable foundation of the dam

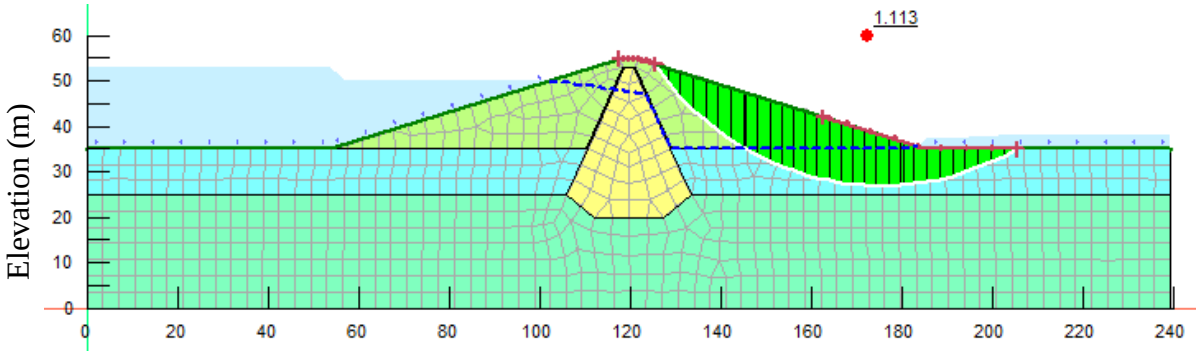

Appendix D.7: 1V:3.2H downstream slope stability of 10 meter thick liquefiable foundation of the dam corresponding to 0.37g earthquake shaking

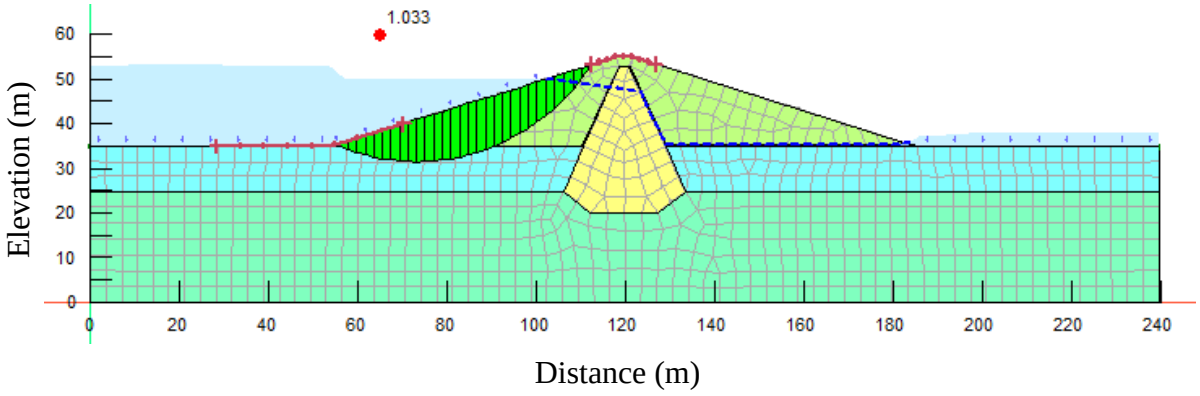

Appendix D.8: 1V:3.2H upstream slope stability of 10 meter thick liquefiable foundation of the dam corresponding to 0.37g earthquake shaking

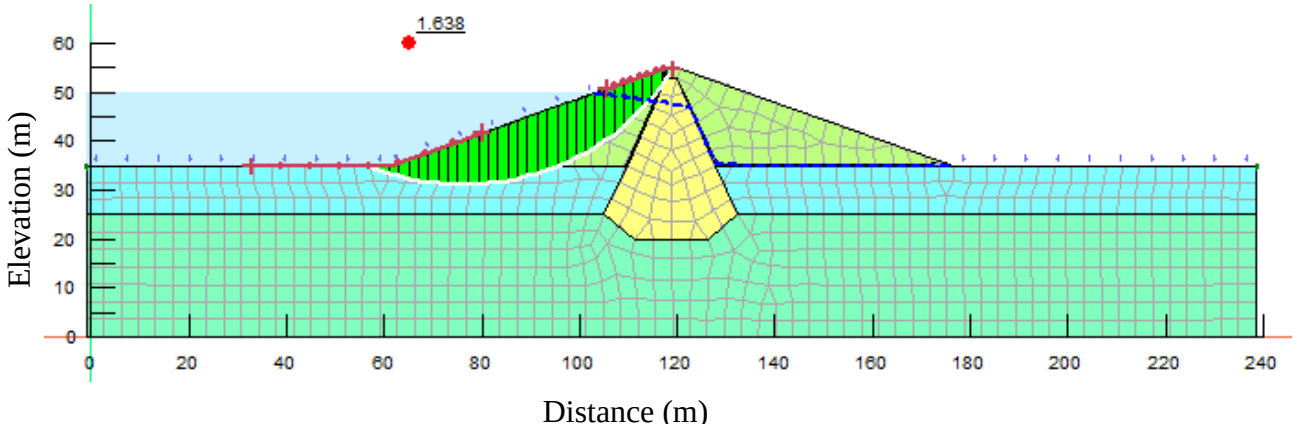

Appendix D.17: 1V:2.8H upstream slope stability of 10 meter thick liquefiable foundation of the dam

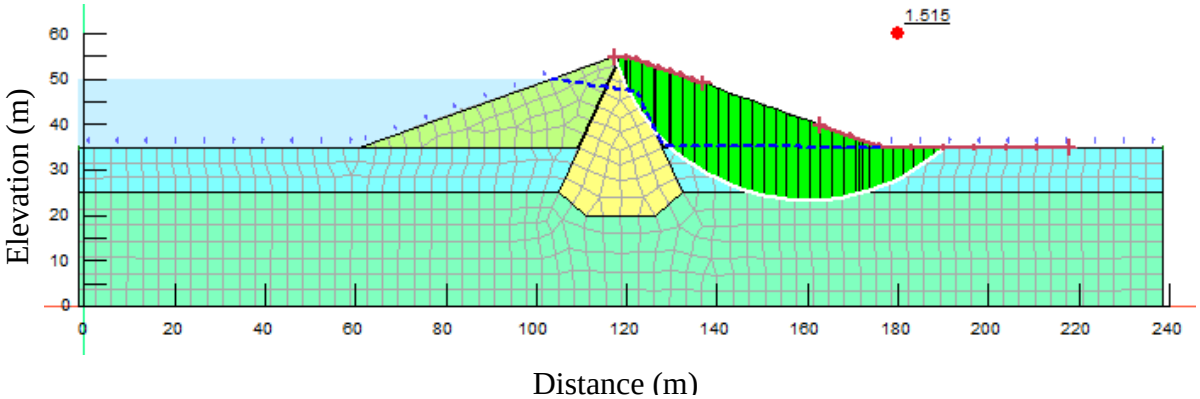

Appendix D.18: 1V:2.8H downstream slope stability of 10 meter thick liquefiable foundation of the dam

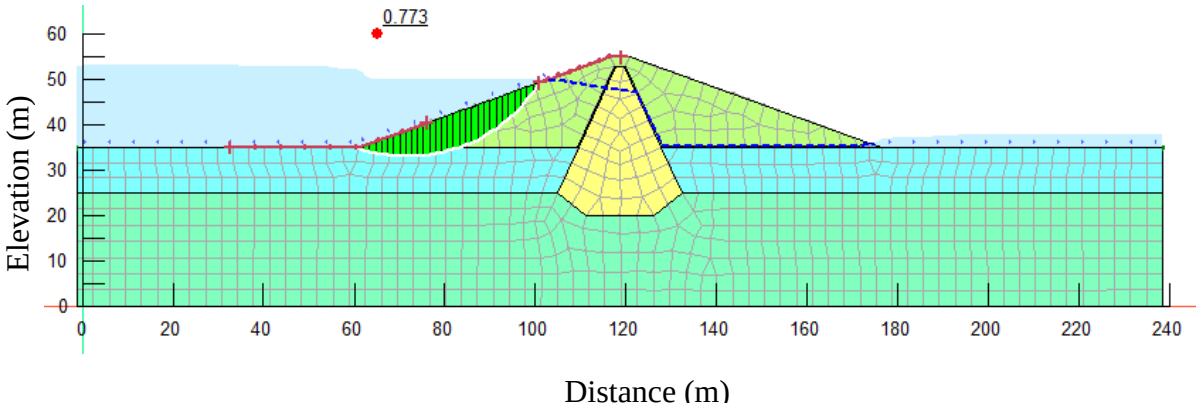

Appendix D.19: 1V:2.8H upstream slope stability of 10 meter thick liquefiable foundation of the dam corresponding to 0.37g earthquake shaking

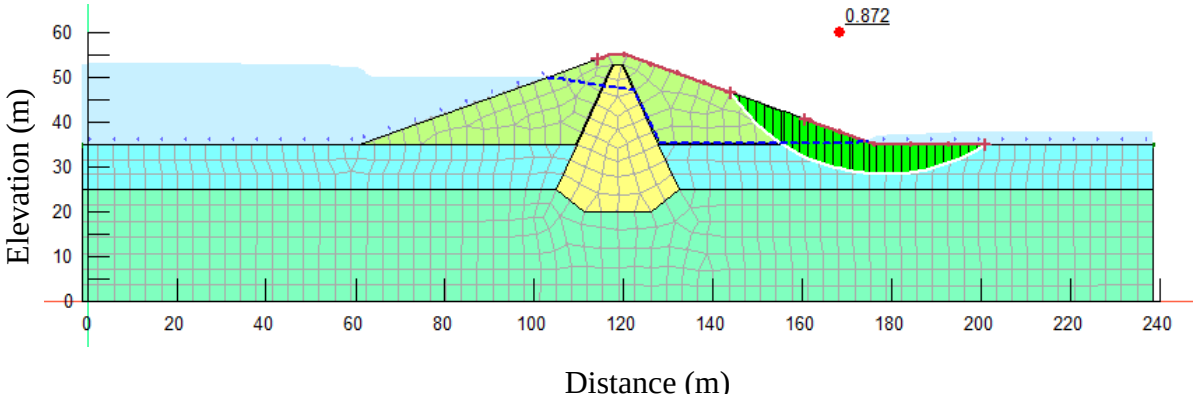

Appendix D.20: 1V:2.8H downstream slope stability of 10 meter thick liquefiable foundation of the dam corresponding to 0.37g earthquake shaking

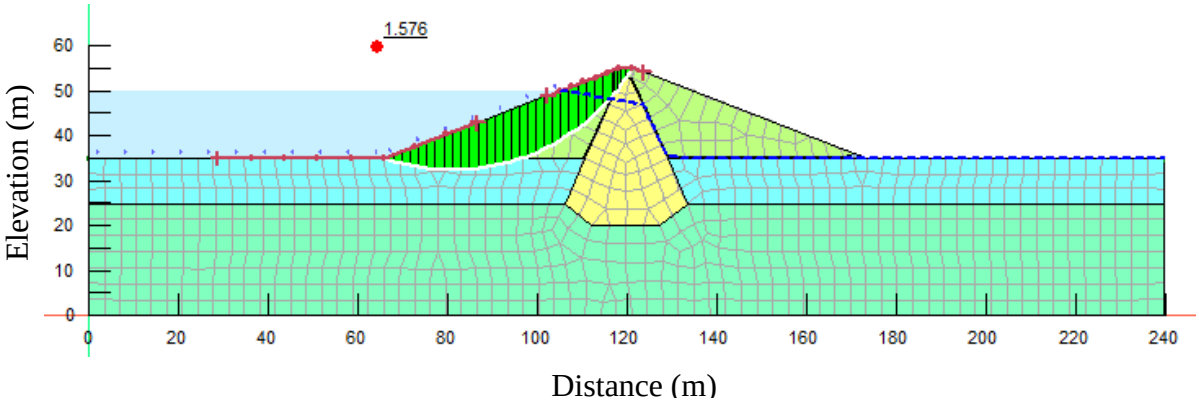

Appendix D.21: 1V:2.6H upstream slope stability of 10 meter thick liquefiable foundation of the dam

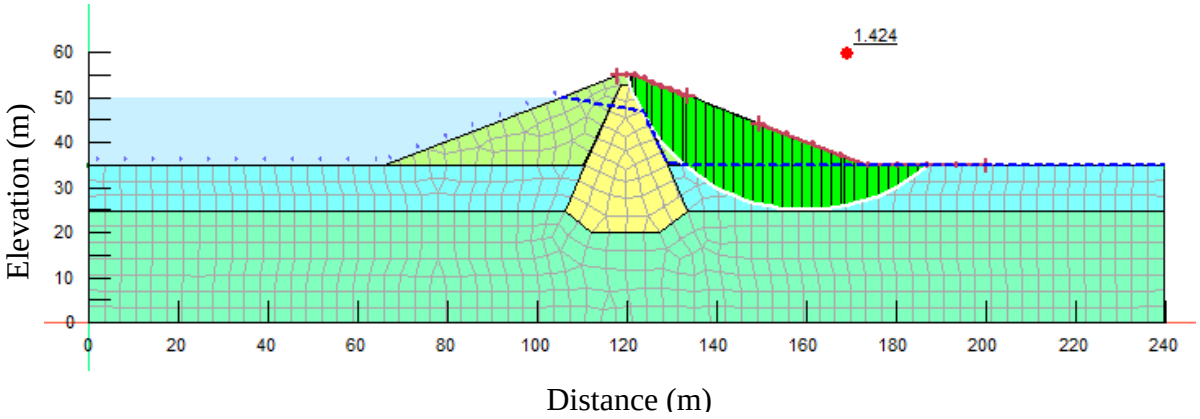

Appendix D.22: 1V:2.6H downstream slope stability of 10 meter thick liquefiable foundation of the dam

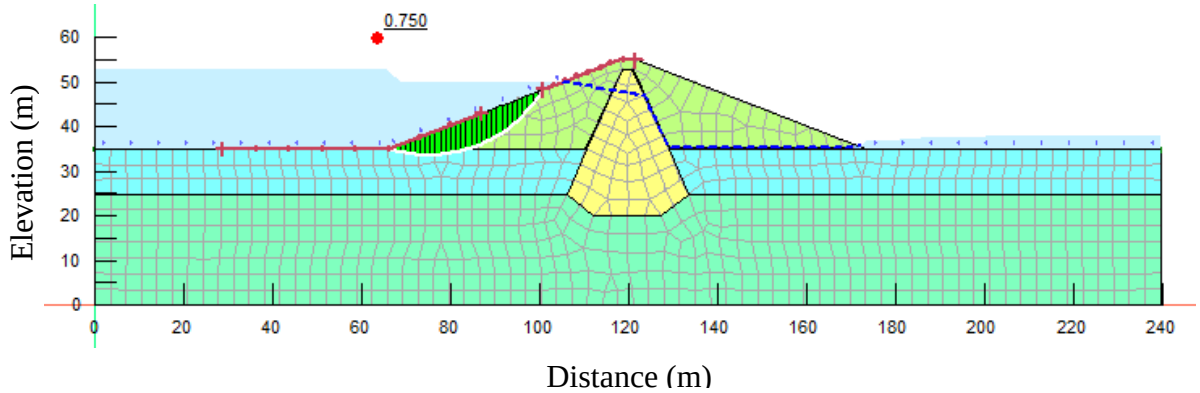

Appendix D.23: 1V:2.6H upstream slope stability of 10 meter thick liquefiable foundation of the dam corresponding to 0.37g earthquake shaking

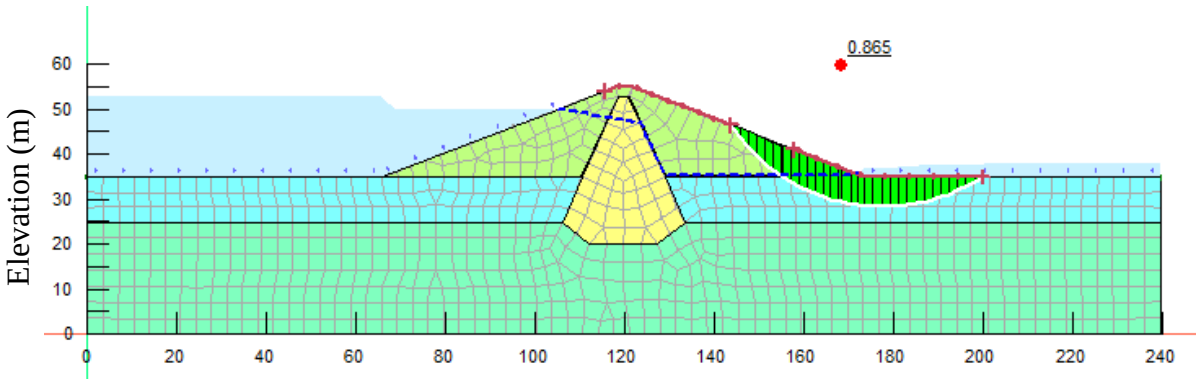

Appendix D.24: 1V:2.6H downstream slope stability of 10 meter thick liquefiable foundation of the dam corresponding to 0.37g earthquake shaking

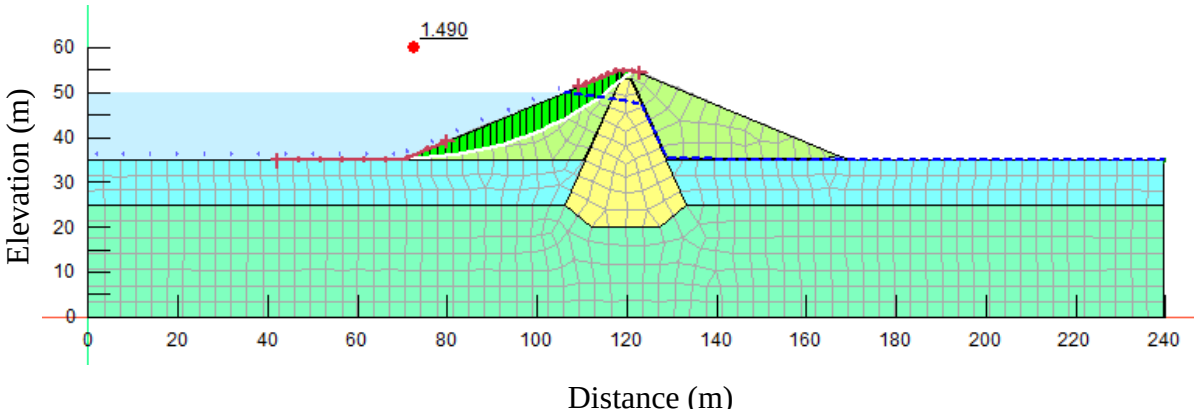

Appendix D.25: 1V:2.4H upstream slope stability of 10 meter thick liquefiable foundation of the dam

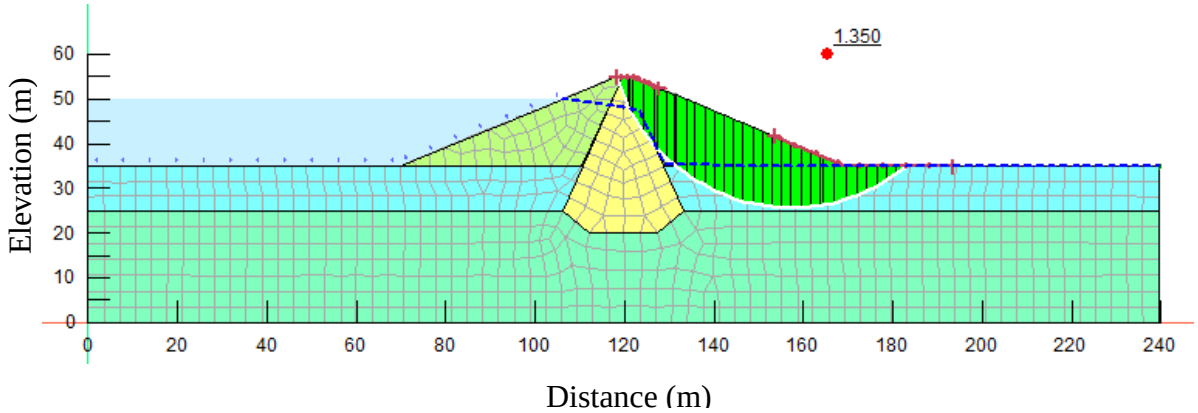

Appendix D.26: 1V:2.4H downstream slope stability of 10 meter thick liquefiable foundation of the dam

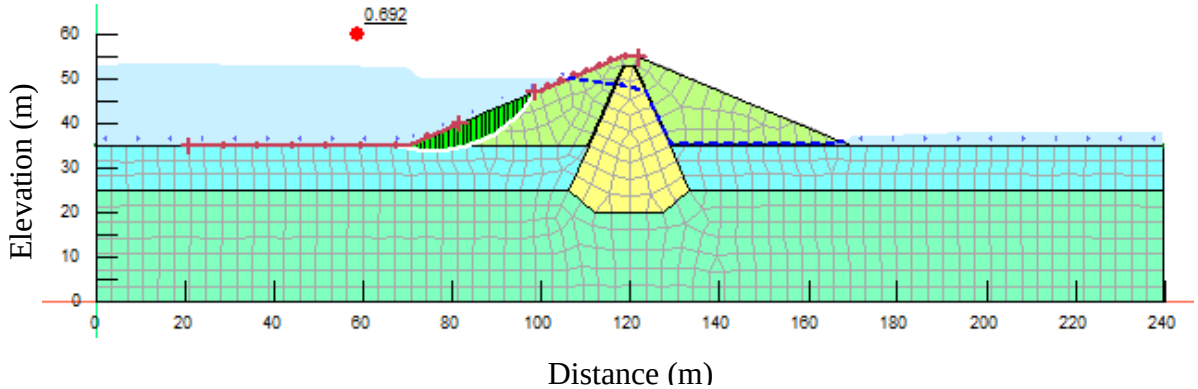

Appendix D.27: 1V:2.4H upstream slope stability of 10 meter thick liquefiable foundation of the dam corresponding to 0.37g earthquake shaking

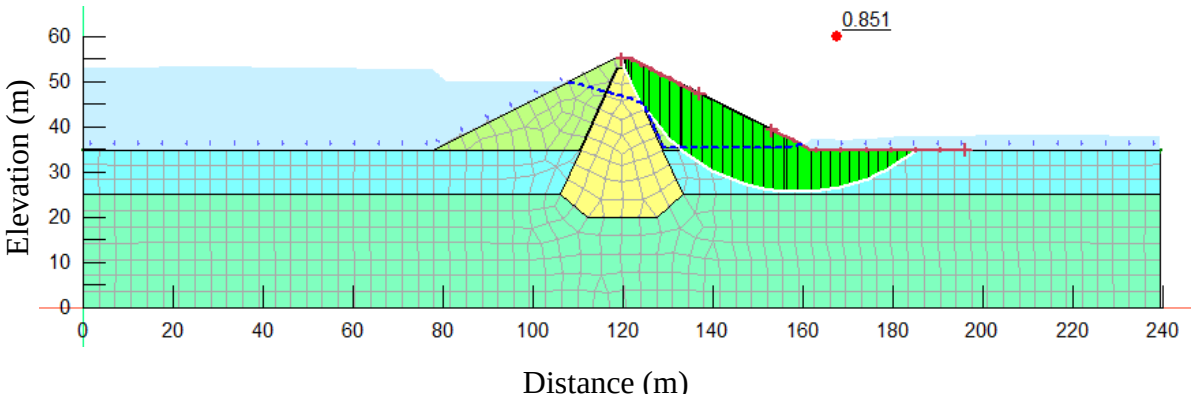

Appendix D.28: 1V:2.4H downstream slope stability of 10 meter thick liquefiable foundation of the dam corresponding to 0.37g earthquake shaking

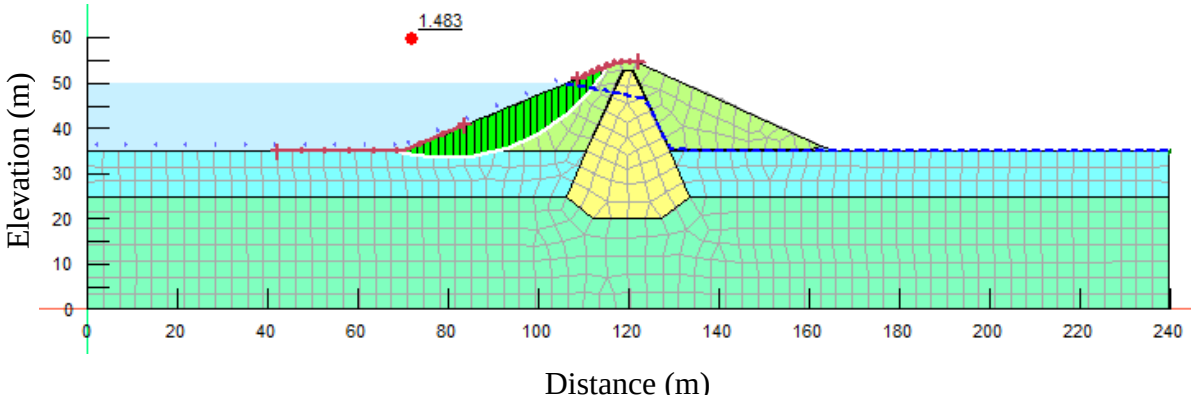

Appendix D.29: 1V:2.2H upstream slope stability of 10 meter thick liquefiable foundation of the dam

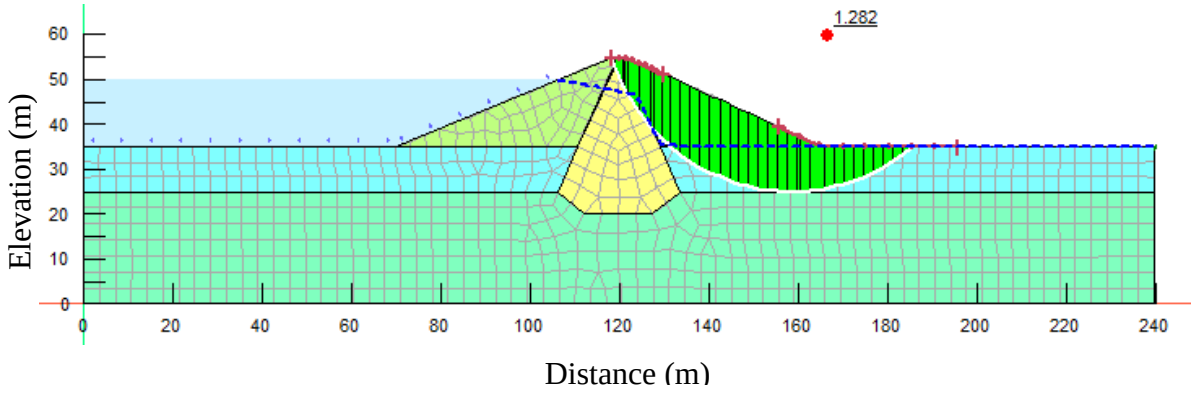

Appendix D.30: 1V:2.2H downstream slope stability of 10 meter thick liquefiable foundation of the dam

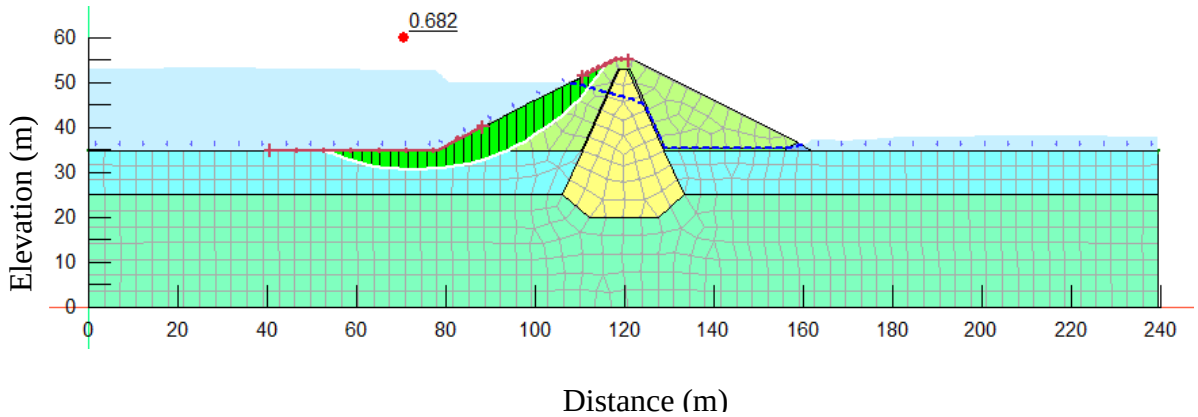

Appendix D.31: 1V:2.2H upstream slope stability of 10 meter thick liquefiable foundation of the dam corresponding to 0.37g earthquake shaking

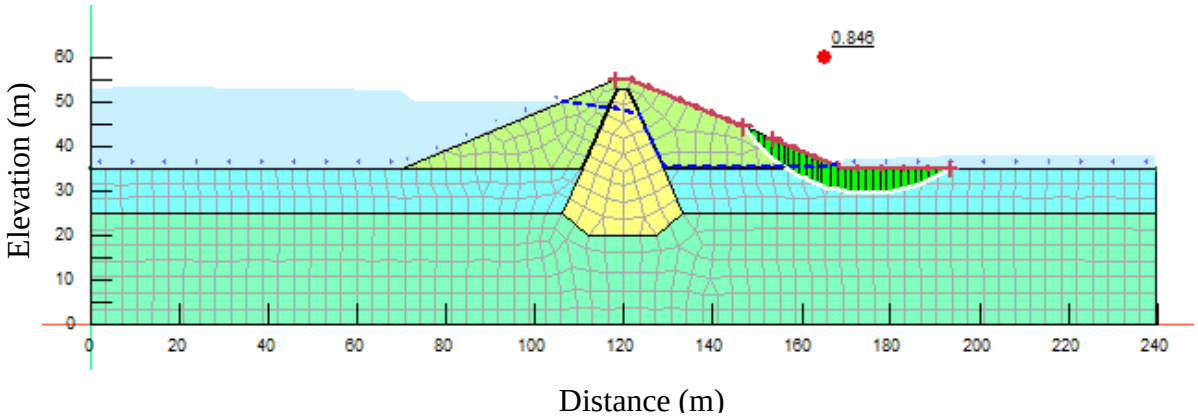

Appendix D.32: 1V:2.2H downstream slope stability of 10 meter thick liquefiable foundation of the dam corresponding to 0.37g earthquake shaking

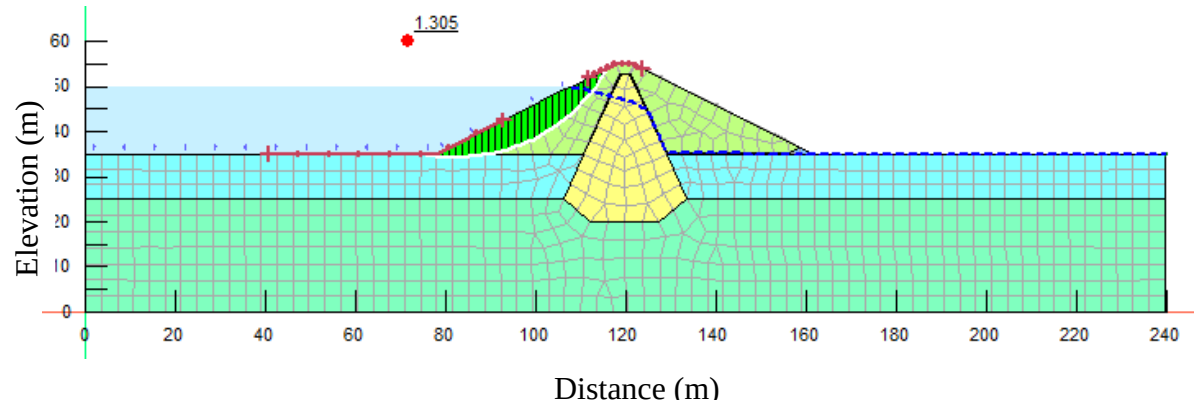

Appendix D.33: 1V:2H upstream slope stability of 10 meter thick liquefiable foundation of the dam

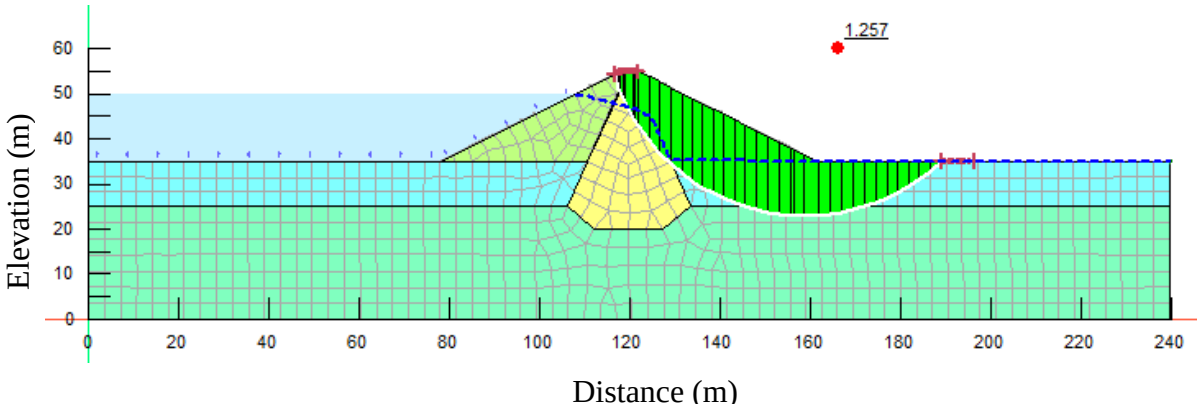

Appendix D.34: 1V:2H downstream slope stability of 10 meter thick liquefiable foundation of the dam

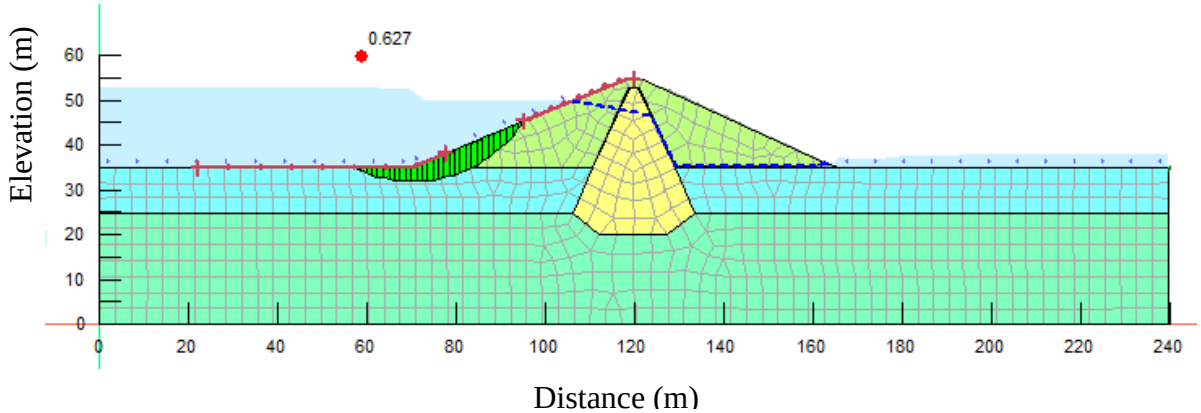

Appendix D.35: 1V:2H upstream slope stability of 10 meter thick liquefiable foundation of the dam corresponding to 0.37g earthquake shaking

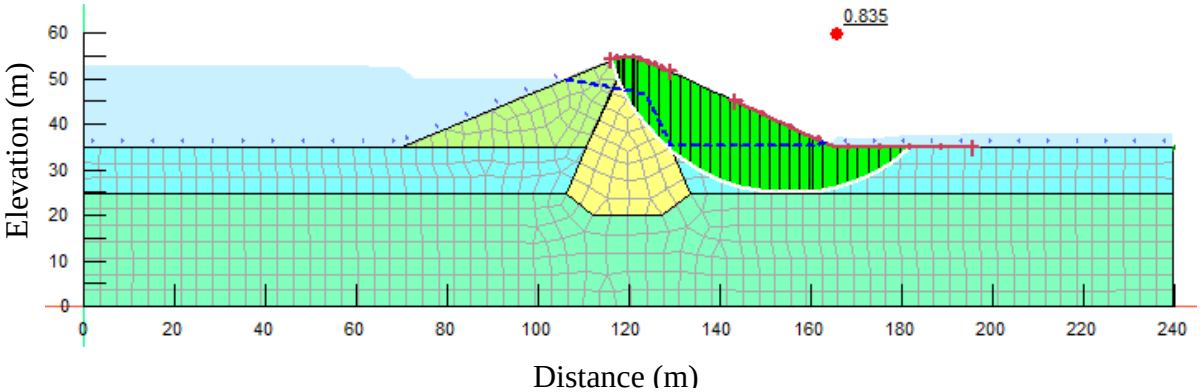

Appendix D.36: 1V:2H downstream slope stability of 10 meter thick liquefiable foundation of the dam corresponding to 0.37g earthquake shaking

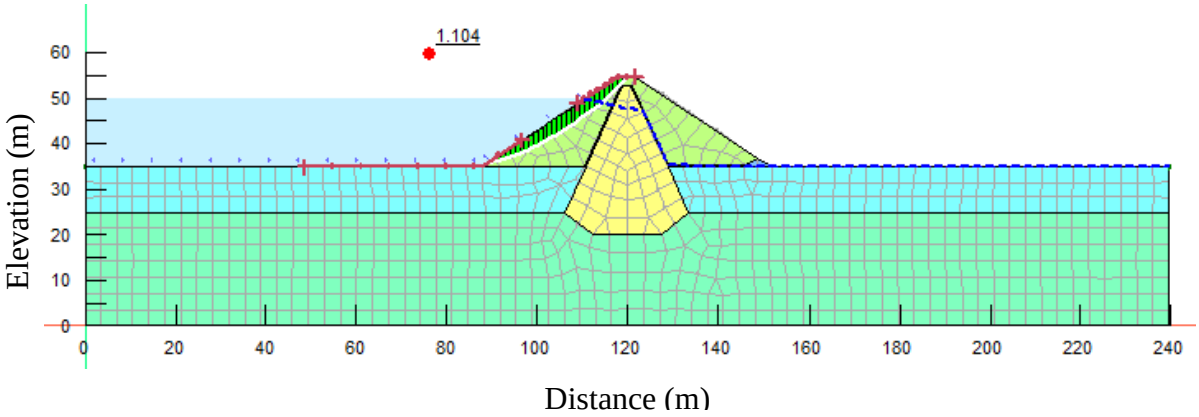

Appendix D.37: 1V:2H upstream slope stability of 10 meter thick liquefiable foundation of the dam

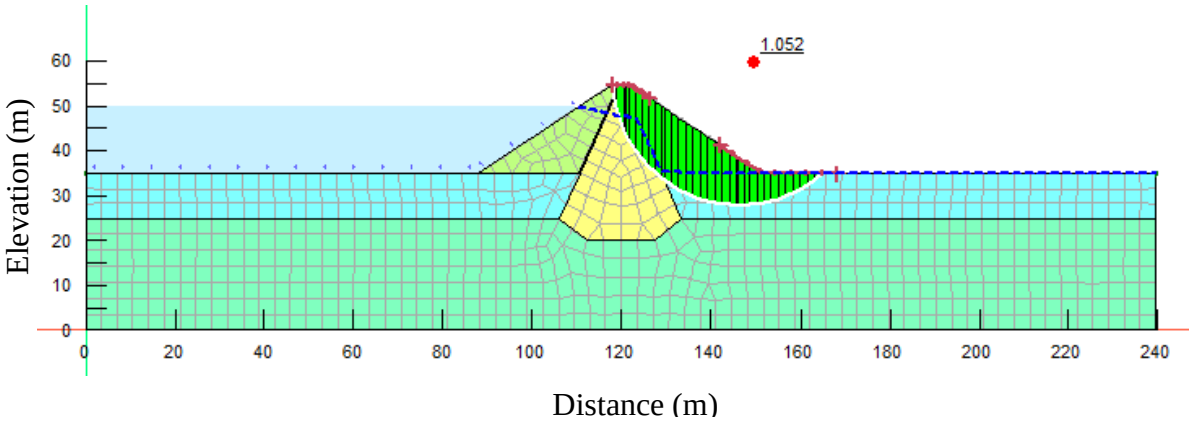

Appendix D.38: 1V:1.5H downstream slope stability of 10 meter thick liquefiable foundation of the dam

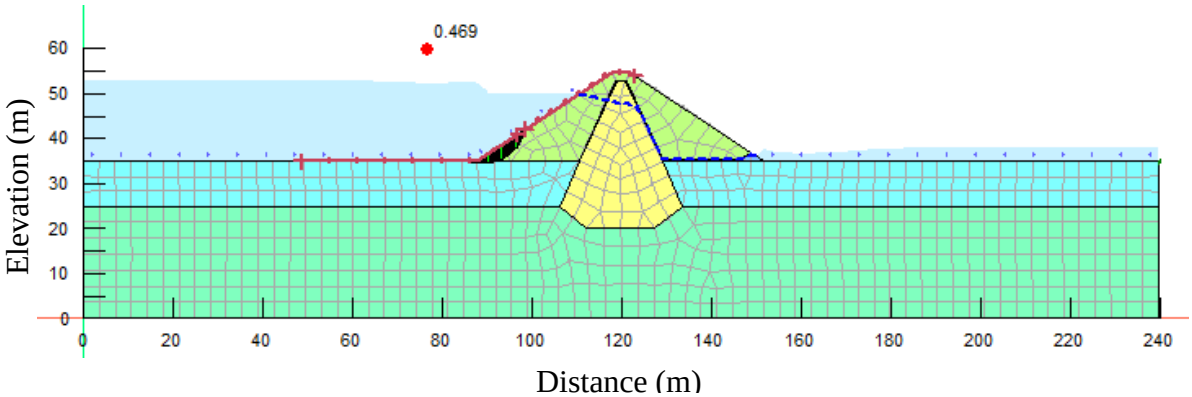

Appendix D.39: 1V:1.5H upstream slope stability of 10 meter thick liquefiable foundation of the dam corresponding to 0.37g earthquake shaking

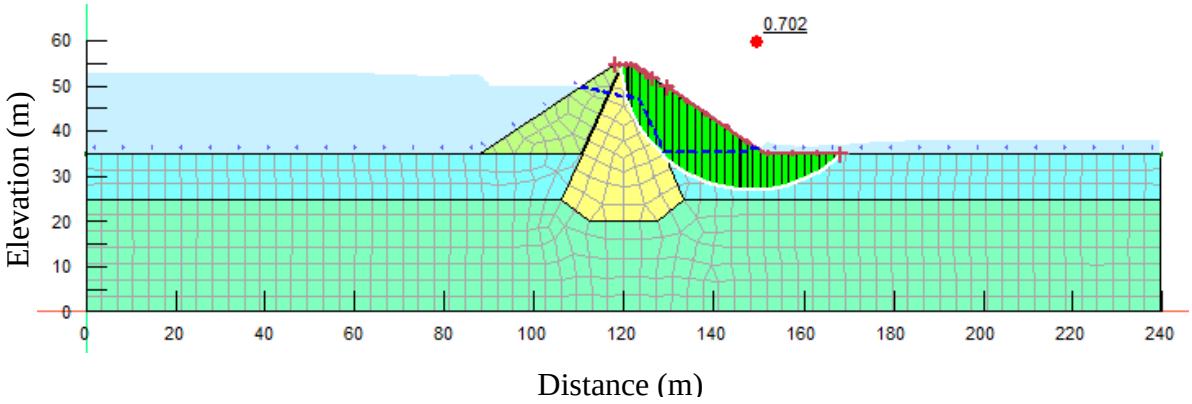

Appendix D.40: 1V:1.5H downstream slope stability of 10 meter thick liquefiable foundation of the dam corresponding to 0.37g earthquake shaking

Appendix E: During Earthquake Acceleration Response at the Dam Crest

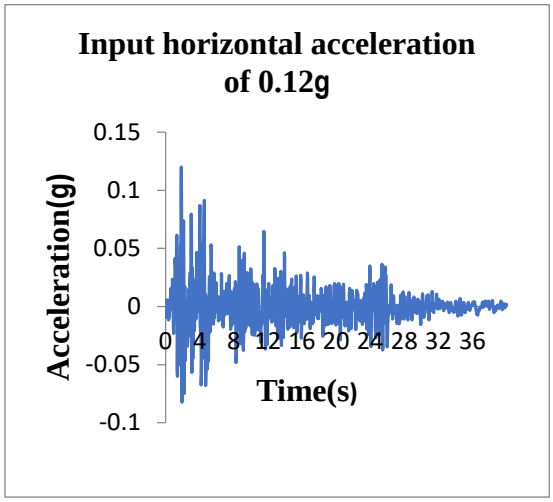

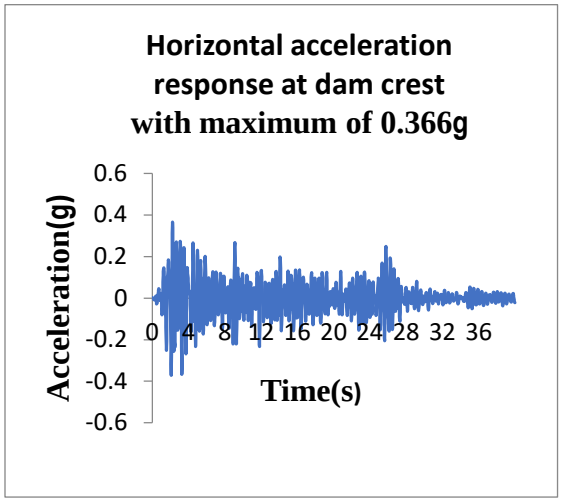

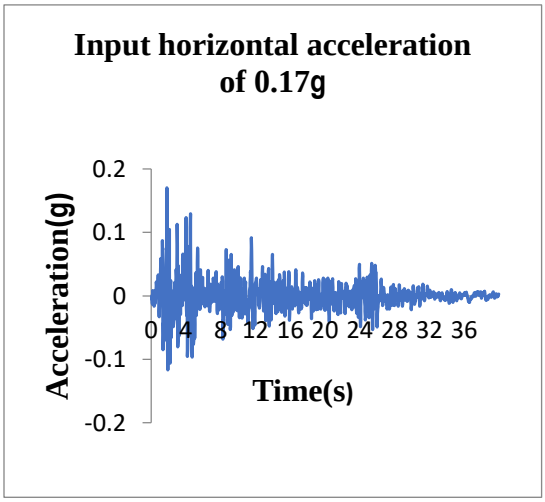

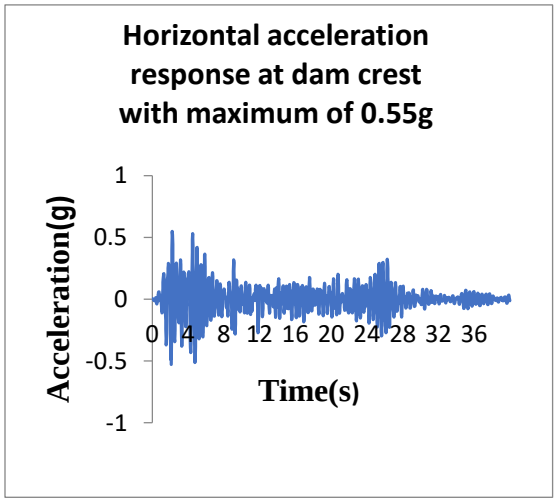

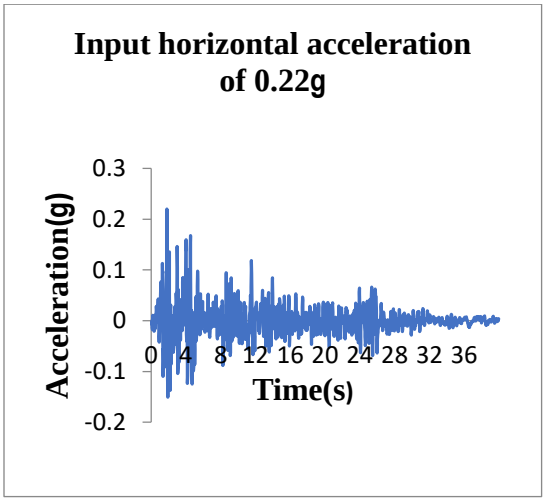

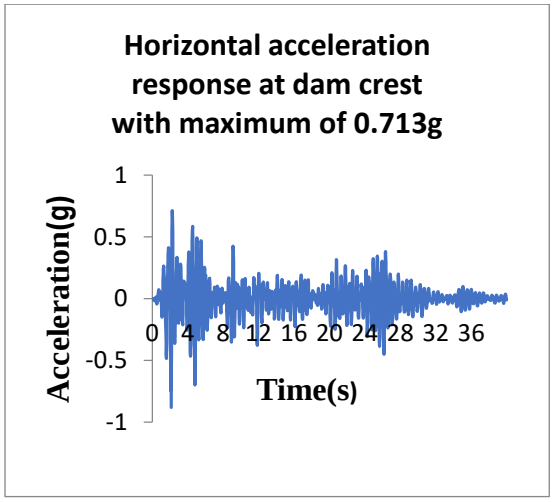

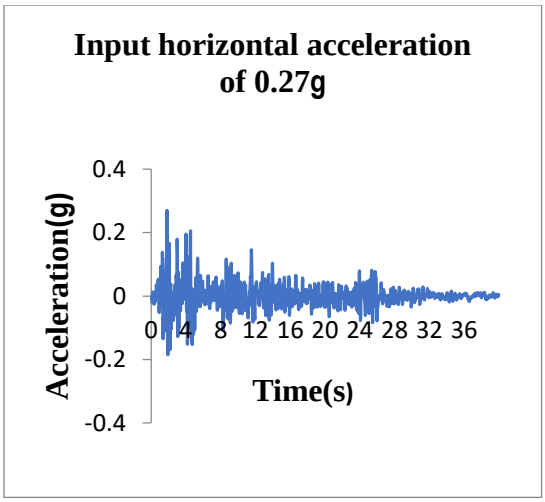

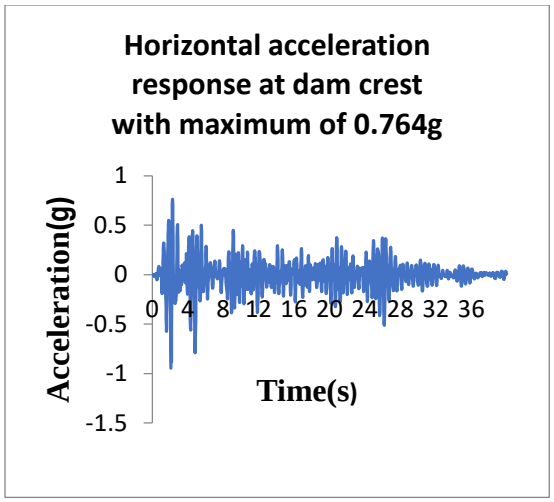

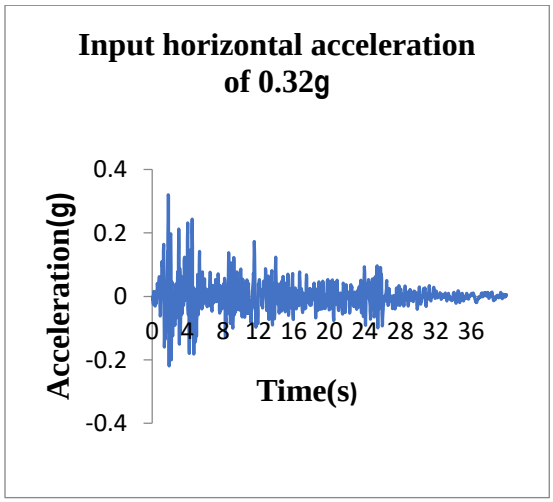

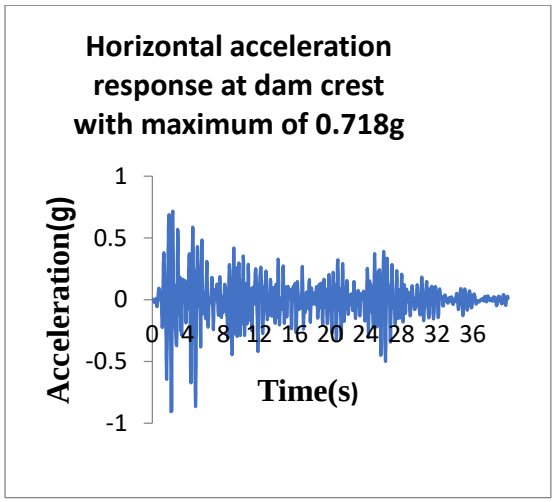

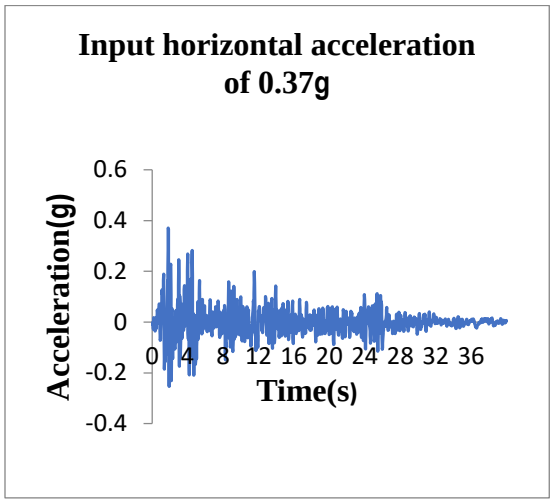

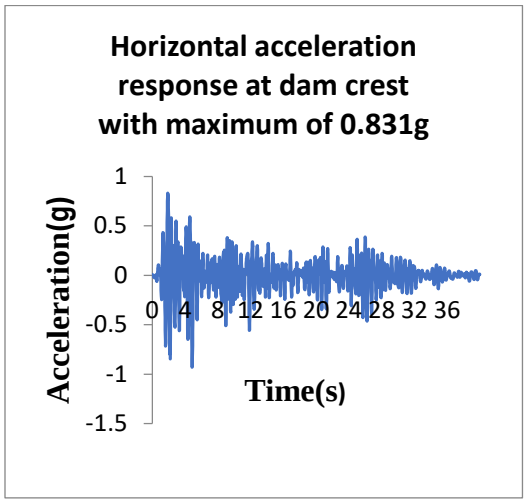

Appendix C.1: Acceleration response at crest of the dam for HACHINOHE earthquake record